The University School for Advanced Studies IUSS Pavia

Interplay of radiation response in fibrosarcoma: effects on immune response and complement activation

A Thesis Submitted in Partial Fulfilment of the Requirements
for the Degree of Doctor of Philosophy in

THE HADRON ACADEMY: Risk and complexity in high tech medical innovation

by

Gaia Volpi

Supervisors:
Angelica Facoetti (CNAO Pavia)
Andrea Spanu (IUSS Pavia)

External Supervisors:
Claudia Fournier (GSI Darmstadt)

March 2026

Contents

1. List of figures

Supplementary figures

2. List of Tables

3. List of abbreviations

• ATP	Adenosine triphosphate
• BSA	Bovine serum albumin
• C-ion	Carbon ion
• CRT	Calreticulin
• CXCL	Chemokine (C-X-C motif) ligand
• DAMPs	Damage-associated molecular patterns
• DAPI	4', 6'-diamidino-2-phenylindole
• DCs	Dendritic cells
• DDR	DNA damage repair
• DMSO	Dimethylsulfoxide
• DNA	Deoxyribonucleic Acid
• DSBs	Double-strand breaks
• ECM	Extracellular matrix
• ELISA	Enzyme-linked immunosorbent assay
• EMT	epithelium mesenchymal transition
• ER	Endoplasmic reticulum
• FCS	Forward scatter
• FITC	Fluorescein isothiocyanate

• GM-CSF	Granulocyte-macrophage colony-stimulating factor
• h	Hours
• HIF-1α	Hypoxia-Inducible Factor-1 alpha
• HMGB1	High mobility group box 1
• HR	Homologous recombination repair
• ICD	Immunogenic cell death
• IC50	Half-Maximal Inhibitory Concentration
• ICIs	Immune checkpoint inhibitors
• IFN	Interferon
• IL	Interleukin
• LET	Linear energy transfer
• MAC	Membrane attack complex
• MDSCs	Myeloid-derived suppressor cells
• MFI	Median fluorescence intensity
• MMP-2	Matrix Metalloproteinase-2
• NF-kB	Nuclear factor-kappa B
• NHEJ	Non-homologous end joining
• NK	Natural killer
• OER	Oxygen enhancement ratio

• PAMPs	pathogens-associated molecular patterns
• PBS	Phosphate-buffered saline
• PD1	Programmed cell death 1
• PD-L1	Programmed death-ligand 1
• PFA	Paraformaldehyde
• PHD	Prolyl 4-hydroxylase
• PTCOG	Particle therapy co-operative group
• RBE	Relative biological effectiveness
• ROS	Reactive oxygen species
• RPMI	Roswell park memorial institute medium
• SOBP	Spread-out Bragg peak
• SSC	Side scatter
• TAAs	Tumour-associated antigens
• TCR	T-cell receptor
• TLR4	Toll-like receptor 4
• TME	Tumor microenvironment
• TNF	Tumor necrosis factor

4. Introduction

4.1. Radiotherapy and Particle therapy

According to the World Health Organisation, in 2022, nearly 20 million new cancer cases were diagnosed, accompanied by 9.7 million cancer-related deaths, with a different geographical distribution worldwide. **(Figure 1a)**. Lifetime risk estimates indicate that approximately one in five men and women will develop cancer, while approximately one in nine men and one in twelve women will die from the disease (Bray et al. 2024).

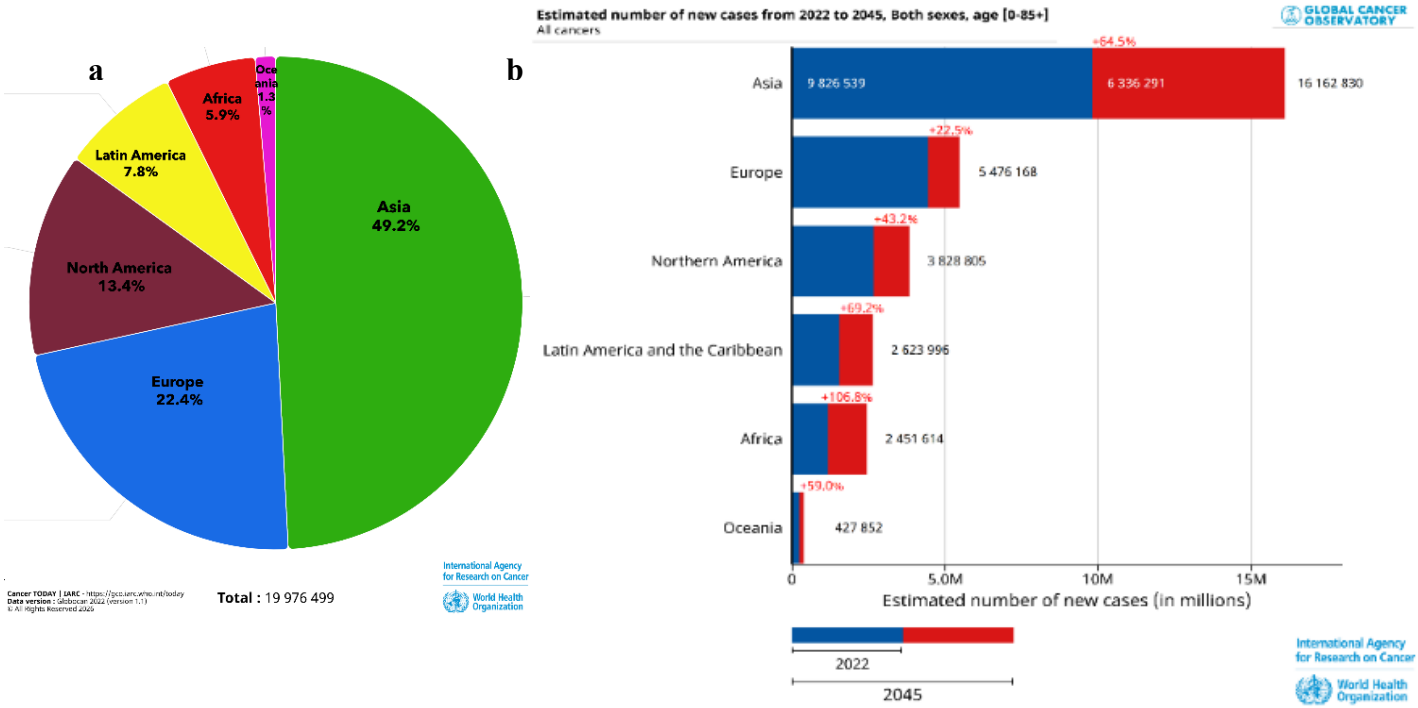

Figure 1: International Agency for Research on Cancer (IARC) of the global incidence and estimation of cancer cases

(a) Absolute numbers, Incidence, Both sexes, in 2022 in the different the continents (https://gco.iarc.fr/today/en/dataviz/pie)

(b) Estimated number of new cases from 2022 to 2045, Both sexes, age [0-85+] (https://gco.iarc.who.int/tomorrow/en/dataviz/bars)

Projections suggest that new cases will increase by 60% globally by 2050, compared with 2022 (**Figure 1b**), underscoring the importance of prevention strategies that target key risk factors to avert millions of diagnoses and yield substantial economic and societal benefits (Bray et al. 2024). Over recent decades, mortality rates have decreased due to advancements in treatments and improved tumour profiling (Durante, Orecchia, and Loeffler 2017).

Surgery and chemotherapy represent the frontline strategies for treatment, while radiotherapy has evolved from a primarily palliative modality, with nearly half of all cancer patients currently receiving it also for curative purposes (Orth et al. 2013). However, in parallel with advances in radiotherapy techniques, increased recognition of tumour radioresistance has driven the integration of particle therapy since the 1990s, especially for these radioresistant and inoperable tumours. This shift highlights the ongoing need to refine therapeutic strategies to enhance local tumour control and patient survival (Sengedorj et al. 2022). By the end of 2022, more than 350,000 patients had undergone particle therapy, according to the Particle Therapy Co-operative Group (PTCOG) database (https://www.ptcog.site)(Zink et al. 2024) (**Figure 2**).

One of the key drivers for the development and adoption of alternative modalities is the toxicity associated with photon-based radiotherapy to surrounding normal tissue. Refinements in imaging, planning, and delivery have enabled precise tumour targeting, expanding the therapeutic window (Reda et al. 2020). Building on these distinct interaction mechanisms, the concept of the "4 Rs of hadrontherapy indications" has been introduced to define the main clinical settings in which particle therapy provides therapeutic advantages: rare, radioresistant, recurrent, and radio-induced tumours (Vischioni et al. 2025). The following sections will explore each category in detail, illustrating how the biological rationale and clinical evidence support the use of particle therapy in these specific cases.

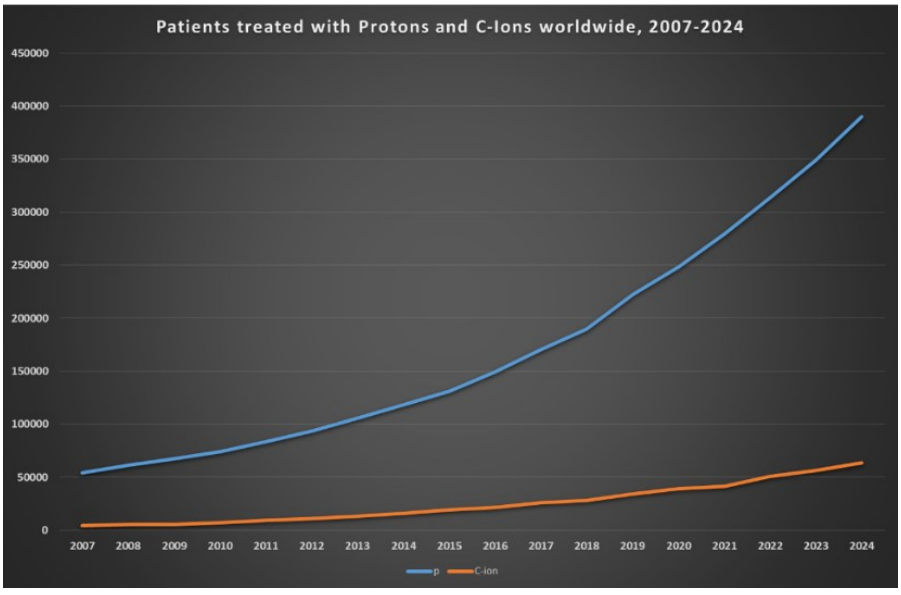

Figure 2: Worldwide number of patients treated with charged particles from 2007 to 2024

A steady increase is observed in the number of patients treated with proton therapy (p, blue) and carbon-ion therapy (C-ion, orange) worldwide. The graph was downloaded on 20 January 2026 from https://www.ptcog.site/index.php/patient-statistics.

Rare tumours, characterised by low incidence, complex anatomy, and frequent resistance to standard treatments, present significant challenges for delivering adequate doses with conventional photon radiotherapy. At the same time, particle therapy spares surrounding healthy tissues better than conventional photon radiotherapy (Loeffler and Durante 2013). Particle therapy provides dosimetric and radiobiological advantages that can improve local control and reduce side effects (Durante, Debus, and Loeffler 2021). Due to its physical and biological characteristics, particle therapy is commonly used to treat radioresistant tumours with reduced sensitivity to photon irradiation, tumour recurrence, radio-induced tumours, and paediatric tumours (Vischioni et al. 2025). Currently, treatments using particle therapy include head and neck, prostate, gynaecological, pancreatic, and liver cancers, chondrosarcomas and sarcomas (https://fondazionecnao.it/en/pathologies-than-can-be-treated).

4.1.1. Physical, Chemical, and Biological Bases of particle therapy

Particle therapy exploits the distinctive physical behaviour of charged particles as they traverse matter, particularly their characteristic inverse depth–dose distribution. Unlike photons, which deposit energy exponentially with depth and deliver a substantial exit dose, carbon ions exhibit a low entrance dose that progressively increases as the particles slow down, culminating in a sharp Bragg peak, followed by an abrupt distal dose fall-off (**Figure 3**) (Helm et al. 2021; Schardt, Elsässer, and Schulz-Ertner 2010). The initial particle energy primarily determines the position of the Bragg peak. It can be accurately modulated to coincide with the tumour depth, enabling highly conformal dose delivery while minimising irradiation of surrounding healthy tissues and organs at risk (Loeffler and Durante 2013). By superimposing multiple Bragg peaks of different energies, a spread-out Bragg peak (SOBP) can be generated to uniformly cover the tumour volume while preserving the favourable distal fall-off characteristic of heavy ions (Durante and Loeffler 2010).

In addition to their depth–dose advantages, carbon ions display reduced lateral scattering compared with photons, resulting in straighter trajectories and sharper lateral penumbrae. This improved spatial precision is particularly advantageous for the treatment of tumours located near critical structures or in anatomically complex regions (Graeff, Volz, and Durante 2023; Liu et al. 2024).

A central parameter governing the physical and chemical characteristics of carbon-ion irradiation is the linear energy transfer (LET), defined as the average energy deposited per unit path length by a charged particle:

$$\mathrm{LET} = -\frac{\mathrm{d}E}{\mathrm{d}x}$$

where $\mathrm{d}E$ is the differential energy loss over a distance $\mathrm{d}x$, typically expressed in keV/µm. As carbon ions traverse tissue, LET increases continuously as their velocity decreases, reaching its maximum in the proximity of the Bragg peak. This spatial variation in LET is a defining feature of heavy-ion beams and distinguishes them from low-LET photon radiation, in which energy deposition is relatively uniform along the beam path (Hall, Eric J. & Giaccia 2018.).

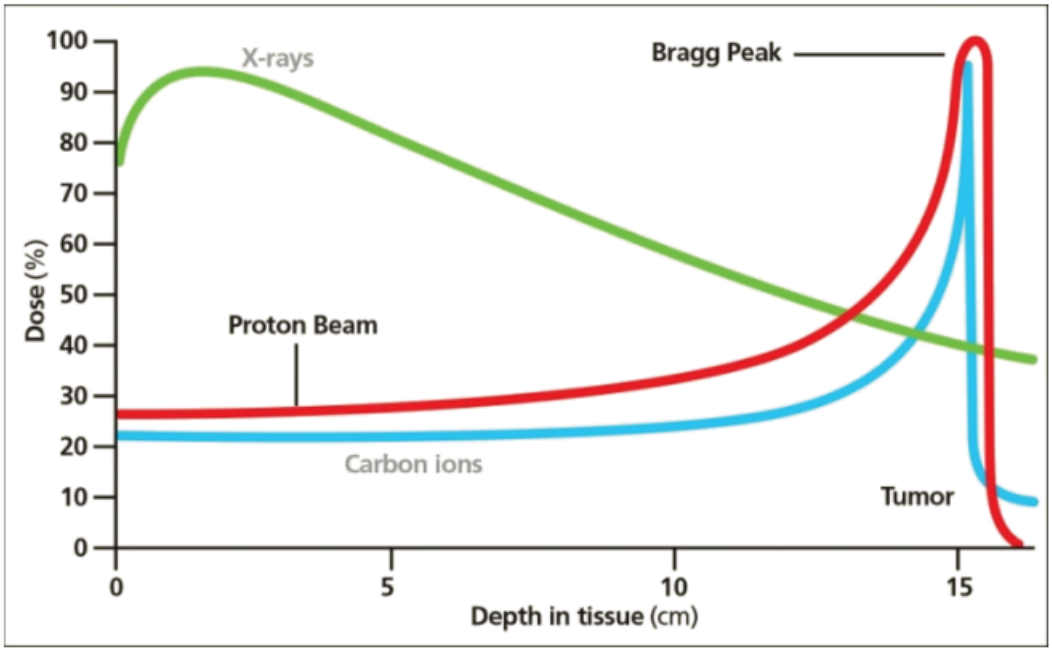

Figure 3: Relative dose as a function of depth in water for different types of radiation used in cancer therapy (B. Mustapha et al. 2020)

The rise in LET towards the end of the particle range reflects an increased frequency of ionisation events and a higher local density of energy deposition (Sokol and Durante 2023). This coupling between depth–dose and LET profiles provides a mechanistic basis for the increased effectiveness of carbon ions within the target volume. It also underlies their ability to overcome the limitations of conventional photon radiotherapy, particularly in hypoxic tumour regions where indirect, oxygen-mediated damage pathways are less dominant (Sokol and Durante 2023; Tinganelli and Durante 2020).

At the microscopic scale, the elevated LET of carbon ions leads to the formation of densely ionising tracks with complex spatial structure. During the physical phase of radiation interaction, occurring within femtoseconds to picoseconds, carbon ions generate closely spaced ionisations within nanometric volumes, in contrast to the sparse ionisation pattern produced by photons **(Figure 4)**. This track structure establishes the initial conditions for the subsequent chemical phase, which unfolds over picoseconds to microseconds and is dominated by water radiolysis (Camazzola et al. 2023).

With photon irradiation, the relatively low density of ionisations allows reactive species such as hydroxyl radicals to diffuse away from their site of origin, favouring indirect chemical interactions and inducing DNA damage mainly indirectly (Camazzola et al. 2023; Mohamad et al. 2017). In contrast, the dense ionisation tracks of high-LET carbon ions promote radical–radical recombination within the track core, limiting diffusion and creating highly localised regions of intense chemical reactivity (Sokol and Durante 2023; H. Wang et al. 2019).

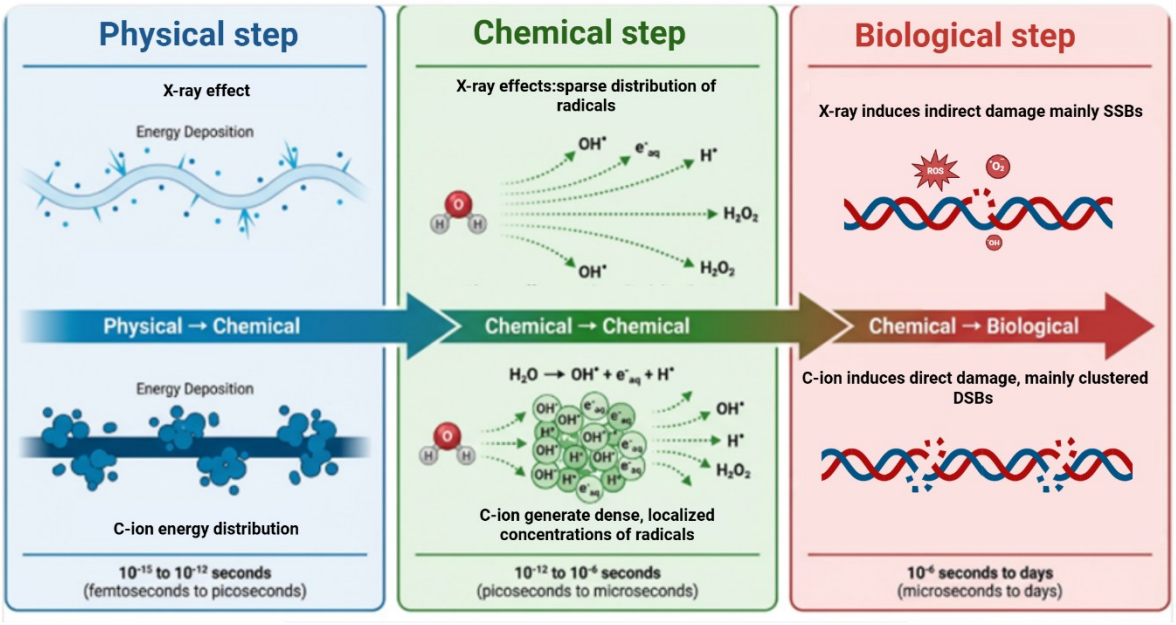

Figure 4: Particle therapy and radiotherapy phases along the time

Created in https://BioRender.com

This distinct chemical microenvironment, characterised by elevated local concentrations of radiolytic products within the track core, represents the crucial link between physical energy deposition and the subsequent biological lesions (section 4.1.2). While photon-induced damage relies predominantly on the indirect action of diffusing reactive oxygen species (ROS), leading to sparse, easily repairable DNA lesions, the dense ionisation tracks of carbon ions favour direct action

on the DNA sugar-phosphate backbone (H. Wang et al. 2019)(Baldacchino et al. 2019; Schardt, Elsässer, and Schulz-Ertner 2010).

Overall, the combination of a well-defined Bragg peak, reduced lateral scattering, and a depth-dependent increase in LET underpins the physical and chemical uniqueness of carbon-ion therapy (A. S. Wozny and Rodriguez-Lafrasse 2023). These features allow for precise dose localisation and generate radiation qualities that differ fundamentally from those of conventional photon beams, laying the foundation for the distinct radiobiological effects discussed in the following chapter (section 4.1.2.)

4.1.2. Biological effect of charged particle and Hallmarks of Particle therapy

The cascade of physical and chemical events initiated by irradiation ultimately manifests as a spectrum of biological consequences that determine therapeutic outcome. Following exposure, cells detect damage to the DNA and other cellular structures and activate checkpoint pathways that transiently arrest cell-cycle progression, to allow repair (Mohamad et al. 2017). While this response is often effective after low-LET photon irradiation, the increased complexity and spatial clustering of lesions induced by high-LET particle beams frequently compromise repair fidelity (Helm and Fournier 2023). In such cases, cells may fail to resume normal proliferation or may propagate unrepaired or misrepaired damage, increasing the probability of cell death through apoptosis, mitotic catastrophe, or permanent growth arrest in the form of senescence (Fournier et al. 2007). A central concept linking radiation quality to biological outcome is the relative biological effectiveness (RBE), defined as the ratio of the dose of a reference radiation (typically photons) to the dose of a test radiation, required to produce the same biological effect (Hall, Eric J. & Giaccia 2018), as expressed by the following formula:

$$RBE = \frac{Dose\ (ref)}{Dose\ (test)}$$

From a biological perspective, the high RBE values observed for carbon ions reflect the increased efficiency of high-LET radiation in converting physical energy deposition into lethal cellular damage. This enhanced effectiveness arises from the predominance of direct interactions and the formation of complex lesions that are intrinsically more challenging for tumour cells to process than the predominantly isolated, indirect damage induced by photons (Hall, Eric J. & Giaccia 2018; A. S. Wozny and Rodriguez-Lafrasse 2023).

To provide a comprehensive framework for these effects, the biological advantages of particle therapy can be conceptualised as a set of "Hallmarks of Particle Therapy" **(Figure 5)** that directly counteract the acquired capabilities of cancer cells defined by Hanahan and Weinberg (Hanahan 2022). These hallmarks include enhanced DNA damage complexity, a reduced oxygen enhancement ratio, cell death, angiogenesis, modulation of tumour microenvironment (TME) and the immune system, all contributing to superior tumour control.

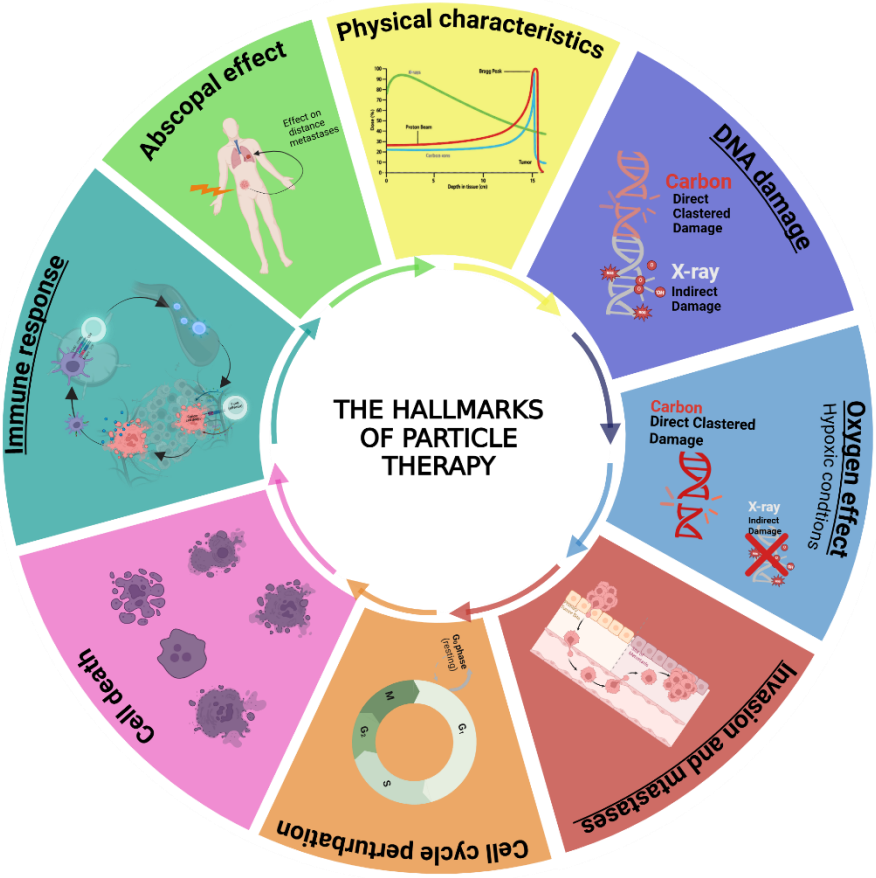

Figure 5: The hallmarks of particle therapy

The underlined topic are the ones that we will investigate.

Inspired by **(Hanahan 2022)** created in https://BioRender.com

Moreover, high-LET particle irradiation fundamentally alters the balance between damage induction and repair. Carbon ions cause tightly clustered DNA damage within very small volumes, making it difficult for the cell's repair machinery to process these lesions(Helm and Fournier 2023). As a result, tumour cells frequently enter mitosis with incompletely repaired chromosomes, leading to mitotic catastrophe and irreversible loss of clonogenic survival (Mohamad et al. 2017). Although some evidence suggests activation of alternative or compensatory repair pathways following high-LET exposure, the extent to which tumour cells can adapt to such damage remains an area of active investigation (Helm and Fournier 2023). These uncertainties highlight the biological complexity

underlying particle therapy responses. The biological advantages of particle therapy are particularly evident in radioresistant tumours, often associated with efficient DNA repair mechanisms, robust antioxidant defences, or hypoxic microenvironments that limit radical-mediated damage (Mohamad et al. 2017; Sokol and Durante 2023). Carbon ions partially overcome these resistance factors through their high-LET damage profile: direct energy deposition reduces oxygen dependence, complex lesion patterns saturate repair capacity, and dense ionisation limits the protective effects of cellular antioxidant systems. Consequently, tumour cell killing by carbon ions is less dependent on cell-cycle phase and microenvironmental oxygenation than photon-based radiotherapy (Tinganelli and Durante 2020).

Overall, the biological effectiveness of radiotherapy reflects a complex interplay among radiation quality, intrinsic tumour radiosensitivity, repair capacity, microenvironmental conditions such as hypoxia, and immune composition (Barker et al. 2015). By inducing qualitatively different biological responses compared with photons, high-LET particle therapy provides a mechanistic basis for improved control of resistant tumours and supports its role as a complementary modality within modern precision radiotherapy (Durante, Orecchia, and Loeffler 2017).

4.2. Tumour hypoxia and its impact on radiotherapy outcomes

The effectiveness of radiotherapy is strongly influenced by the tumour microenvironment, with hypoxia representing one of the main causes of resistance in tumour treatment (Sørensen and Horsman 2020). As solid tumours expand beyond a critical size, oxygen diffusion from surrounding normal tissue becomes insufficient, necessitating the formation of new blood vessels through angiogenesis. However, tumour-driven angiogenesis is typically disorganised and inefficient due to the rapid proliferation of cancer cells, resulting in the formation of abnormal vasculature characterised by irregular vessel morphology, incomplete endothelial linings, and unstable blood flow (Jain 2005). These structural abnormalities give rise to spatially and temporally heterogeneous regions of reduced oxygen tension, nutrient deprivation, and acidosis. Early histopathological evidence of such hypoxic niches was provided by Thomlinson and Gray (1955), who identified viable tumour cells surrounding necrotic cores in human lung carcinomas, highlighting hypoxia as an intrinsic feature of solid tumours (Thomlinson and Gray 1955).

Hypoxia has a dual influence on tumour cells. While temporary oxygen deprivation imposes metabolic stress and can limit cell proliferation, severe and chronic hypoxia promotes cellular adaptation and malignant progression (Lee et al. 2023). Under low-oxygen conditions (0.1-5%), tumour cells activate hypoxia-responsive signalling pathways that drive metabolic and proteomic

reprogramming, enhancing cell survival, invasion, and metastatic potential. These adaptations lead to genetic instability and attenuated apoptotic responses, allowing the selection and expansion of hypoxia-tolerant subpopulations and reinforcing a self-perpetuating cycle of hypoxia, tumour aggressiveness, and therapeutic resistance (Kunachowicz et al. 2025; Lee et al. 2023; Vaupel, Mayer, and Höckel 2004). Hypoxic responses have a time-dependent effect. Acute hypoxia, occurring within seconds to hours (<24 hours), rapidly impairs oxygen-dependent enzymes and induces immediate metabolic and protein homeostasis adjustments that support short-term survival (Lee et al. 2023; Vito, El-Sayes, and Mossman 2020). In contrast, chronic hypoxia develops after 24 hours to several days and is characterised by sustained transcriptional and chromatin remodelling, establishing stable programs that support altered metabolism, angiogenesis, stem-like properties, and long-term tolerance **(Figure 6)** (Quartieri et al. 2023).

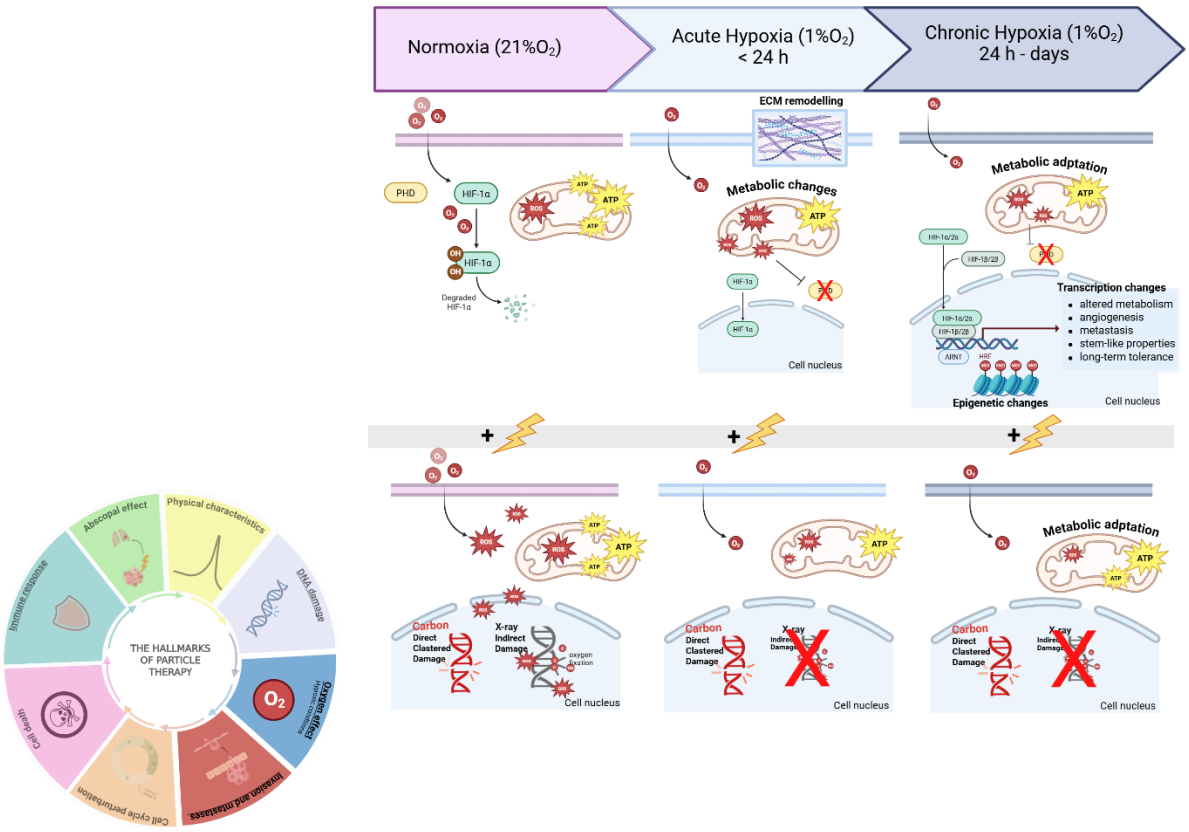

Figure 6: Influence of hypoxia in tumor cells and following irradiation

Graphical representation of radiation response in tumor environments. First raw: Temporal evolution of cellular phenotypes as a function of oxygen concentration. Second raw: Differential efficacy of X-ray and C-ion therapy in normoxic versus hypoxic environments, organised by oxygen tension and time. Created in https://BioRender.com

HIF-α is a key marker and regulator of hypoxic signalling. Under normoxia, it is ubiquitinated and degraded, whereas hypoxia inhibits PHD activity, triggering HIF-α stabilisation, nuclear translocation, and transcription of hypoxia-responsive genes that drive migration, extracellular matrix remodelling, immune evasion, and tumour progression (Vito, El-Sayes, and Mossman 2020).

From a radiobiological perspective, radioresistance is driven by hypoxia, particularly with low-LET radiation such as photons and protons. Low-LET modalities primarily induce DNA damage indirectly through the radiolysis of water, generating ROS that interact with DNA radicals. Under normal oxygen conditions (normoxia), molecular oxygen reacts with radiation-induced DNA radicals to form stable peroxyl adducts, effectively "fixing" the damage and preventing its restitution by cellular repair processes (H. Wang et al. 2019). This mechanism, known as the oxygen fixation hypothesis, renders DNA lesions chemically permanent and increases their biological lethality (Hall, Eric J. & Giaccia 2018). In hypoxic environments, the absence (or lower amount) of oxygen allows DNA radicals to be chemically restored by endogenous reducing agents, such as glutathione and thioredoxin, thereby increasing the probability of successful repair and cell survival.

The oxygen level, which is quantified by the oxygen enhancement ratio (OER), modulates radiation response It expresses the ratio of doses required to achieve the same biological effect under hypoxic and normoxic conditions.

$$OER = \frac{Dose\ (Hypoxia)}{Dose\ (Normoxia)}$$

For low-LET radiation, OER values typically range between 2.2 and 3, underscoring the substantial protective effect of hypoxia against photon-induced damage (Telarovic, Wenger, and Pruschy 2021; Tenforde et al. 1980; Williams 2019).

In contrast, the dense ionisation tracks of high-LET carbon ions promote direct DNA damage and complex lesions that are independent of oxygen-mediated chemical fixation, effectively neutralising the radioresistance of hypoxic tumour regions (OER for C-ion 1.9) (Sokol and Durante 2023; Tenforde et al. 1980; Tinganelli and Durante 2020). Preclinical and clinical evidence indicate that the relative biological effectiveness of carbon ions remains comparatively stable under hypoxic conditions, supporting their use in the treatment of tumours characterised by extensive hypoxia and intrinsic resistance to photon therapy (Sokol and Durante 2023; Tinganelli et al. 2015).

4.3. Migration capacity influenced by hypoxia and radiotherapy

Tumour cell migration is a dynamic, multistep process regulated by interactions with the TME. Cells utilise various migratory modes, individual (amoeboid or mesenchymal) or collective (clusters and chains), depending on their tissue of origin and local cues. Collective chain migration, observed in lobular breast carcinoma, ovarian cancer, and melanoma, represents a highly effective penetration mechanism linked to poor prognosis (Friedl and Wolf 2003). Conversely, individual amoeboid migration facilitates rapid movement through confined spaces, while mesenchymal migration depends on extracellular matrix (ECM) remodelling, typical for sarcomas and carcinomas (Enterline and Coman 1950). Crucially, tumour cells exhibit high migratory plasticity, switching modes in response to hypoxia, ECM composition, and therapeutic stress (Pourjafar and Tiwari 2024).

The epithelial–mesenchymal transition (EMT) is a central driver of this adaptability. Through EMT, epithelial cells reversibly acquire mesenchymal traits, characterised by what is known as the cadherin switch, by the downregulation of epithelial E-cadherin and the upregulation of mesenchymal cadherins such as N-cadherin. This switch weakens cell–cell adhesion while promoting increased motility, invasiveness, and enhanced interactions with the surrounding stroma. including enhanced motility, cytoskeletal reorganisation, and proteolysis (Loh et al. 2019; Thiery 2002). This phenotypic shift is intrinsically linked to stem-like features, metastatic competence, and resistance to therapy (Friedl and Wolf 2003). Ultimately, microenvironmental signals like paracrine communication and vesicle exchange converge to drive the invasive phenotypes responsible for local infiltration and systemic dissemination (Glaviano et al. 2025).

Hypoxia is a central but context-dependent regulator of migration, with its effects strongly influenced by oxygen availability. While hypoxia is a potent inducer of EMT through the activation of hypoxia-responsive transcriptional programs, its interplay with radiotherapy reveals a critical hallmark of particle therapy (Tinganelli and Durante 2020). Conventional photon radiotherapy has been shown to enhance cancer cell migration and invasion at clinically relevant doses (2–20 Gy) during the acute post-irradiation period (20–48 hours) (Hanley et al. 2023). This pro-migratory effect is driven by the uniform distribution of ROS throughout the cell, which activates signalling networks including EMT pathways (Snail, Twist), matrix metalloproteinases (MMP-2), integrin and cadherin expression and CXCR4/SDF-1 axes (Friedl and Wolf 2003, Eckert et al. 2018). However, photon-induced enhancement is significantly attenuated under hypoxic conditions (e.g., 1% O_2), likely because limited oxygen availability restricts the ROS-mediated signalling needed to trigger the migratory shift. Aggressive metastatic cell lines like HT1080 (fibrosarcoma) and T98G (glioblastoma) show robust photon-induced migration, while other lines like HCT116 (colon

cancer) exhibit dose-dependent suppression, indicating that pro-migratory responses are governed by cell-specific thresholds and intrinsic phenotypes (Goetze et al. 2009; A. Wozny et al. 2019).

In contrast, particle therapies, particularly carbon ions, consistently suppress migration and invasion and stemness in a dose-dependent manner across diverse cancer models (Barcellini et al. 2025). This suppression represents the unique biological hallmark of oxygen-independent anti-metastatic activity. Unlike photons, carbon ions concentrate high levels of ROS along narrow ion tracks, a localised distribution that fails to trigger pro-migratory signalling pathways. Mechanistically, carbon ion therapy prevents HIF-1α stabilisation and inhibits MMP-2 expression even under hypoxic conditions, whereas photon may activate these factors (A.-S. Wozny et al. 2019). This consistent effectiveness regardless of oxygenation status provides a strong mechanistic rationale for using particle therapy to target radioresistant, hypoxic tumour regions where metastatic potential is highest.

4.4. The role of the immune system in cancer and radiotherapy response

The immune system functions as a pivotal regulator in cancer development, eliciting a dual influence that can either suppress tumour growth or, conversely, promote its advancement. This multifaceted relationship is most effectively framed through the concept of the cancer immunity cycle **(Figure 7),** a dynamic and self-perpetuating sequence of immunological events necessary for a productive anti-tumour response (Chen and Mellman 2013). The cycle begins when neoantigens and tumour-associated antigens (TAAs), arising from somatic mutations during oncogenesis or emitted after genotoxic treatments, are released from dying malignant cells and subsequently internalised and processed by dendritic cells (DCs). For this priming phase to be effective, it needs to occur in an immunostimulatory milieu, often orchestrated by immunogenic cell death (ICD)(Galluzzi et al. 2017). ICD is defined by the spatiotemporally coordinated release and exposure of damage-associated molecular patterns (DAMPs), which confer the adjuvant signals required for effective immune recognition. Among the principal DAMPs, calreticulin (CRT) is exposed on the cell surface and acts as an "eat-me" signal to facilitate dendritic cell–mediated phagocytosis. Extracellular ATP serves as a "find-me" signal that attracts and activates antigen-presenting cells through purinergic receptors. Additionally, High-Mobility Group Box 1 (HMGB1) binds Toll-like receptor 4 (TLR4), thereby promoting optimal antigen processing and cross-presentation **(Figure 7A)** (Fucikova et al. 2021; Krysko et al. 2012). Collectively, these signals orchestrate a robust immunostimulatory context in which tumour-associated antigens are efficiently captured, processed, and presented, ultimately driving the priming and expansion of tumour-specific cytotoxic T lymphocytes (Galluzzi et al. 2023; Kepp and Kroemer 2023). Following antigen capture, mature dendritic cells (DCs) move to the draining lymph nodes, where they initiate and expand tumour-specific cytotoxic $CD8^+$ T lymphocytes. Once generated, these effector T cells must enter the circulation, extravasate into the tumour microenvironment (TME), and identify malignant cells through T-cell receptor (TCR) recognition, ultimately inducing cytolytic killing (Chen and Mellman 2013). This ordered interplay between immune cells and tumour is central to cancer immunoediting, which is conventionally divided into three phases: elimination, in which nascent transformed cells are detected and eradicated; equilibrium, during which residual malignant cells survive in a state of controlled dormancy; and escape, marked by uncontrolled tumour expansion and dissemination as immune surveillance becomes ineffective (Mittal et al. 2014). Tumours transition into the escape phase by disrupting multiple steps of this cycle, for example, by upregulating immune checkpoint molecules such as PD-1 and their ligands like PD-L1, thereby driving T-cell anergy or functional impairment **(Figure 7B)**. The TME itself contributes to immune resistance through components like

hypoxia, metabolic reprogramming, and stromal cells that hinder immune cell infiltration and activation (Tufail, Jiang, and Li 2025).

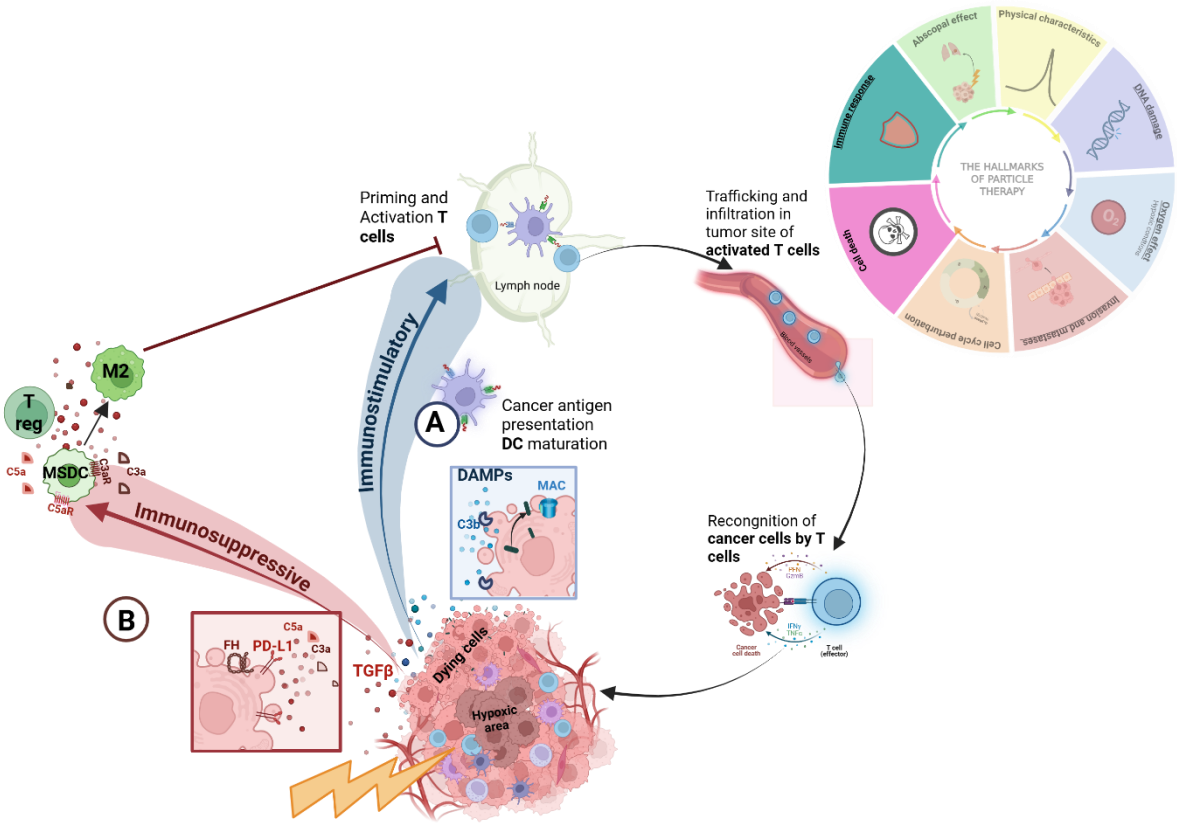

Figure 7: Cancer immunity cycle influenced by irradiation

Graphical overview of irradiation-induced immune modulation within the tumour microenvironment, illustrating the balance between immunostimulatory mechanisms (A) and immunosuppressive pathways (B). Inspired by **(Mellman et al. 2023)** Created in https://BioRender.com

While adaptive immune responses coordinate most anti-tumour effects, their efficacy is profoundly shaped by innate immune mechanisms. Among these, the complement system has emerged as a pivotal "master regulator" that integrates innate and adaptive immunity. Complement role in TME is tumour type dependent, can trigger cell killing, but also in promoting tumor growth (Magrini et al. 2021; Meri et al. 2023). The tumour-promoting pathway induced by complement activation emerged in the last decades and includes cell survival, proliferation, migration, epithelial-mesenchymal transition (EMT), and stemness, or indirect effects via immunosuppression or angiogenesis (Garlanda, Dambra, and Magrini 2025).

In this context, radiotherapy has emerged as a powerful modulator of tumour immunity, capable of reshaping several steps of the cancer immunity cycle. Beyond its direct cytotoxic effects, ionising radiation can enhance tumour immunogenicity (Demaria et al., 2005; Galluzzi et al., 2020).

However, the immunological consequences of radiotherapy are highly context-dependent and influenced by dose, fractionation, radiation quality, and the tumour microenvironment, underscoring the need to better understand how advanced modalities such as particle therapy may be leveraged to overcome immune resistance and improve therapeutic synergy with immunotherapy, that we explain more in details in following chapter 4.5 ((Durante et al., 2017; Formenti & Demaria, 2013).

4.4.1. Innate immunity and complement system in tumour microenvironment

The complement system is increasingly recognised as a multifaceted regulator within the intricate cancer-immunity cycle, extending its influence far beyond its classical role in host defence. As highlighted by Pio et al. in "Complementing the Cancer-Immunity Cycle" (Pio et al. 2019), this system wields a dual capacity, capable of either fostering robust anti-tumour immunity or establishing an immunosuppressive tumour microenvironment (Pio et al. 2019).

4.4.1.1. The complement cascade: activation and effector mechanisms

The complement system constitutes a complex cascade including more than 50 soluble and membrane-associated proteins, functioning as a primary effector of innate immunity and a vital link to adaptive immune responses (Pio, Ajona, and Lambris 2013; Sonderegger et al. 2023). Primarily produced in the liver but also synthesised locally by immune and stromal cells in tissues, these proteins exist in circulation as inactive zymogens activated via three primary pathways: classical, lectin, and alternative (Meri et al. 2023; Roumenina et al. 2019). Activation of the classical pathway occurs when the C1 complex binds to antigen-antibody complexes or danger-associated molecular patterns on compromised cells. The lectin pathway is activated by mannose-binding lectin or ficolin, DAMPs or PAMPs (pathogen-associated molecular patterns), recognising carbohydrate structures on microbial surfaces or altered host cells (**Figure 8**). In contrast, the alternative pathway maintains low-level constitutive activity via spontaneous C3 hydrolysis, acting as a monitoring system that intensifies on surfaces deficient in regulatory proteins (Artero et al. 2025).

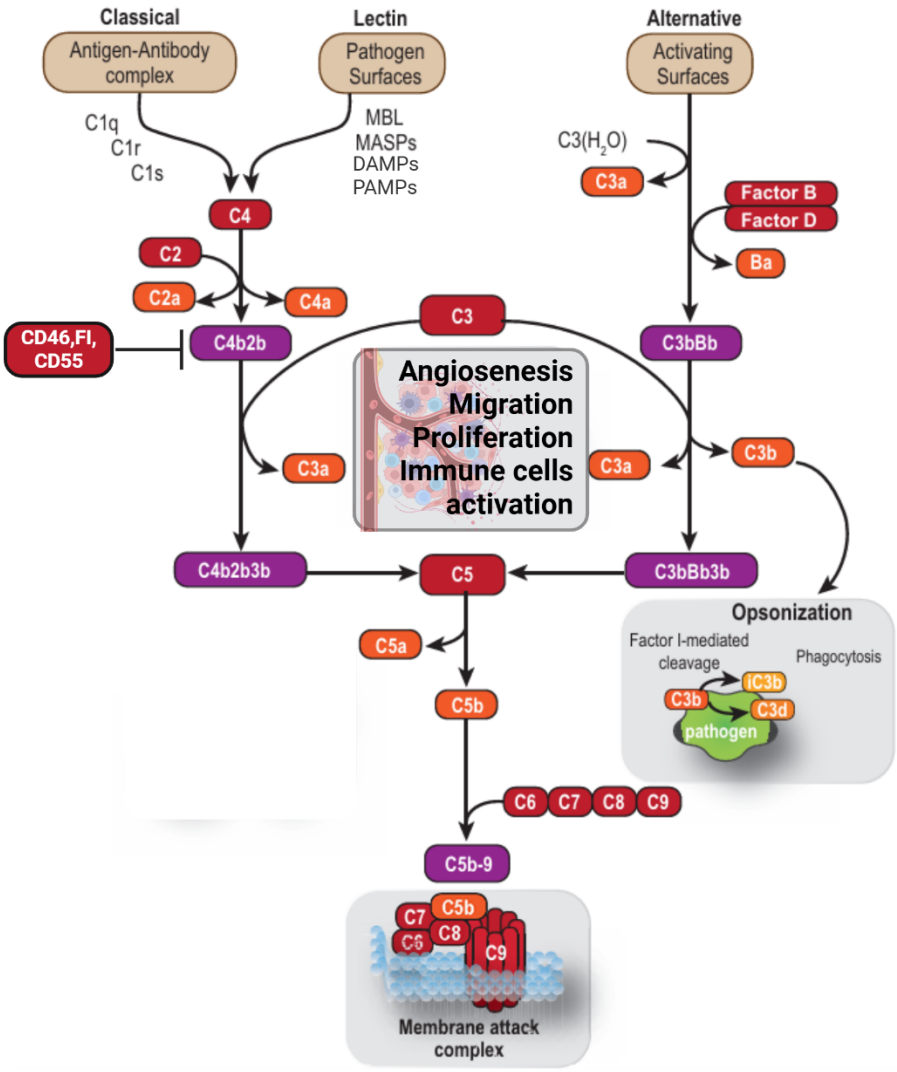

Figure 8: Complement system cascade

Modified from **(Sonderegger et al. 2023)** with https://BioRender.com

Regardless of the initiating stimulus, convergence occurs at C3 convertases, which proteolytically process the pivotal C3 protein into the anaphylatoxin C3a and opsonin C3b. Surface-bound C3b propagation forms C5 convertases that cleave C5, yielding the proinflammatory mediator C5a and the C5b fragment (Sonderegger et al. 2023). The latter triggers the formation of the membrane attack complex, a lytic pore that embeds in target membranes, provoking osmotic lysis and cytotoxicity. The anaphylatoxins C3a and C5a mobilise and stimulate immune cells, fostering inflammation and modulating adaptive immunity by engaging C3aR and C5aR receptors. Host tissue protection is ensured by diverse soluble and membrane regulators that suppress convertase activity or MAC (membrane attack complex) formation (Morgan 2016). Recent discoveries have further highlighted the capacity for intracellular complement activation, a non-canonical mechanism independent of the

established cascade, which significantly expands the functional repertoire of complement proteins within the cellular milieu (Garlanda, Dambra, and Magrini 2025; West and Kemper 2023).

4.4.1.2. Complement system in tumour microenvironment

As mentioned in section 4.4 , the complement system can trigger dual and opposite outcomes in TME: anti-tumour responses and tumour progression. On one hand, complement components can orchestrate potent anti-tumour responses (Revel et al. 2020). For instance, C3b opsonisation of tumour cells serves as an "eat-me" signal, significantly augmenting antibody-dependent phagocytosis by macrophages and dendritic cells. This enhances antigen presentation and triggers the activation of cytotoxic T lymphocytes, leading to effective antitumour immunity **(Figure 7 (A))** (Pio et al. 2019).

However, the complement system can also be co-opted by tumours to promote progression and to evade immune surveillance (fibrosarcoma (Magrini et al. 2021)), melanoma (Y. Wang et al. 2016), breast cancer (Vadrevu et al. 2014), colon carcinoma (Downs-Canner et al. 2016), lung cancer (Ajona et al. 2017)). Central to this pro-tumourigenic role, the anaphylatoxins C3a and C5a drive inflammation and tumour growth through mechanisms such as chemotaxis, ROS production, enhanced vascular permeability, and direct stimulation of cell proliferation and metastasis (Jeon et al. 2018; O'Brien et al. 2021). These components shift immunity towards a suboptimal T helper cell Th2 phenotype (Kolev et al. 2022) and are instrumental in recruiting and polarising tumour-associated macrophages towards an M2-like protumour state (Artero et al. 2025), which actively suppresses cytotoxic T-cell infiltration and activity. Similarly, C5a is known to recruit myeloid-derived suppressor cells that impair the effectiveness of antitumour CD8+ T-cell responses **(Figure 7 (B))** (O'Brien, Lynam-Lennon, and Olcina 2023). Adding another layer of complexity, tumour cells can themselves engage in intracellular complement activation, a non-canonical mechanism where they synthesise and process C3 internally (King and Blom 2023; Kolev et al. 2022). The secreted C3a from this process can then bind to C3a receptors on TAMs in the tumour microenvironment, activating the PI3Kγ pathway and further reprogramming these macrophages into an immunosuppressive M2 state (Roumenina et al. 2019). Tumours further develop evasion strategies by upregulating complement inhibitors like Factor H and CD46, which convert immunostimulatory C3b into iC3b, thereby conveying tolerogenic "super-self" signals to myeloid cells (Roumenina et al. 2019). Notably, hypoxia represents a critical contextual factor of TME that can also influence and complement activity toward its pro-tumourigenic functions within the tumour microenvironment. Hypoxia-inducible signalling has been shown to enhance the expression of complement components and anaphylatoxin receptors, including C3, C3aR, and C5aR, thereby

reinforcing C3a- and C5a-mediated immunosuppressive signalling (Monica M Olcina 2019). Through this mechanism, hypoxic tumour regions preferentially sustain complement-driven inflammation and immune evasion, further limiting effective anti-tumour immune surveillance. This context-dependent duality underscores the pivotal role of complement as a master regulator that can either suppress or promote tumour development (Yang, Fu, and Liao 2025).

4.4.1.2.1. Intracellular complement activation: *the complosome*

Challenging the conventional perspective of complement as an extracellular serum-mediated process, the "complosome" denotes an intracellular complement apparatus wherein proteins such as C3 and C5 function within cells to govern essential homeostatic functions, including metabolism and cell viability (Kolev et al. 2022). Originally identified in T lymphocytes, where intracellular C3a signalling supports homeostasis and Th1 (T helper cells) differentiation, this atypical activation significantly influences tumour advancement and immune escape. Tumour cells independently synthesise and process C3 intracellularly, frequently through alternative proteinases like cathepsin L, yielding active fragments such as C3a (Ding et al. 2022; O'Brien, Lynam-Lennon, and Olcina 2023). The real role of intracellular complement is still not fully clear, but it was demonstrated in recent studies that intracellularly produced C3 acts as an autocrine signalling hub in tumour cells, supporting cell survival, proliferation, and metabolic fitness (Bennion, Lysaght, and Lynam-Lennon 2026; Zha et al. 2019). Tumour-derived C3 can be cleaved intracellularly and activate downstream signalling pathways (e.g., mTOR, NF-κB), independent of serum complement. This intracellular complement system promotes resistance to stress, apoptosis, and therapies. It also contributes to immune evasion by shaping inflammatory and immunosuppressive signalling programs. Thus, intracellular C3 is not merely an immune protein but a core regulator of tumour cell biology (Zha et al. 2019).

4.5. Particle therapy and advantages in combination treatment

Over the past 25 years, our understanding of the hallmarks of cancer has expanded, showing that tumours are dynamic system that evolve traits driving proliferation, aggressiveness, and therapeutic resistance. Traditional pillars of cancer treatment, surgery, radiotherapy, and systemic therapies (including chemotherapy, targeted therapy, and immunotherapy), target tumours through different mechanisms, but none alone is sufficient for long-lasting control in many patients (Hanahan 2022). Although surgery, radiotherapy, and systemic therapies remain the backbone of cancer treatment, durable tumour control often requires rational combination strategies. In this context, there has been growing interest in the immunological effects of radiotherapy, particularly in combination with immune checkpoint inhibitors, which have shown promising synergistic activity in recent clinical and preclinical studies (Formenti and Demaria 2013; Li et al. 2023). The immunogenicity of the radiation response is primarily governed by two factors: antigenicity, driven by the generation of neoantigens, and adjuvanticity, mediated by the release of danger-associated molecular patterns during cell death and stress responses (Wennerberg et al. 2017). These properties likely enhance immunogenic cell death, enabling particle therapy to more efficiently convert immunologically "cold" tumours into "hot" tumours (Demaria, Coleman, and Formenti 2016). Carbon ion radiotherapy may further bias this balance towards immunostimulants due to its high linear energy transfer and unique DNA damage signatures (Formenti and Demaria 2013; Totis et al. 2025). Consistently, preclinical studies have shown that carbon ion therapy combined with immune checkpoint inhibitors, such as anti-PD-1 and anti-CTLA-4, achieves superior abscopal effects and reduces metastatic burden compared to conventional radiotherapy (Helm et al. 2021).

Radiotherapy profoundly reshapes tumour–immune interactions through mechanisms centred on immunogenic cell death and complement activation, generating responses that can either stimulate or suppress antitumour immunity (Charpentier et al., 2022). The radiation-induced inflammatory response resets tumour–immune crosstalk, with the outcome determined by the balance between immunostimulatory pathways that promote antigen presentation and T-cell activation, and immunosuppressive mechanisms that limit tumour rejection (De Martino, Daviaud, and Vanpouille-Box 2021).

The complement system exemplifies this duality. While it contributes to antitumour immunity, it also plays a key role in the non-inflammatory clearance of apoptotic cells, a process that can promote immune tolerance (Elvington et al., 2014). Experimental evidence indicates that tumour-targeted modulation of complement activity can shift this balance toward inflammation, enhancing dendritic cell maturation and T-cell activation (Elvington et al. 2014; O'Brien et al. 2021).

Finally, the success of these strategies critically depends on the temporal coordination of radiotherapy, immunogenic cell death, complement activation, and TME composition. The timing and sequence of interventions determine whether radiation-induced immune responses evolve towards durable immune activation or towards compensatory immunosuppression, a process strongly influenced by tumour biology and the tumour microenvironment (De Martino et al., 2021; Charpentier et al., 2022). The integration of complement modulation with radiotherapy, particularly advanced modalities like carbon ion therapy, represents a transformative frontier in precision oncology. In clinical practice, the primary objective of such combinations is to disrupt the pro-tumor homeostasis of the microenvironment by strategically inhibiting specific complement components.

5. Aim of the thesis

C-ion irradiation exhibits higher efficacy than conventional X-rays in reducing cell survival and suppressing migratory capacity, particularly within the radioresistant context of hypoxic tumors. While the interplay between conventional radiotherapy and the adaptive immune system is well documented, emerging evidence suggests that C-ion irradiation may possess superior immunogenicity supporting its potential as a promising partner for combinatorial treatment strategies (Helm et al. 2021). Increasing studies show the importance of innate immunity in tumor microenvironment, highlighting the pivotal role of complement system. Sarcomas, such as fibrosarcoma, present a critical clinical challenge due to their mesenchymal origin, anatomical complexity, and intrinsic or microenvironment-mediated radioresistance (Sbaraglia, Bellan, and Dei Tos 2021, Baumann et al. 2016). These tumors frequently exhibit hypoxic and immunosuppressive TMEs that may be selectively modulated by the high-LET properties of carbon ions. This provides a strong biological rationale for investigating C-ion-induced immune modulation in sarcoma models.

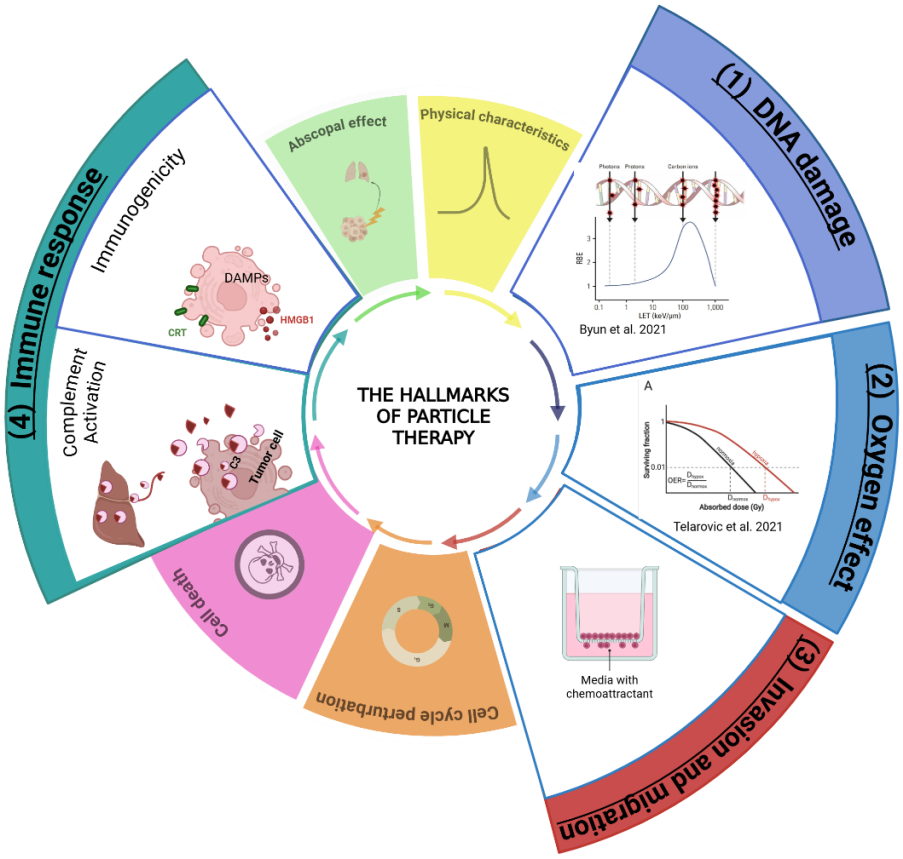

Figure 9: Aims of the thesis highlighted in the hallmarks of particle therapy

Schematic overview of the main topics in particle radiobiology, with those investigated in this work highlighted in white: (1) cell survival related to DNA damage, (2) oxygen effect and hypoxia in radiation response, (3) post-

irradiation invasion and migration, and (4) immune response, including immunogenic cell death and complement activation. Inspired by **(Hanahan 2022)** created in https://BioRender.com

A central component of this research involves the first radiobiological characterisation of the MN/MCA1 fibrosarcoma model following X-ray and C-ion irradiation **(Figure 9 (1-3))**, highlighting the central role of hypoxia in a representative tumour cell line **(Figure 9 (2))**. Following an initial investigation into C-ion immunogenicity, this thesis subsequently focuses on the activation of the complement system **(Figure 9 (4))**. Despite its importance, the relationship between radiation and complement signalling remains poorly understood and often contradictory, likely due to tumour-specific contexts and the bifunctional nature of the cascade. This work seeks to bridge these gaps by investigating the capacity of carbon ions to trigger complement activation within the MN/MCA1 cell line. We build upon the recent discovery that some immune and tumour cells are capable of local complement production, though the functional role of this "complosome" remains unclear. These *in vitro* findings are essential for clarifying the mechanistic role of the complement system following radiation treatment, an area that remains poorly understood and highly tumour-specific, with the future goal to investigate whether the combination of particle therapy and modulation of the complement system can have a synergic effect.

6. Materials and Methods

6.1. Biological materials and models

6.1.1. *In vitro* model: thawing, passaging, cryopreservation of cell lines

The MN/MCA1 fibrosarcoma cell line, provided by collaborators from Humanitas University in Milan, was used for the *in vitro* experiments described in this study. This cell line was originally isolated in 1978 from a 3-methylcholanthrene (3-MCA)-induced tumour in a C57BL/6 mouse at the Research and Pharmacological Institute "Mario Negri" in Milan. It was the only member of a series of similarly induced tumours that developed spontaneous metastases to the lungs (Giavazzi et al. 1980). Cells were cultured under two conditions, normoxia and hypoxia, with hypoxic cells maintained using the InvivO2 manipulator. For both conditions, a new vial of cells was thawed two weeks before the experiment. The vial was briefly removed from liquid nitrogen, slightly opened to allow degassing, and then rapidly thawed in a 37°C water bath. Afterwards, the content was transferred dropwise into a 50 mL Falcon tube containing complete Roswell Park Memorial Institute medium (RPMI-1640) (10% Fetal Bovine Serum (FBS), 1% Penicillin-Streptavidin) at room temperature. To remove DMSO, cells were centrifuged for 5 minutes at 1500 rpm, resuspended in 15 mL of complete RPMI, and plated in a T75 flask. Upon reaching 80-90% confluence, cells were split into a new T75 flask (75 cm^2 growth area), typically twice per week, following the protocol outlined below. After microscopic examination, the medium was removed, and a wash with PBS-/- (Sigma-Aldrich®) was performed. Cells were incubated with Accutase (Sigma-Aldrich®) for 4 minutes at 37°C. Accutase was inactivated by adding at least 3 volumes of complete medium, and the cell suspension was gently pipetted to disaggregate the cells. To seed the appropriate number of cells into a new T75 flask, cells were counted using Trypan Blue (1:1) and an automated cell counter (Bio-Rad Laboratories Inc.) (range: 6-23 µm), then incubated at 37°C, 5% CO_2, and 21% O_2. After one week of thawing, hypoxic cells were transferred to a hypoxic manipulator and maintained for at least one week at 37°C, 5% CO_2, 1% O_2, and 70% relative humidity. Cell passage procedures were identical for both conditions and performed in a standard flow box. However, due to the slower proliferation rate of hypoxic cells, the number of cells seeded was adjusted accordingly. To maintain an appropriate number of viable cells at low passage and to minimize potential mutations during passaging and freeze-thaw cycles, a frozen cell stock was prepared between passages 2 and 6. A total of 2×10^6 cells were frozen per vial in a mixture of 90% FBS and 10% DMSO, to reach a final volume of 1.8 ml. For gradual freezing, cells were stored at -80°C for 24 hours, then transferred to liquid nitrogen for long-term storage. The experiments are performed following the scheme in **Figure 10.**

For some experiments we used as comparison also the mammary carcinoma 4T1 cells (viability and C3b deposition) were purchased from ATCC® (CRL-2539TM) and melanoma B16-F10 cells (C3b deposition) purchased from ATCC® (CRL-6475TM) cultured in RPMI-1640.

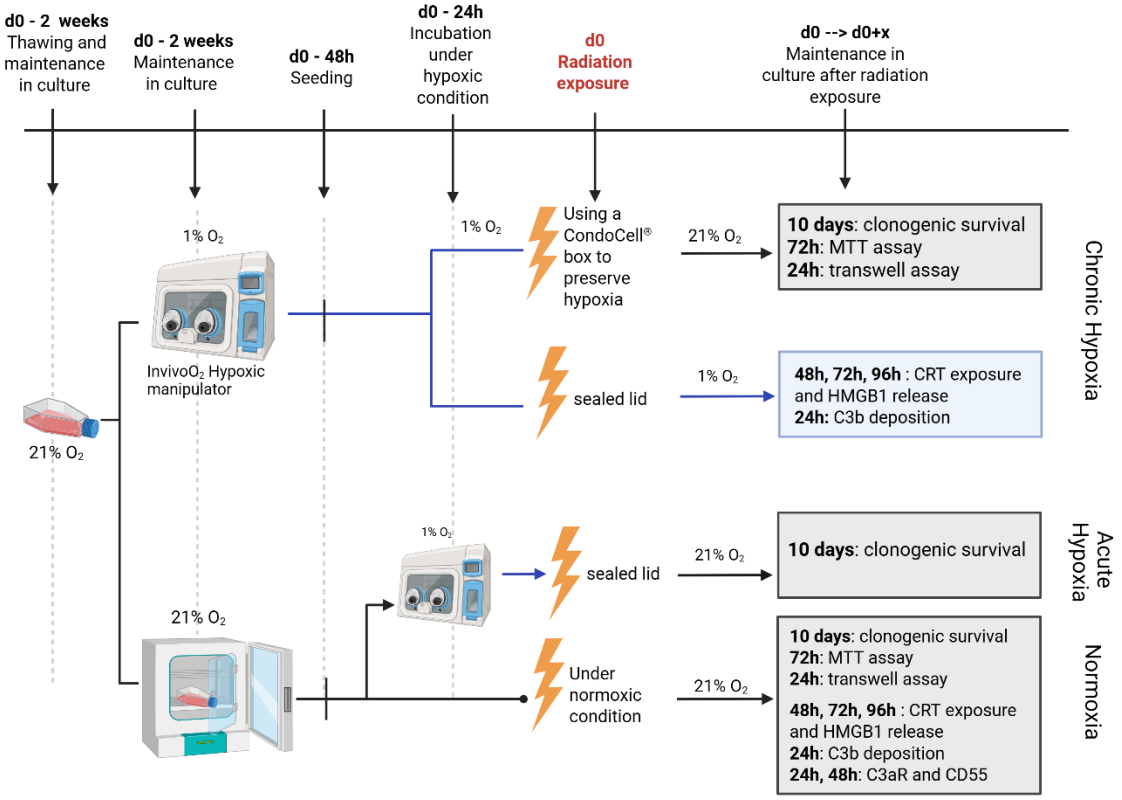

Figure 10: Schematic representation of the experiments' workflow, in normoxic and hypoxic conditions

The timeline (left to right) illustrates the main experimental steps, from cell thawing to the day of the experiment, with Day 0 defined as the day of irradiation. Black lines indicate periods of cell culture under normoxic conditions, whereas blue lines denote periods of hypoxic culture. Experiments were performed in biological replicates. Figure created with BioRender.com

6.1.2. *In vivo* mouse model: housing, cell injection and tumour growth

All animal experiments were conducted in accordance with the institutional guidelines and regulations of the local animal care committee and approved by the Regierungspräsidium Darmstadt. Female, 9-week-old C57BL/6 mice wt and $C3^{-/-}$ (obtained from Charles River Laboratories) were used for the study.

Animals were housed under specific pathogen-free (SPF) condition in individually ventilated cages (IVC). The IVC system ensured a regulated environment, with air changes per hour (ACH), constant temperature (22±1°C), and humidity (55 ± 10%). A controlled 12-hour light/dark cycle was maintained, and the mice had unrestricted access to food and water. The cages, along with the bedding and enrichment, were changed once per week.

After one week of acclimatisation, 0.5 x 10^6 MN/MCA1 cells resuspended in 20 µl of $PBS^{-/-}$ were injected subcutaneously into the mice's limb. Data were shown as tumour incidence and tumour volume, measured with a calliper, calculated according to the formula: Volume = (D×d2)/2, where D = larger tumour diameter and d = smaller tumour diameter (**Figure 11**).

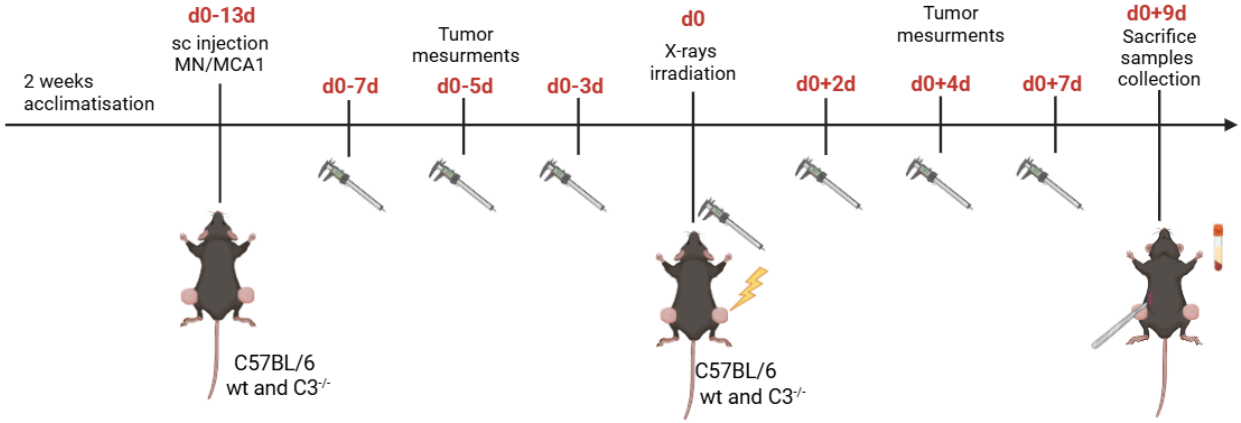

Figure 11: Experimental set up of *in vivo* experiments

Timeline of *in vivo* experiment from cells inoculation to sacrifice. We considered Day 0 the day of the irradiation, all the other steps were considered starting from day 0. The periodic tumour measurements were graphically reparented with the calliper.

6.2. Irradiation

6.2.1. *In vitro* irradiation

For *in vitro* experiments, the cells were irradiated with different radiation qualities and in different facilities. We aimed to maintain consistent irradiation parameters and repeated certain experiments to ensure that differences in the irradiation set up did not influence the results.

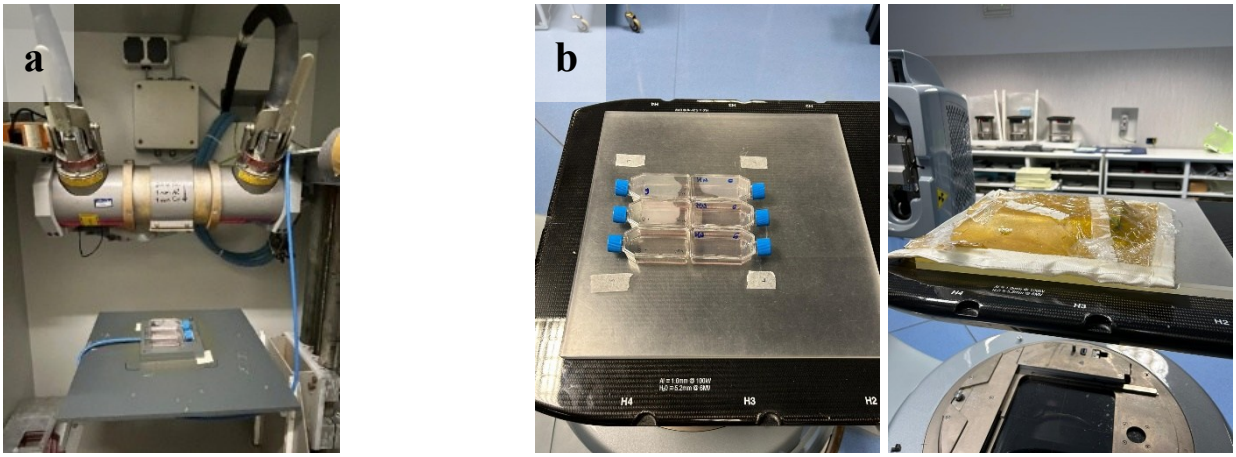

Figure 12: Experimental set up for X-ray irradiation at GSI (Darmstadt) and at Istituti Clinici Scientifici Maugeri (Pavia)

(a) X-ray generator Isovolt DS1 at Gesellschaft fuer Schwerionenforschung GSI, Helmholtz Center for Heavy Ion Research GmbH, Darmstadt, Germany, with 2 T25 flask positioned and ready to be irradiated. (b) Samples (6 T25) positioned on the patients' treatment couch and cover with water equivalent bolus (yellow phots on the right) and ready to be irradiated with Linear accelerator at Radiation Oncology Department of Istituti Clinici Scientifici Maugeri (Pavia, Italy).

Cells were seeded in 25 cm^2 tissue culture flasks 48h before the irradiation except for the clonogenic survival and migration assays, in which the cells were seeded 72h before treatment. For X-ray irradiation, two flasks were placed horizontally in the irradiation cabinet (X-ray generator Isovolt DS1, 7 mm beryllium, 1 mm aluminium, and 1 mm copper filter system, at 250 kV/16 mA, dose rate 2 Gy/min at the *Gesellschaft fuer Schwerionenforschung* GSI, Helmholtz Center for Heavy Ion Research GmbH, Darmstadt, Germany) **(Figure 12a).** Some X-ray irradiations were also performed at Radiation Oncology Department of Istituti Clinici Scientifici Maugeri (Pavia, Italy), using 6 MV linear accelerator (LINAC), where we placed a maximum of 6 flasks per irradiation session, on a 1.5 cm plexiglass platform within the homogeneity region of a 20 × 20 cm^2 irradiation field and covered with a 1 cm thick water-equivalent bolus, to maintain electronic equilibrium. The photon beam was delivered from below, at an angle of 180° (**Figure 12b).**

C-ion irradiation ($^{12}C^{+6}$) was performed at the National Center for Oncological Hadrontherapy (CNAO) in Pavia (Rossi 2015), Italy and at the Marburger Ionenstrahl-Therapiezentrum (MIT, Marburg Ion Beam Therapy Center, Marburg, Germany, MIT-2022-03) with doses between 0.5 Gy and 10 Gy. In CNAO, cells were irradiated in T25 flasks using a fixed horizontal clinical beamline and an active scanning dose delivery technique. A spread-out Bragg peak (SOBP) was optimized to achieve a homogenous physical dose level across the target region by modulating an energy range of 220-240 MeV/u. The flasks were positioned at the centre of the 4 cm modulated region of the SOBP with a mean dose averaged LET of 75 keV/ µm inside a water phantom, with the entrance window aligned at the room's isocentre. **Figure 13** shows an example of the experimental setup and positioning of the samples for the irradiation in a patient treatment room in CNAO (Italy). For the irradiation at the MIT facility ((Zink et al. 2024), for a technical overview of the facility), 4 x 10^5 cells were seeded in 75 cm2 tissue culture flasks 72 hours before irradiation. On the day of irradiation, cells were harvested in a 50 mL tube and counted using 10 µL of cell suspension (range 7-28 µm). 7 x 10^6 cells were transferred into a new 15- or 50-mL tube and centrifuged for 5 minutes at 300 x g at room temperature. Afterwards, the cell pellet was resuspended in 5 mL of supplemented medium and transferred into a 5 mL cryovial. Irradiation was performed with an energy range of 220-240 MeV/u (active energy scanning, mean dose averaged LET of 75 keV/µm; 4 cm SOBP).

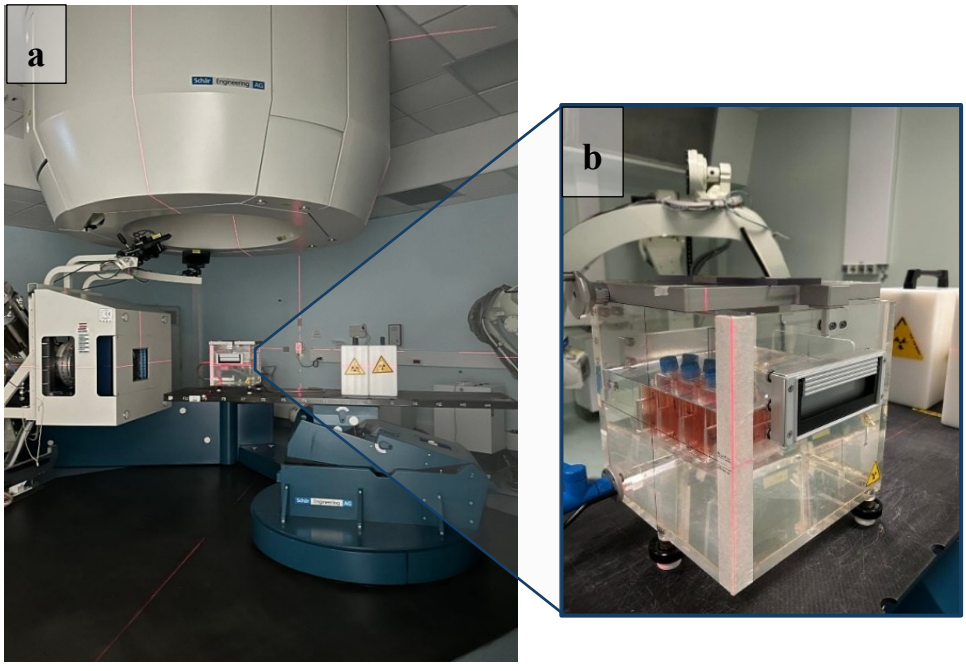

Figure 13: Set up carbon ion irradiation in the patient treatment room at CNAO

(a) Treatment room in CNAO. From the left of the picture, we have the nozzle and the beam window. The water phantom inside our samples is positioned on the patient's couch, aligned with 3 lasers. (b) Image showing a magnified view of the water phantom with the positioned samples. Specifically, six T25 flasks were arranged along two parallel lines, with the cell-seeded surfaces oriented toward the centre (back-to-back configuration).

Sedimentation of the cells at the bottom of the cryovials (which could lead to the formation of a oxygen heterogeneous environment) was avoided by mixing the tubes every 20 minutes. Immediately after irradiation and transportation, the cells were seeded in 25 cm2 tissue culture flasks.

6.2.2. *In vivo* irradiation

When the tumours reached visible dimensions (day 13 after injection) we irradiated the mice with X-rays **(Figure 14a).** Photon irradiation was performed with the SARRP machine, irradiating two mice for each shot, under constant isoflurane anaesthesia. An initial computed tomography (CT) scan was used to determine the isocentre and to precisely set the beam on the tumour **(Figure 14b).** Immediately after irradiation, mice were placed in a separate cage, in a warm environment (using a red warm-up lamp) until they recovered from anaesthesia.

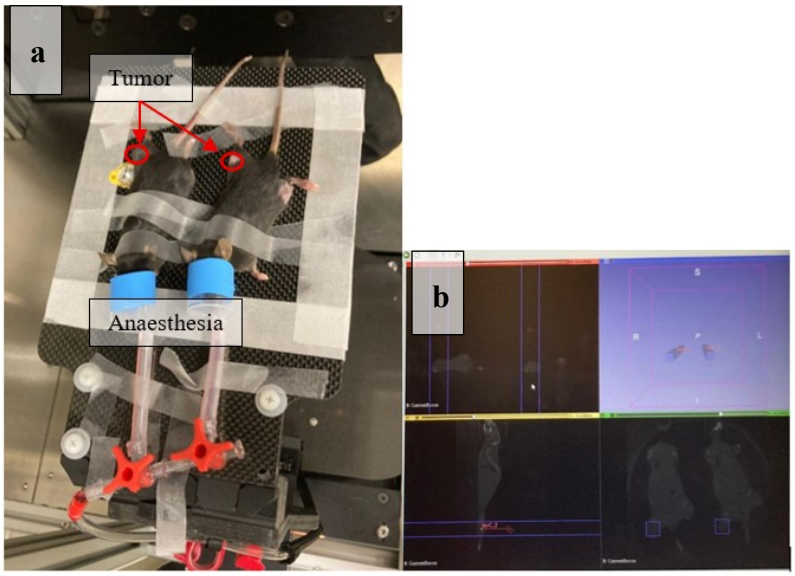

Figure 14: Irradiation set up for the *in vivo* experiment

(a) Mice positioning on the small couch and stabilised with tape. The tumour on the limb is circled in red and the anaesthesia set up is highlighted. (b) The SARRP system software was used to control mouse positioning through CT imaging and to define and configure the irradiation beams.

6.3. Experimental set up and protocol

6.3.1. Growth curve

Cells were seeded in a 25cm^2 culture flask and cultured at 37°C at 21%O_2 or 1%O_2. To evaluate the growth of the cells, one flask, for each biological replicate, was detached every day and the cell suspension was counted with Trypan Blue 1:1. The cell count was normalised on the cell-seeded and plotted using GraphPad Prism software.

6.3.2. Clonogenic survival assay

The clonogenic survival was performed under normoxic and hypoxic conditions, following X-ray and C-ion irradiations. The cells were cultured as described above **(6.1.1)** at 21%O_2 or 1% O_2 conditions for two weeks. Cells were seeded 72h before irradiation, and, immediately after treatment, were harvested counted and plated in a new 25 cm2 tissue culture flasks at appropriate densities calculated to allow the formation of 100 colonies, using the formula:

$$Volume\ (\mu L) = \frac{1000 * 100}{cell\ number * expected\ survival * PE}$$

PE (plating efficiency): number of colonies obtained relative to the total number of cells seeded;
1000: for the conversion into µL;
100: number of colonies/flasks needed in the end

For re-seeding, three technical replicates were performed for each dose, and the experiment was repeated at least three times in order to have three biological replicates. Both normoxic and hypoxic cells were incubated for 10 days at 21%O_2 , 37°C, 5% CO_2. Afterwards, the cells were fixed and stained with methylene blue solution or a combination of May-Grunwald/Giemsa.

Colonies containing at least 50 cells were counted by eyes or with a microscope and the survival fraction (SF) was defined by the formula:

$$Survival\ fraction\ (SF) = \frac{n°colonies\ (more\ than\ 50\ cells)}{n°\ of\ cells\ you\ re-seeded}$$

The obtained survival fractions were fitted using the Linear-Quadratic (LQ) model using GraphPad Prism software:

$$Y = C \cdot e^{-(\alpha \cdot X + \beta \cdot X^2)}$$

Y = fraction of cells surviving, X = dose of irradiation, C = is a normalization factor introduced to account for variability in plating efficiency and experimental conditions, allowing adjustment of the

surviving fraction at zero dose, α = coefficient for linear killing/ single DNA damage, β = coefficient for quadratic killing/ double DNA damage.

The RBE was calculated at 10% survival with the formula: $RBE = \frac{Dose\ (X-ray)}{Dose\ (C-ion)}$

For hypoxia, the OER was calculated at 10% survival with the formula: $OER = \frac{Dose\ (Hypoxia)}{Dose\ (Normoxia)}$

6.3.3. MTT assay

The MTT (3-[4,5-dimethylthiazol-2-yl]-2,5 diphenyl tetrazolium bromide) assay is based on the conversion of MTT into formazan crystals by living cells, which determines mitochondrial activity. Since for most cell populations, the total mitochondrial activity is related to the number of viable cells, this assay is broadly used to measure the *in vitro* cytotoxic effects of drugs on cell lines or primary patient cells (Berridge, Herst, and Tan 2005). MN/MCA1 and 4T1 cells were seeded and irradiated as mentioned above (section 6.2.1.). After irradiation, $1x10^3$ cells were seeded in 96 well plates, with six technical replicates for each condition; to avoid evaporation, the external wells were filled with PBS-/-. 72h after, the medium was removed and incubated for 2h with 50µl of 0,5mg/ml MTT solution, diluted in complete medium.

The MTT internalization was observed under the microscope and approximately after 2h the reaction was stopped by adding 50µl of SDS solution (SDS powder dissolved in distilled water 1:10). To completely dissolve of the formazan crystals, the plate was incubated for a maximum of 24h at 37°C.
All the procedures were performed in the dark. The absorbance was measured using a microplate reader, at 570nm. The external wells filled with PBS-/- were used as background and subtracted to all values. Each value was normalised on the sham control (non-irradiated samples) of the respective biological replicate.

6.3.4. Migration assays

6.3.4.1. Scratch assay

Following irradiation cells were seeded at high density ($2\text{-}3 \times 10^5$) in a 48-well plate. 24h after seeding, when the cells reached 100% confluency, a straight scratch in the centre of each well was performed using a 1000µl tip. After one wash with PBS-/-, each well was filled with complete medium; a mix of medium + 100ng/ml of SDF-1 was added in treated samples.

Photos of the same wells were taken at the microscope immediately after performing the scratches (0h timepoint), and up to 72 hours, to assess the closure of the wound area. Images were then analysed using Fiji software to delineate the wound area.

From the wound areas, measurements were determined as follows:

- The difference in wound area over time, normalized to the area at time zero: Δ wound area: Area t_{0+x} / Area t_0
- Migration rate from time 0 to 72h
  Migration rate (h^{-1}): $(At0-At0+x)0 \cdot 24\ h$

6.3.4.2. Transwell assay (or Boyden chamber)

The Transwell migration assay is an *in vitro* technique designed to study and quantify cell migration(Justus et al. 2023). The assay utilizes a chamber divided into two compartments by a microporous membrane (0.8 μm). Cells are seeded in the upper compartment, referred to as the Transwell insert, and migrate through the membrane pores into the lower chamber in response to a chemoattractant gradient established by the addition of 20% serum to the lower compartment, as shown in **Figure 15** .

Migration capacity was evaluated using Boyden chambers (Greiner Bio-one). Each well of a 24-well plate was filled with 700 µl of complete medium containing 20% fetal bovine serum (FBS). Following irradiation as previously described, 3×10^4 cells re-suspended in 250 µl were seeded into the upper wells of the Boyden chambers, with two wells selected for each dose. The plates were then incubated for 24 hours at 21% O_2 and 37°C.

Following the incubation period, the Transwell inserts were carefully removed from the plate. Any non-migrated cells remaining on the upper surface of the membrane were gently wiped away using a cotton swab. The medium from the lower chamber was aspirated, and 1 ml of sterile 1X PBS was added to wash the chamber and the insert, then the PBS was removed. The cells that successfully migrated through the membrane were then fixed by adding 2 ml of ethanol to the lower chamber, with the Transwell insert placed back in for 5 minutes. After fixation, the ethanol was removed, and another quick PBS wash was performed.

For the staining, 1 mL of May-Grünwald dye was added to each lower chamber for 2 minutes. Without removing the stain, water was added and incubated for an additional 2 minutes. The staining solution was then discarded, and Giemsa stain was applied for 10 minutes. Wells were subsequently

rinsed thoroughly with running water and allowed to air dry. The number of migrated cells, stained and visible under the microscope, was then quantified using Fiji software to assess cell migration.

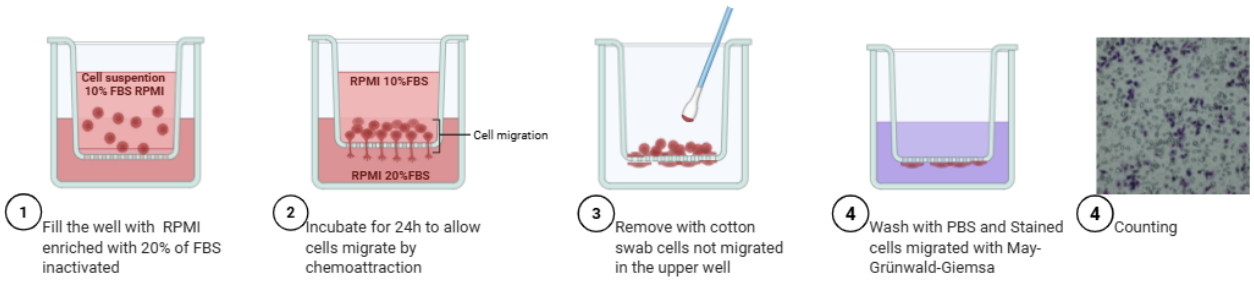

Figure 15: Schematic representation of Transwell assay steps

6.3.5. Flow cytometry analyses

Complement and immunogenic cell death factors were detected using flow cytometry in MN/MCA1, 4T1 and B16 cell lines. $1x10^5$ cells were seeded 48h before irradiation, then harvested and stained at different time points, as described in **Figure 10.** The cell concentration was determined, and 10^6 cells for each condition were centrifuged at 500 x g for 5 minutes at 4°C and washed with 500 µL of cold PBS-/-. From this point onward, the cells were kept on ice, protected from light, and all solutions used were pre-cooled at 4°C. For dead cell staining, $5x10^5$ cells were incubated for 30 minutes at 56°C, for positive control of death cells and then mixed with live half a million cells, centrifugated and resuspended in 1 mL of PBS-/- and incubated with all the other samples for 30 minutes at 4°C, after the addition of 1 µL of fixable viability dye (FVD) eFluorTM 506. For CRT, C3 exposure, CD55 and C3aR after incubating with FVD, the cells were centrifuged (500 x g for 5 minutes at 4°C), and the pellet was washed with 500 µL of FACS buffer (2% BSA in PBS) (for C3 staining, CD55 and C3aR, the FACS buffer was incubated for 1h). Following the final centrifugation, the cells (excluding unstained and FVD-only samples) were stained with 100 µl of primary antibody solution **(Table 1)** at 4°C for 1h. Subsequently, the samples were washed twice and incubated with 100 µl of secondary antibody solution at 4°C in the dark. Following two PBS washes, cells were fixed with 0.25% PFA to prevent plasma membrane permeabilization. Residual fixative was removed by additional PBS washes, and the pellet was resuspended in FACS buffer for acquisition. Over 30.000 events were acquired for all samples, and each experiment included an unstained sample and a positive control FVD-only.

6.3.5.1. C3b deposition assay

To evaluate complement activation by measuring C3b deposition on MN/MCA1, 4T1 and B16-F10 cells, we harvested the cells 24h after irradiation and incubated them with untreated or heat-inactivated mouse serum from C57BL/6 mice at 37°C for 5 minutes. Then, complement activation was immediately blocked by keeping the cells on ice and adding EDTA to a final concentration of 10 mM. Cells were washed, blocked in PBS-/- containing 2% BSA and 5% Normal Donkey Serum, for 30 min at RT, and then incubated with 5µg/ml anti-mouse C3b/iC3b/C3c (Hycult Biotech, clone 2/11) primary antibody for 1h at RT. After three washing steps, samples were incubated with 2 µg/ml AF488-donkey anti-rat IgG secondary antibody for 1h at RT. In selected experiments (C3b deposition), sarcoma cells were preincubated overnight at 37°C with 10 µg/ml tunicamycin (Sigma-Aldrich) or vehicle (0.1% DMSO) in complete medium, then subjected to the C3 deposition assay.

Table 1: Antibody for flowcytometry experiments and respective dilution

Marker	**Antibody**	**Dilution**
CRT	Calreticulin Recombinant Rabbit Monoclonal Antibody (SU37-03)	1:100
C3	Thermofisher (PA1-29715) Complement C3 Polyclonal Antibody	1:100
C3b	Hycult (HM1065) C3b/iC3b/C3c, Mouse, mAb 2/11	1:20
C3aR	Catalog (HM1123) C3aR, Mouse, mAb 14D4	1:50
CD55	Catalog (HM1115) CD55, Mouse, mAb 3D5	1:50
Fixable viability dye 506	Thermofisher (65-0866-14) eBioscience™ Fixable Viability Dye eFluor™ 506	1:1000
Fixable viability dye 450	Thermofisher (65-0863-14) eBioscience™ Fixable Viability Dye eFluor™ 450	1:1000

6.3.5.1.1. Flow cytometry measurement and analysis

Two different cytometers were used for the acquisition: CRT exposure was measured with a Beckman counter Cytoflex KO525 to exit FVD and FITC to detect CRT conjugated with Alexafluor 488; C3, C3aR, CD55 and C3b deposition exposure were measured by a Thermofisher Attenuate cytometer. In both experiments, debris and duplets were excluded by gating shown in **Figure 16**.

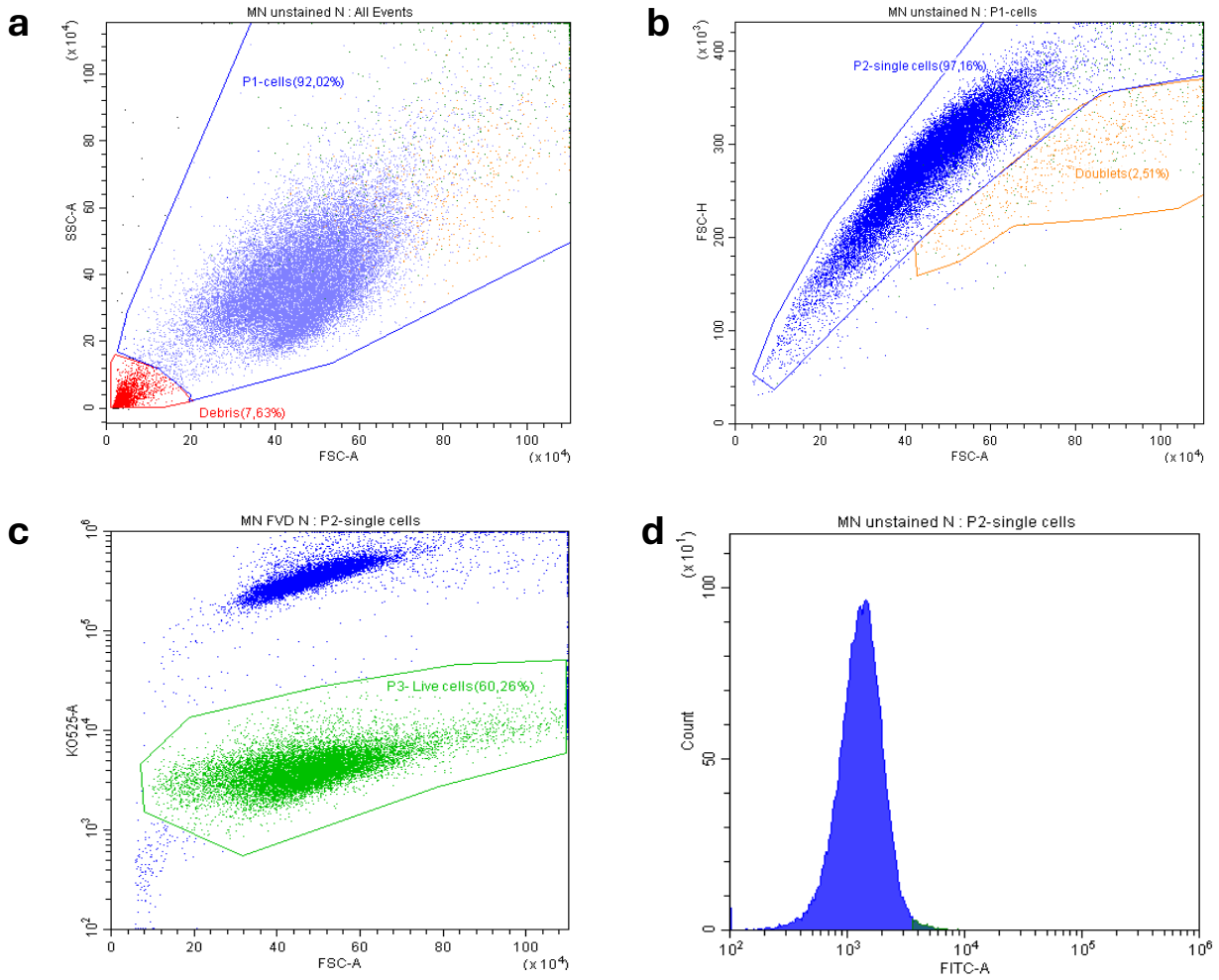

Figure 16: Gaiting strategy for CytExpert analyses

(a) The first gating is to exclude cells debris (in red) and consider only the population of cells (P1 in light purple). (b) The P1 is subsequently gated to exclude doublets (in orange) resulting in a population of single cells (P2 in blue). (c) When is necessary we also exclude death cells (in blue) stained with FVD 506 and detected in KO525-A channel, resulting in P3- Live cells in green. (d) The acquisition gains for FITC channels were adjusted to have the median fluorescence intensity (MFI) of the unstained between 10^3 and 10^4.

For most experiments, we included an unstained sample for each dose to reduce the influence of irradiation-induced cell enlargement **Figure 17**, and the signal for each dose was then subtracted from the unstained sample.

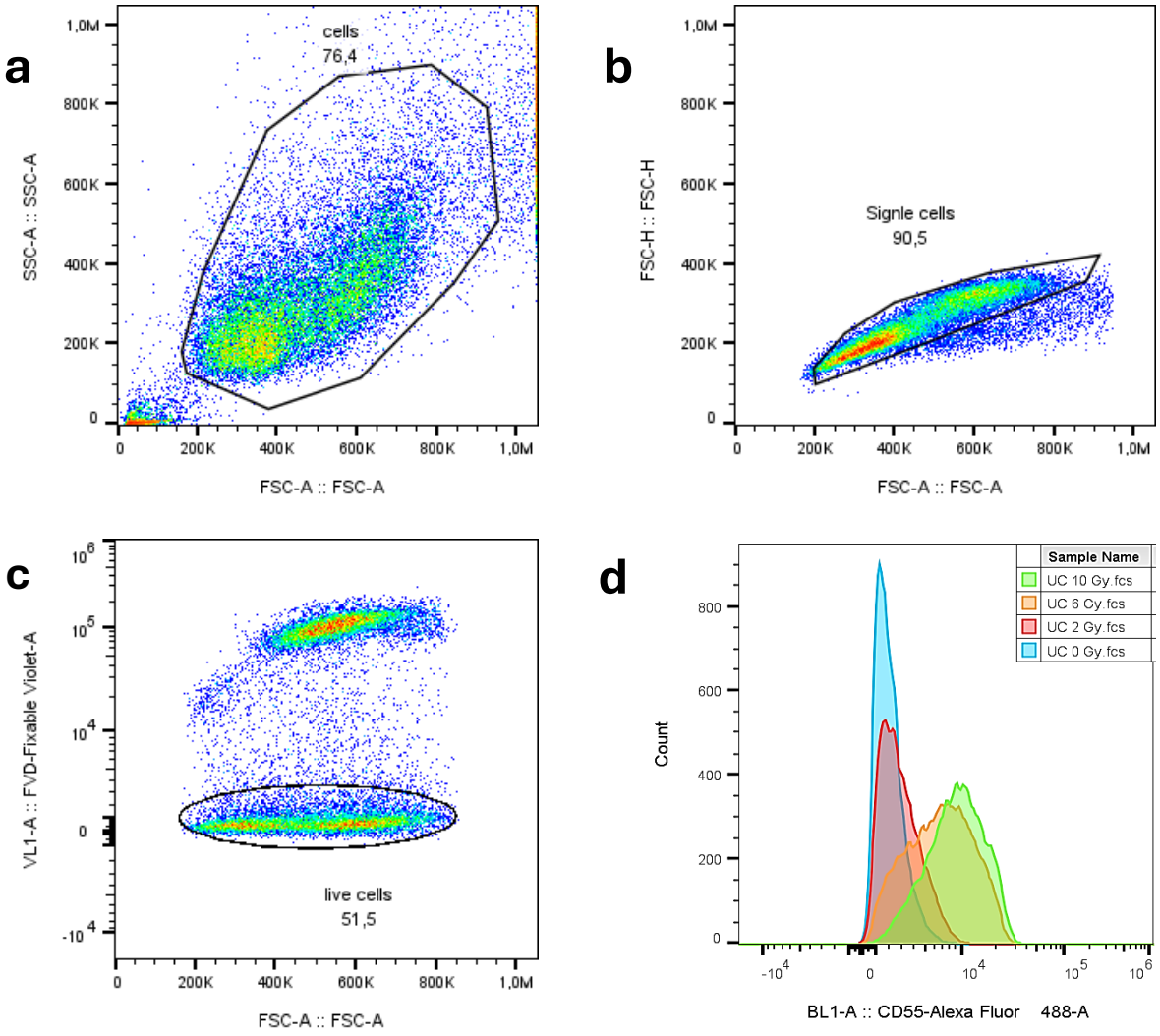

Figure 17: Gaiting strategy FlowJo analysis

The firsts two gating are to exclude cells debris and doublets (a) and (b) resulting in a population of single cells (P2 in blue). (c) When is necessary we also exclude death cells (in blue) stained with FVD 506 and detected in VL1-A channel, resulting in Live cells. (d) Histograms showing the increase in autofluorescence of the unstained sample at increasing doses.

6.3.6. Tumour tissue homogenization

Part of tumour tissues were snap frozen the day of the sacrifice in liquid nitrogen and stored at -80°C. The day of the experiment, the frozen tissues were kept in ice and homogenised with Tissuelyser bead mill for 5min at 50Hz, with steal beads and cold lyses buffer (1 g tumour tissue/ml): 50mM Tris-HCl pH 7.5 containing: 2mM EDTA, 1% Triton X-100, Immediately before use add protease inhibitors.

The homogenised solution was transferred into a new 1.5ml tube and centrifugated for 20 min (15.000 rcf) at 4°C. The interface liquid was collected and either stored at 80°C or processed for protein quantification using the DC Protein Assay Kit (Bio-rad) according to the manufacturer's instructions.

6.3.7. ELISA assay

The release of cytokines and other factors were measured in the supernatant by Enzyme-Linked Immunosorbent Assay (ELISA). Cells were seeded 48h before the irradiation and 1,8ml of cells' supernatant was collected at different timepoints and stored at -80°C. **(Figure 11).** HMGB1 quantification was performed with the HMGB1 ELISA kit (IBL International GmbH), according to the manufacturer's instructions. Due to the high concentration of this factor in the cells, supernatant required additional dilutions (Normoxia 1:3, Hypoxia 1:10). At the end of the protocol the absorbance was measured at 450nm and 630nm (background subtracted to 450nm) using the BioTek EL808 Microplate Reader and Gen5 software. The exact concentration of the analyte was calculated using a 4-parameter fit based on the standard values, with parameters derived from www.mycurvefit.com. Additionally, the positive control provided in the kit was measured to ensure that its value fell within the acceptable range specified in the QC certificate.

C3a ELISA was performed to quantify the analyte concentration in cell supernatants, tumour tissue homogenates, and mouse serum, according to the manufacturer's instructions with the addition of 10 mM EDTA to each kit solution. The absorbance obtained at 450nm was used for the analyses. The standard curve values were used to generate a linear regression or 4-parameter fit to determine the precise C3a concentration.

For cell supernatants, the results were normalized to the total number of adherent cells in each sample. The resulting analyte concentration (given in ng per 10^5 cells) was further normalized to the respective 0 Gy control at each time point.

6.3.8. Multiplex ELISA assay

The multiplex ELISA assay was used to determine the analyte concentration in the supernatant of MN/MCA1 cell line, but also to evaluate the concentration of ten different analytes in C3H mouse serum. The release of GM-CSF, tumour necrosis factor (TNF)-α, chemokine (C-X-C motif) ligand (CXCL) 10, Interleukin (IL)-6, and IFN-β after irradiation of MN/MCA1 cells was quantified from cell culture supernatant. A customized U-PLEX Custom Biomarker Group 1 (ms) Assay kit from MSD® was performed following the manufacturer's instructions. Technical duplicates were performed for both the standards and the samples. For analysis, the MSD Discovery Workbench software was used, and the results were normalized to the total number of adherent cells in each sample.

6.3.9. Tumor tissue frozen section and staining

The fixed tumor samples were de-hydrated in growing gradients of sucrose solution (10%, 20% and 30% in PBS, Roth, Karlsruhe, Germany). After the last solution, all the samples were embedded in Optimal Cutting Temperature Compound (OCT Embedding Matrix for Frozen Sections, CellPath, Roth, Karlsruhe, Germany) by cutting them into slices and placing them into cryomolds (vinyl Tissue-Tek® Cryomold®, Sakura Finetek Inc., Torrance, CA, USA). The cryomolds were let to cool down to -22˚C for at least four hours and then transferred to the -80˚ C freezer for long-term storage. To soften the samples for cutting, they were transferred in the cryostat (Leica CM1860 UV, Leica Biosystems, Nussloch, Germany), two hours prior, with the temperature set at -22˚C. Upon use, they were mounted on the cryostat holder to cut slices of 8 µm, then were collected on glass slides (Microscope slides, adhesive and salinized, 75x25x1 mm, LABSOLUTE) and let dry at room temperature for 30 minutes. Afterwards, they were stored at -22˚C until staining. For the staining the frozen sections were taken out of the freezer, let soften at room temperature for 10 mins, rinsed in PBS for 5 mins and then stained. After the delimitation of tumor tissue with hydrophobic barrier pen and two additional washing steps the unspecific binging were blocked for 30min with blocking solution (5% serum NGS (normal goat serum), 2%BSA and 0.8% Triton in PBS-T 3). Tumor sections were than incubated for 1h, at RT with primary antibodies (anti-mouse C3b/iC3b/C3c (Hycult Biotech, clone 2/11, 5 µg/ml)) diluted 1:20 in PBS++ pH 7.4 containing 2% BSA (Sigma-Aldrich), 5% NGS and 0.25% Triton X-100 (Sigma-Aldrich). Two washes were carried out to eliminate excess antibody. Then tissues were incubated with Alexa Fluor 488 diluted 1:400 in in in PBS++ pH 7.4 containing 2% BSA (Sigma-Aldrich), 5% NGS and 0.25% Triton X-100 (Sigma-Aldrich) for 1 at RT. The nuclei were stained for 15 minutes with DNA detection, 4',6-diamidino-2-phenylindole (DAPI) (300nM, Invitrogen), after two washing steps. To conclude the staining

tissue were washed and leave it dry for a couple of hours before the mounting with the VectaShield antifade medium (Vector laboratories). Pictures were taken using Leica DMI 4000B confocal microscope.

6.4. Statistical analyses

Technical replicates were defined as repeated measurement of the same sample, used to account for variability in instruments or protocols. Biological replicates were considered as independent measurements of biologically distinct samples, derived from different cell cultures processed either at different times or simultaneously. Data were analysed with Microsoft Excel and GraphPad Prism software. The differences between the irradiation qualities were considered statistically significant for p - values ≤ 0.05, comparing the same physical dose. Statistical significance in the graphs is indicated by: (*) < 0.033, (**) < 0.002, (***) <0.001; denoting differences compared to the corresponding non-irradiated control of each experiment (radiation effect). The reported p-values indicate the statistical significance between the two conditions compared within each graph (e.g., normoxia vs hypoxia or X-rays vs C-ions, time points).

7. Results

This study presents the first comprehensive radiobiological and immunological characterization of a specific fibrosarcoma cell line (MN/MCA1), originally isolated at the Mario Negri Institute in Milan in 1978 (Giavazzi et al. 1980). The fibrosarcoma is a highly aggressive malignancy characterised by significant metastatic potential and inherent radioresistance(Augsburger et al. 2017). To establish for the first time a robust radiobiological profile for MN/MCA1cell line, its response was compared to two established models of radioresistant cells: the 4T1 triple-negative breast cancer (TNBC) and the B16-F10 melanoma lines. The comparative analysis between the novel MN/MCA1 line and the established 4T1 and B16 models is instrumental in dissecting the interplay between radiation response and complement activation, the core of this work. While 4T1 and B16 are widely studied in particle therapy research, they also offer distinct basal profiles regarding complement components; utilizing them as reference points allows for a more precise contextualization of the MN/MCA1 immunological behaviour.

A primary objective of this study was to evaluate the potential of Carbon-ion therapy to overcome the radioresistance of MN/MCA1 cell line compared to conventional X-ray. Radiobiological efficacy was assessed through clonogenic survival assays and the quantification of cellular migration capacity, at multiple time points. C-ion irradiations were performed under clinically relevant conditions within the Spread-Out Bragg Peak (SOBP), utilizing a mean dose-averaged Linear Energy Transfer (LET) of 75 keV/µm. The therapeutic gain of C-ion over photons was quantitatively defined by calculating the Relative Biological Effectiveness (RBE) across specific survival fractions.

Furthermore, given the superior immunogenicity discussed for high-LET radiation, we analysed the induction of Immunogenic Cell Death (ICD) markers to evaluate the capacity of C-ions to stimulate the immune system (Galluzzi et al. 2017; Helm et al. 2021). Specifically, we monitored the kinetics of HMGB1 release and the cell-surface translocation of calreticulin at multiple time points up to 96 hours post-irradiation.

Given the increasing key role of the complement system in modulating the immune landscape of the tumour microenvironment (TME)(Artero et al. 2025), the study presented here additionally focuses on the irradiation-induced modulation of complement components, with a particular focus on the effects of C-ion exposure. While complement factors are traditionally regarded as systemic products within the TME, we investigated whether irradiation influences the endogenous production of C3-derived products directly by tumour cells. To validate these *in vitro* observations, a preliminary *ex vivo* study was conducted in C57BL/6 wild-type (WT) and C3 knockout ($C3^{-/-}$) mouse models.

As hypoxia represents a significant limiting factor in the efficacy of conventional radiotherapy (Brown and Wilson 2004), part of these radiobiological and immunological experiments was performed under hypoxic conditions (1% O_2) during both cell culture and irradiation. This comprehensive approach was designed to determine whether C-ion, characterised by a lower Oxygen Enhancement Ratio (OER) compared to X-ray, can effectively circumvent the radioresistance typically conferred by the hypoxic niche of the MN/MCA1 fibrosarcoma.

7.1. Cell line characterisation

In this study, the focus was on a fibrosarcoma cell line isolated at Mario Negri Institute in 1978 (Giavazzi et al. 1980). Before starting the experiments, we characterised the cell line by performing a growth curve and confirmed the influence of the amount of oxygen on cell proliferation (**Figure 18**).

As already explained in the introduction (section 4.2**)**, hypoxia is a prevalent feature within the sarcoma tumour microenvironment. This reduced oxygen tension is known to induce significant molecular and genetic alterations in cells, substantially contributing to tumour radioresistance. The data derived from the growth curve in **Figure 18** clearly demonstrates that low oxygen concentration attenuates the proliferation rate of the tumour cells. Specifically, cells were cultured in parallel under normoxic and hypoxic conditions for two weeks (**Figure 10**), a strategy designed to mimic the temporary oxygenation gradient, characteristic of the *in vivo* tumour niche.

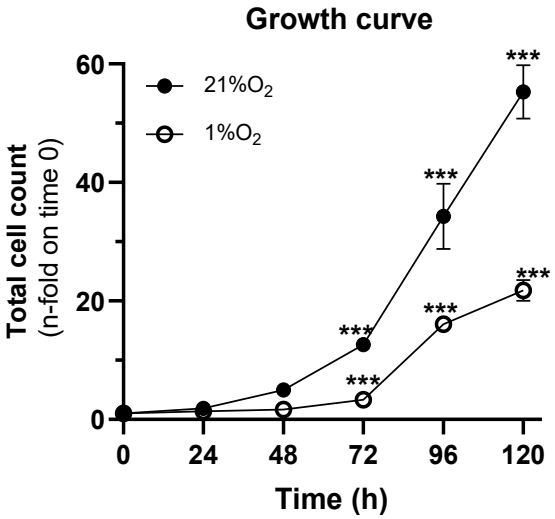

Figure 18: Growth curve of MN/MCA1 cell line at different O_2 concentrations

Comparison of cell growth of MN/MCA1 cells cultured for two weeks under normoxic (21%O_2) and hypoxic (1%O_2) conditions. The graph represents the total cell count at different time points (24, 48, 72, 96 and 120h) normalised on the respective cell seeding number, equal for all the time points. Doubling time was calculated during the exponential growth phase between 48h and 96h (normoxia17.5h, hypoxia 25.67h). Data represent the mean of three technical replicates for each of three independent biological replicates. Error bars indicate the standard error of the mean (SEM). Statistical analysis was performed using two-way ANOVA followed by Sidak's multiple comparisons test. Statistical significance is denoted as follows: *p = 0.033, **p = 0.002, ***p < 0.001, indicating differences relative to the corresponding cell count at 0 h. A significant difference between the two conditions was observed starting from 72 h onward (p < 0.001).

Quantitative analysis of the growth curve revealed a significant difference in cellular proliferation starting at the 48-hour time point. During the exponential growth phase (48-96h), the doubling time (T_d) under normoxia (T_d=17.15h) was 1.5-fold lower than the hypoxic counterpart (T_d =25.67h). This difference underscored the pronounced capability of hypoxia to slow down the proliferative kinetics of the MN/MCA1 cell line.

7.2. Radiobiological characterisation

7.2.1. MN/MCA1 cell survival is influenced by X-ray and carbon ion irradiation and oxygen condition

Table 2: α,β parameters of MN/MCA1 cell line

Radiation qualities	Conditions	α	β	α/β
X-ray	Normoxia	0.5± 0.07	0.07± 0.02	6
	Acute Hypoxia	0.45± 0.07	0.04± 0.03	10
	Chronic Hypoxia	0.42± 0.5	0.02± 0.01	25
C-ion	Normoxia	1± 0.3	≈0	-
	Acute Hypoxia	1± 0.15	≈0	-
	Chronic Hypoxia	0.5± 0.17	≈0	-

The intrinsic radiosensitivity of the MN/MCA1 cell line was assessed for the first time using a clonogenic survival assay. The Linear-Quadratic model analysis of the X-ray survival data yielded an alpha/beta ratio suggesting a high propensity for sublethal DNA damage repair in these cells and increasing value under hypoxic conditions, indicating a progressive decrease in the contribution of the quadratic term with reduced oxygen availability and a oxygen dependence **(Table 2)**. For carbon-ion irradiation (LET ≈ 75 keV/µm), the quadratic term β was not statistically different from zero under all oxygenation conditions. Therefore, carbon-ion survival curves were considered predominantly linear in the investigated dose range, such behaviour is consistent with high-LET radiation, where cell killing is dominated by single-track events and shows reduced sensitivity to and oxygenation. Furthermore, carbon ion irradiation turned out to be more effective than X-ray irradiation and showed a pronounced decrease in cell survival. The enhanced biological effect is reflected in an RBE_{10} of 1.5 at the 10% survival fraction.

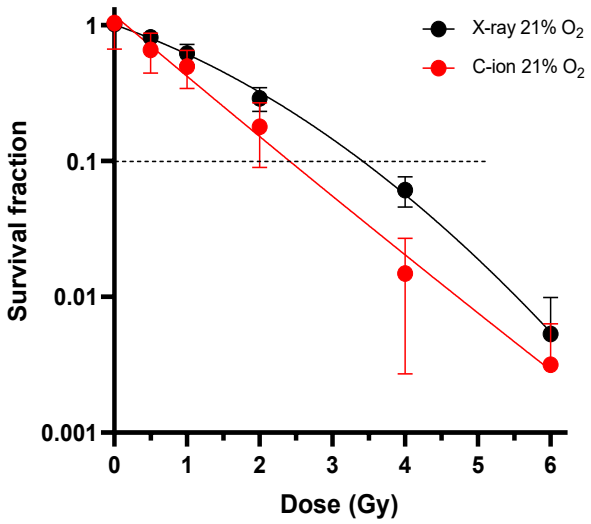

Figure 19: Clonogenic cell survival of MN/MCA1 after X-ray and C-ion irradiation

Survival fraction represents the number of colonies 10 days after irradiation, normalized on not-irradiated samples and fitted using the linear quadratic model. The RBE is calculated at 10% survival, highlighted with dotted line. The data result from the mean of three technical replicates included in four biological replicates. The error bar represents the standard error of the mean (SEM).

As already mentioned before, the hypoxic composition of the sarcoma tumour is one of the limitations in radiotherapy efficacy. We evaluated the survival fraction of MN/MCA1 cells after two weeks under hypoxic conditions. We observed that X-ray and C-ion irradiations cannot overcome the radioresistance induced by prolonged hypoxia **(Figure 20b)**, based on the OER calculated ($OER_{10} = D_{Hypoxia10}/D_{Normoxia10}$) and reported in **Table 3**. Conversely, it is interesting to see in **Figure 20b** that the difference between acute hypoxia (24h under 1%O_2) and normoxia is reduced to non-significant differences, for X-ray and for C-ion exposure. As shown by the OER values in Table 3, there is a distinct relationship between the duration of hypoxia and the resulting cell survival rates after irradiation.

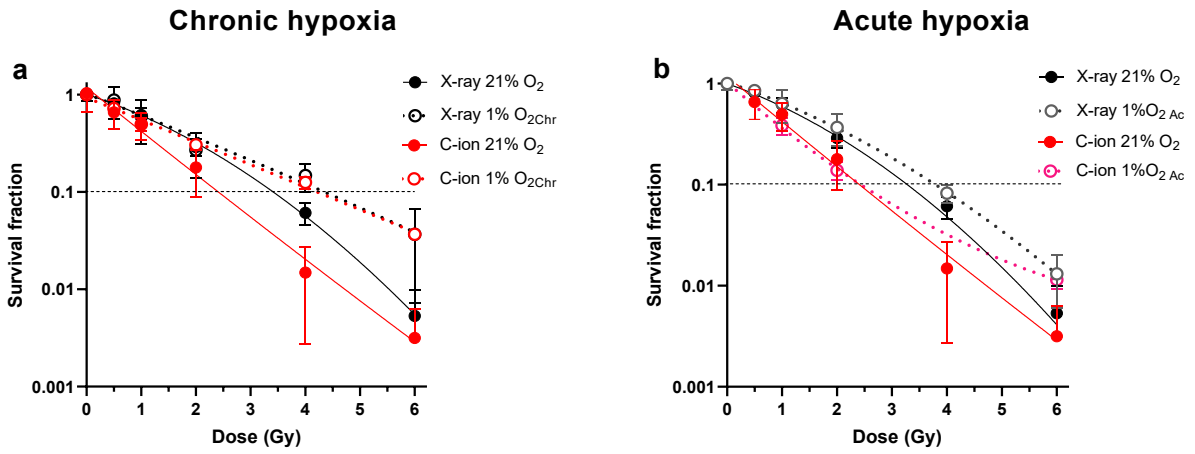

Figure 20: Clonogenic survival under hypoxic conditions (1%O2) of MN/MCA1 after X-ray ad C-ion irradiation

(a) The intrinsic radiosensitivity of the MN/MCA1 cell line was assessed via clonogenic survival assay, following two weeks of pre-incubation under either normoxic ($21\%O_2$; data from **Figure 19**) or chronic hypoxic ($1\%O_2$) conditions. (b) Comparison between normoxia and acute hypoxia (24h at 1% O_2) in survival fraction following x-ray and c-ion irradiation. The plotted data represent the survival fraction measured 10 days post-irradiation, normalized to the respective non-irradiated controls for each oxygenation state. The dose-response data were fitted using the Linear-Quadratic (LQ) model. Each data point represents the mean of three technical replicates per condition. For the hypoxic condition, the experiment was performed in three independent biological replicates.

Table 3: Radiobiological parameters including relative biological effectiveness (RBE) for carbon ions (energy range of 220-240 MeV/u, LET of 75 keV/µ) and oxygen enhancement ratio (OER) measured in MN/MCA1

Cell line	RBE_{10}	Chronic Hypoxia OER_{10}		Acute Hypoxia OER_{10}	
		X-ray	C-ion	X-ray	C-ion
MN/MCA1	1.5	1.4	1.9	1.16	1

7.2.2. Irradiation reduces cell viability in MN/MCA1 and 4T1 cell lines

7.2.2.1. Influence of X-ray and carbon ion irradiation on cell viability in MN/MCA1 at different oxygen concentrations

Cell viability of MN/MCA1 cells was evaluated using a metabolic assay 72 hours post-irradiation, to assess the cytotoxic potential of low and high Linear Energy Transfer (LET) radiation. Both X-ray (low LET) and C-ions (high LET) induced a progressive, dose-dependent reduction in cell viability across the entire dose ranges tested, relative to the non-irradiated control (0 Gy) **Figure 21a**. However, a statistically significant difference was observed in the dose-response.

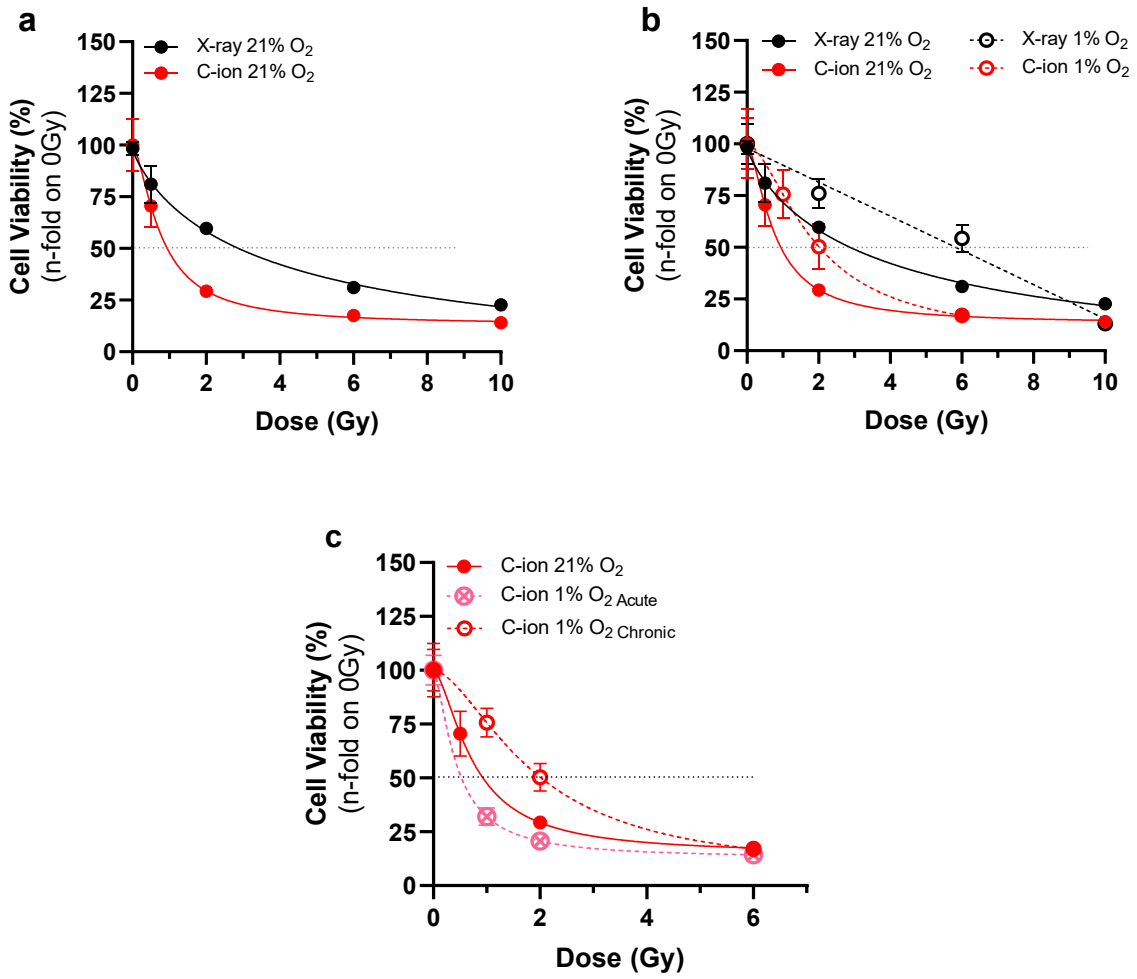

Figure 21: MN/MCA1 cell line viability evaluation following X-ray and C-ion irradiation

(a) The data represent the viability of MN/MCA1 cells 72h after irradiation, evaluated by MTT assay. IC50 was calculated based on the fit, resulting in IC50 for X-ray = 2.8 Gy and IC50 for C-ion = 1 Gy. Dose-response curves were generated via non-linear regression using the 4-parameter logistic model. Differences between datasets were evaluated by comparing a global fit model using an extra sum-of-squares F test (F=3.834, p=0.0136). (b) The data represent the comparison of viability of MN/MNCA1 cells cultured under chronic hypoxic and normoxic condition, 72h

following irradiation with X-ray and C-ion, valuated by MTT assay. IC50 was calculated for hypoxic condition based on the fit, resulting in IC50 X-ray = 5.23 and IC50 C-ion = 2. (c) Comparison of viability of MN/MNCA1 cells cultured under acute and chronic hypoxia and normoxic condition, 72h following irradiation with C-ion, evaluated by MTT assay. IC50 was calculated based on the fit, resulting in IC50 C-ion 21% O_2 = 1 C-ion 1% O_2 Chronic = 2, C-ion 1% O_2 Acute: 0.43 Gy.

All the experiments include three biological replicates with six technical replicates each. The statistical difference between the full dose-response profiles was confirmed by an Extra Sum-of-Squares F-test, which compared the fit of a single curve to two separate curves. The curves exhibited a consistently steeper slope and lower percentage of viable cells compared to the X-ray curve, indicating the superior biological effectiveness of high-LET radiation in reducing the cell population and/or metabolic activity at the 72-hour timepoint**.** The most pronounced difference in the curves occurred within the low-dose region. For instance, at 2 Gy, the viability of cells irradiated with C-ion dropped to approximately 30%, whereas X-ray treated cells maintained a significantly higher value of ~60% **(Figure 21a)**. At 10 Gy, the highest doses examined, the response curves began to reach a plateau, with X-ray resulting in approximately 25% viability, and C-ion inducing a marginally lower viability below 20%. Quantification of the dose required to achieve a 50% reduction in cell viability (IC50, Inhibitory Concentration 50%) further illustrated this differential efficacy. The IC50 for the C-ion group was observed at an approximate dose of 1 Gy. Conversely, a dose of 2.8 Gy was required from X-ray to elicit the equivalent 50% inhibition of viability. This difference demonstrates that the required X-ray dose was two-fold higher than the C-ion dose to achieve the same suppression of cell viability at 72 hours following irradiation.

The radioresistance induced by two weeks of hypoxic culture was further confirmed by the reduced cell viability observed in **Figure 21b**. Cells cultured under chronic hypoxia exhibited higher viability than normoxic cells after low-dose C-ion irradiation, whereas this hypoxia-associated radioresistance was reduced at higher doses. This finding suggests that the radioresistant phenotype induced by two weeks of chronic hypoxia was not completely suppressed by carbon ion irradiation. Consistent with clonogenic survival data **(Figure 19)**, the importance in hypoxia duration come out also in terms of viability and cytotoxicity where C-ion irradiation effectively mitigated resistance under acute hypoxia **(Figure 21c)**.

7.2.2.2. Carbon ions are more effective than X-rays to reduce viability in breast cancer radioresistant cell line (4T1)

Triple negative breast cancer is well known to be a very radioresistant cell line, as demonstrated from the RBE **(Table 3S 1)** and confirmed in **Figure 22.** Comparison of the IC50 showed that C-ion treatment was 2.4-fold more effective compared to X-ray, with a high efficacy already at low doses (2 Gy). Additionally, we can attest a higher radioresistance of 4T1 cells compared to MN/MCA1, based on the IC_{50} following both irradiation types.

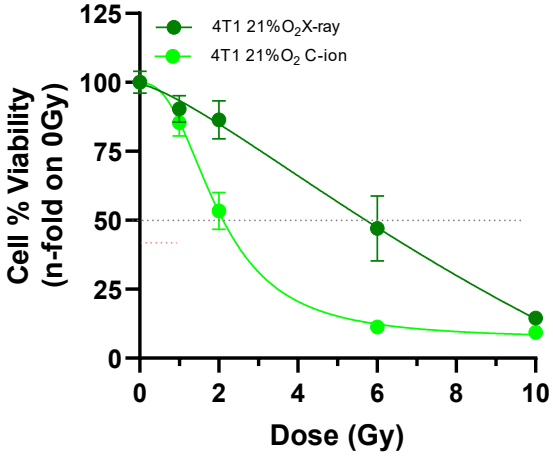

Figure 22: Viability assay following X-ray and C-ion irradiation of 4T1 cell line

(a) The data represent the viability of 4T1 cells 72h after irradiation evaluated by MTT assay. IC50 was calculated based on the fit, resulting in IC50 for X-ray = 5.75 Gy and IC50 for C-ion = 2.13 Gy. Dose-response curves were generated via non-linear regression using the four-parameter logistic model. Differences between datasets were evaluated by comparing a global fit model using an extra sum-of-squares F test (F=13.36, p=<0.0001). All the experiments include three biological replicates with six technical replicates. The statistical difference between the full dose-response profiles was confirmed by an Extra Sum-of-Squares F-test, which compared the fit of a single curve to two separate curves.

7.2.3. Irradiation influences tumour cell migration

Sarcoma and fibrosarcoma are commonly highly metastatic tumour (Damerell, Pepper, and Prince 2021). We investigated the migratory capacity of MN/MCA1 cells following X-ray and C-ion irradiation, specifically focusing on the influence of hypoxia. While hypoxia is a well-established driver of tumor cell motility, it also triggers significant metabolic stress that can, paradoxically, impede migration. To evaluate this, we employed two complementary approaches: scratch assays and transwell assays. Additionally, we explored the potential involvement of the SDF-1/CXCR4 signaling axis, a pathway critical for modulating the tumor microenvironment and directing cell

movement. SDF-1 and its cognate receptor, CXCR4, are critical mediators of cellular trafficking and have been shown to be upregulated following radiotherapy, potentially contributing to tumour regrowth and immune evasion (Duda et al. 2011).

7.2.3.1. Irradiation with X-ray and C-ion reduce collective migration assessed with scratch assay

Scratch assays were performed to assess the migration capacity of cells following irradiation exposure under normoxic and hypoxic conditions. By creating a cell-free gap, this assay removes contact inhibition and triggers collective migration (Rodriguez, Wu, and Guan 2005). The wound area was measured at different time points, thereby highlighting how intrinsic motility is influenced by stressors such as irradiation and hypoxia **(Figure 23)**

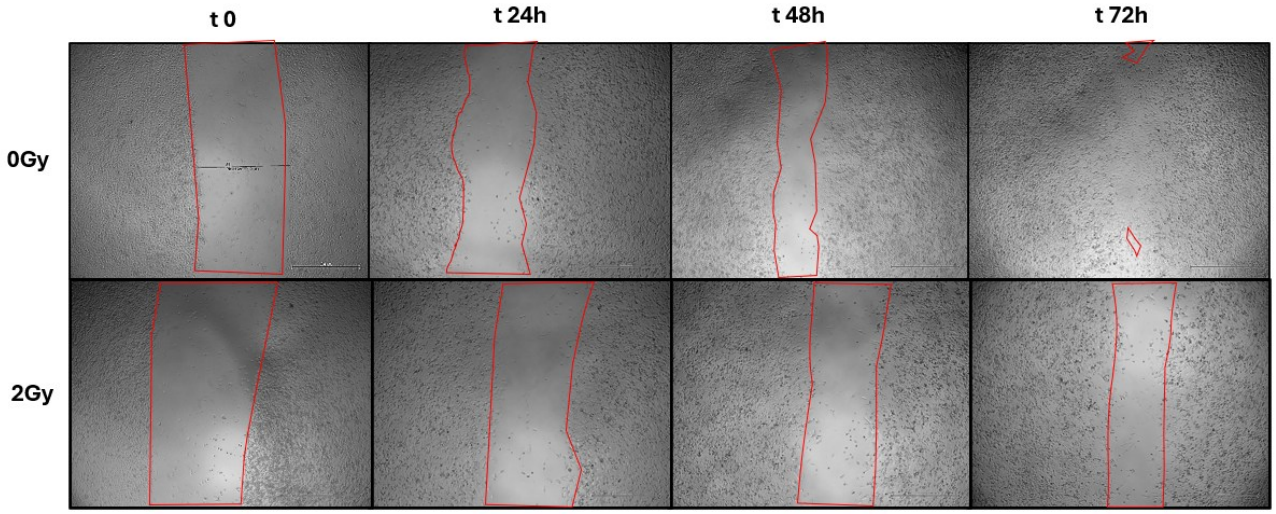

Figure 23: Representative images from *in vitro* scratch wound healing assays

Photos of the same well from time zero (scratch moment) to 72 hours later to assess the area and speed of closure, highlighted in red. Below is a photo of the same well after irradiation with 2 Gy of C-ions from time zero to 72 hours post-scratch.

As we mentioned in section 4.3 hypoxia tends to influence migration capacity in tumor. As shown in **Figure 24,** culturing MN/MCA1 under 1% O_2 trigger and speed up migration capacity.

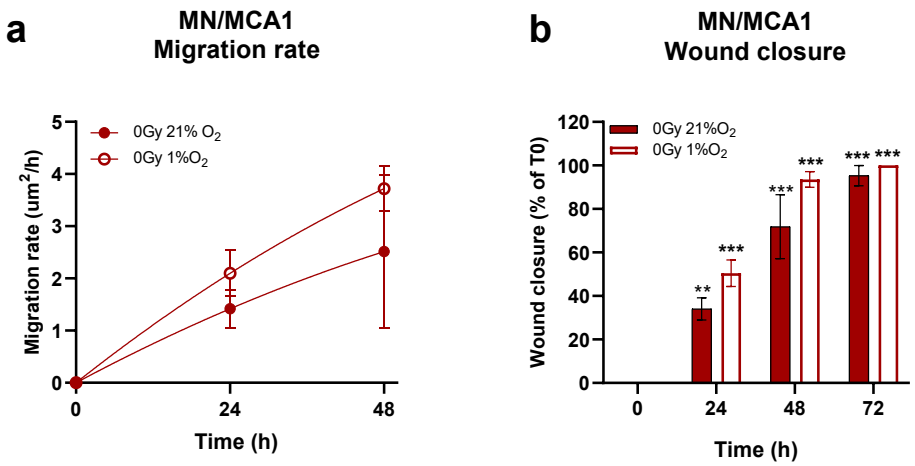

Figure 24: Evaluation of migration ability by scratch assay in MN/MCA1 cell line under hypoxic conditions

Measurement of wound area (um^2) at different time points (24h, 48h, 72h) and O_2 concentrations (21%, 1%) in MN/MCA1 cell. (a) The data represent the migration rate (h^{-1}): $(A_{T0}-A_{Tn})/(A_{T0} *Tn)$ fit with quadratic polynomial formula using GraphPad Prism software. Statistical comparison of the curves was performed using an F-test, revealing significant differences in the overall trends between treatment groups ($p < 0.05$). (b) Percentage of wound area closure over the time in not irradiated sample under 21% and 1% O_2 concentration. Wound area was quantified using Fiji software and is presented as the mean of two technical replicates from three independent biological replicates. Error bars represent the standard error of the mean (SEM). Statistical analysis was performed using two-way ANOVA followed by Sidak's multiple comparisons test. Statistical significance is indicated as follows: *p = 0.033, **p = 0.002, ***p < 0.001, representing differences relative to the corresponding time 0 h.

The migration capacity under hypoxic condition is reduced following irradiation, in particular at high doses compared to not irradiated samples **(Figure 25a)** (statistical analyses suggest a significant difference compared with controls after 6 $Gy_{C\text{-}ion}$ *p: 0.006* and 10 $Gy_{C\text{-}ion}$ *p: 0.008*). Considering 2 Gy as the most representative dose, in **Figure 25c and d** we are not able to see a significant difference in migration capacity over the time comparing normoxic and hypoxic condition, highlighting the capability of irradiation in reducing migration hypoxic trigger.

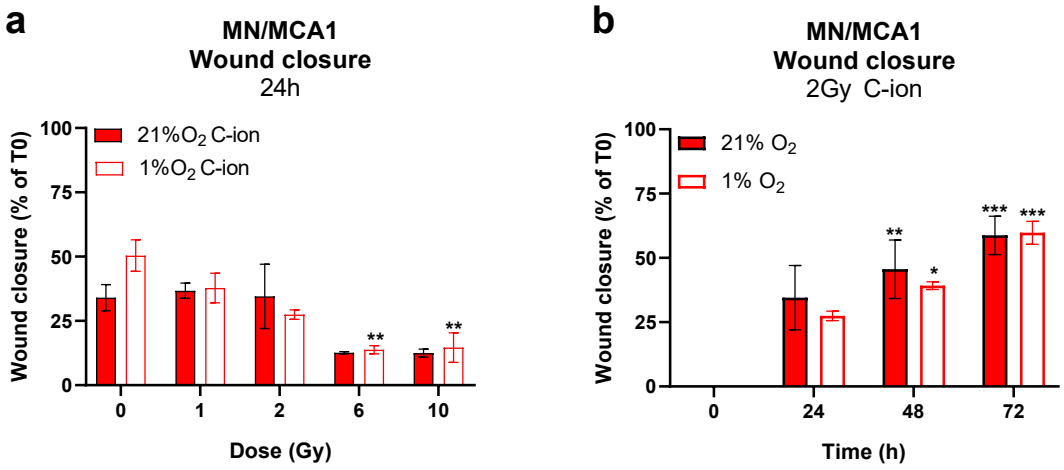

Figure 25: Influence of irradiation in MN/MCA1 migration under normoxic and hypoxic conditions

Measurement of wound area (um^2) at different time points (24h, 48h, 72h) and O_2 concentrations (21%, 1%) in MN/MCA1 cell. (a) Percentage of wound area closure 24h after C-ion irradiation under 21% and 1% O_2 concentration over the doses (from 1 to 10 Gy). (b) Percentage of wound area closure over the time until 72h after irradiation after 2 Gy of C-ion.

Wound area was quantified using Fiji software and is presented as the mean of two technical replicates from three independent biological replicates. Error bars represent the standard error of the mean (SEM). Statistical analysis was performed using two-way ANOVA followed by Sidak's multiple comparisons test. Statistical significance is indicated as follows: *p = 0.033, **p = 0.002, ***p < 0.001, representing differences relative to the corresponding time 0 h or control not irradiated.

Our data show a dose dependent decrease in migration capacity following irradiation with a more effective trend following C-ion irradiation **(Figure 26c)**. In **Figure 26a** we demonstrate the higher capability of C-ion in reducing migration over the time (2 Gy shown as a benchmark for intermediate exposure with initial biological impact of irradiation and the rate of cell death relatively low compared to the higher doses). Comparing the migration rate following irradiation the trend is significantly higher following X-ray **(Figure 26b)** (For a general overview of all resalts see section 10.2).

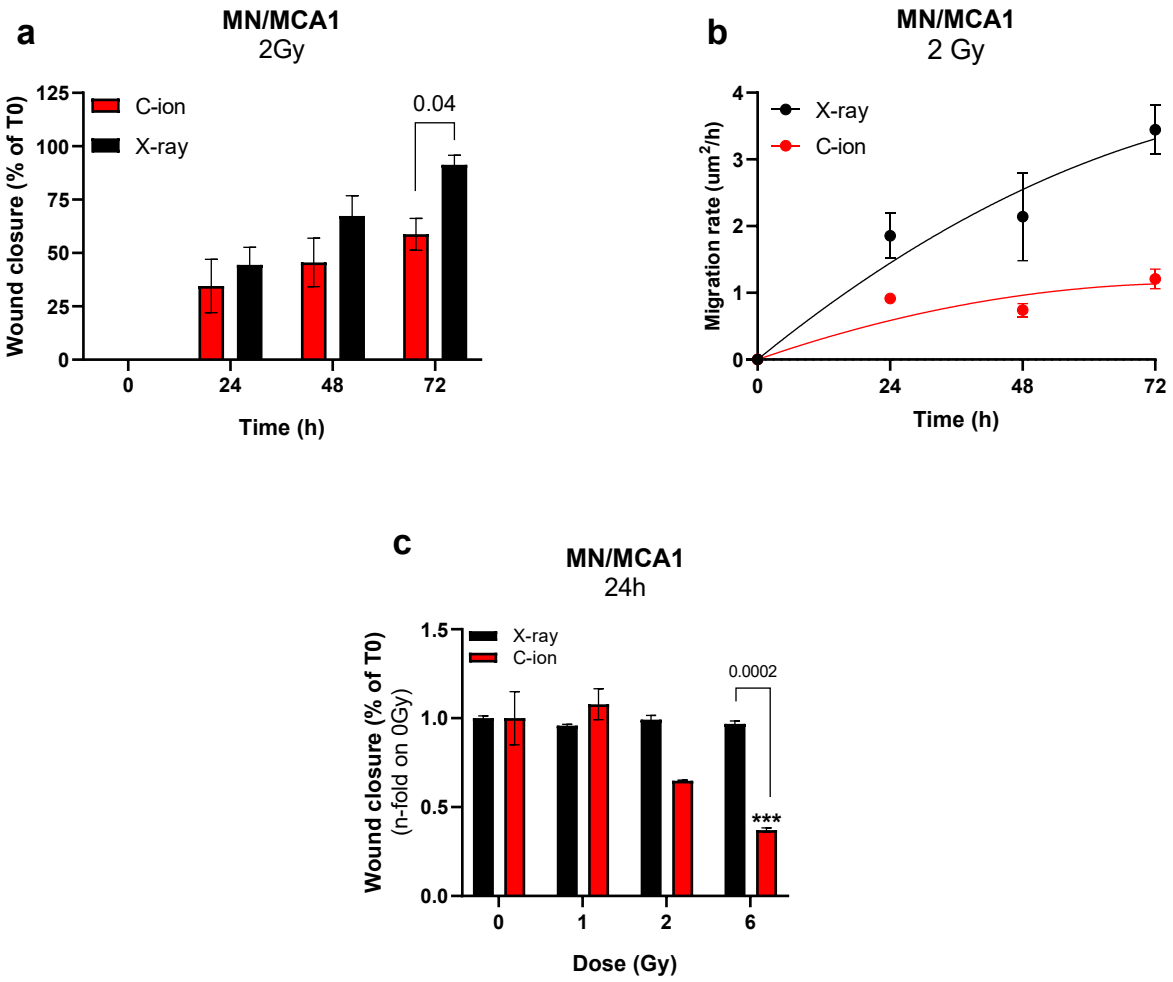

Figure 26: Influence of X-ray and C-ion irradiation in migration capacity of MN/MCA1

Measurement of wound area (um^2) at different time points (24h, 48h, 72h) after X-ray and C-ion irradiation. (a) Comparison between percentage of wound area closure over the time until 72h after irradiation with 2 Gy of X-ray and C-ion. (b) The data represent the migration rate (h^{-1}): $(A_{T0}-A_{Tn})/(A_{T0}$ *Tn) fit with quadratic polynomial formula using GraphPad Prism software. Statistical comparison of the curves was performed using an F-test, revealing significant differences in the overall trends between treatment groups ($p < 0.0001$). (c) Percentage of wound area closure 24h after X-ray and C-ion irradiation at different doses (from 1 to 10 Gy).

Wound area was quantified using Fiji software and is presented as the mean of two technical replicates from three independent biological replicates. Error bars represent the standard error of the mean (SEM). Statistical analysis was performed using two-way ANOVA followed by Sidak's multiple comparisons test. Statistical significance is indicated as follows: *p = 0.033, **p = 0.002, ***p < 0.001, representing differences relative to the corresponding time 0 h or control not irradiated. Differences between the two experimental conditions are reported as exact p-values directly on the graph.

7.2.3.1.1. The migration of MN/MC1 is not influenced by CXCR4- SDF-1 pathway

To complete the results, we evaluated the role of the CXCR4-SDF-1 pathway in migration of MN/MCA1 cells by incubating cells with 100 ng/ml of SDF-1. SDF-1 shows capacity in increasing migration rate in not irradiated MN/MCA1 **(Figure 27**: Migration evaluation by scratch assay of MN/MCA1 cell after X-ray or C-ion irradiation in the presence of SDF-1**a)** with not a significant difference in percentage migration closure **(Figure 27**: Migration evaluation by scratch assay of MN/MCA1 cell after X-ray or C-ion irradiation in the presence of SDF-1. Monitoring the wound area following X-ray and C-ion treatment **(Figure 27c,d)** revealed a persistent reduction in migration capacity post-irradiation with and without SDF-1 incubation. The statistical analyses revealed no significant different with SDF-1 stimulation.

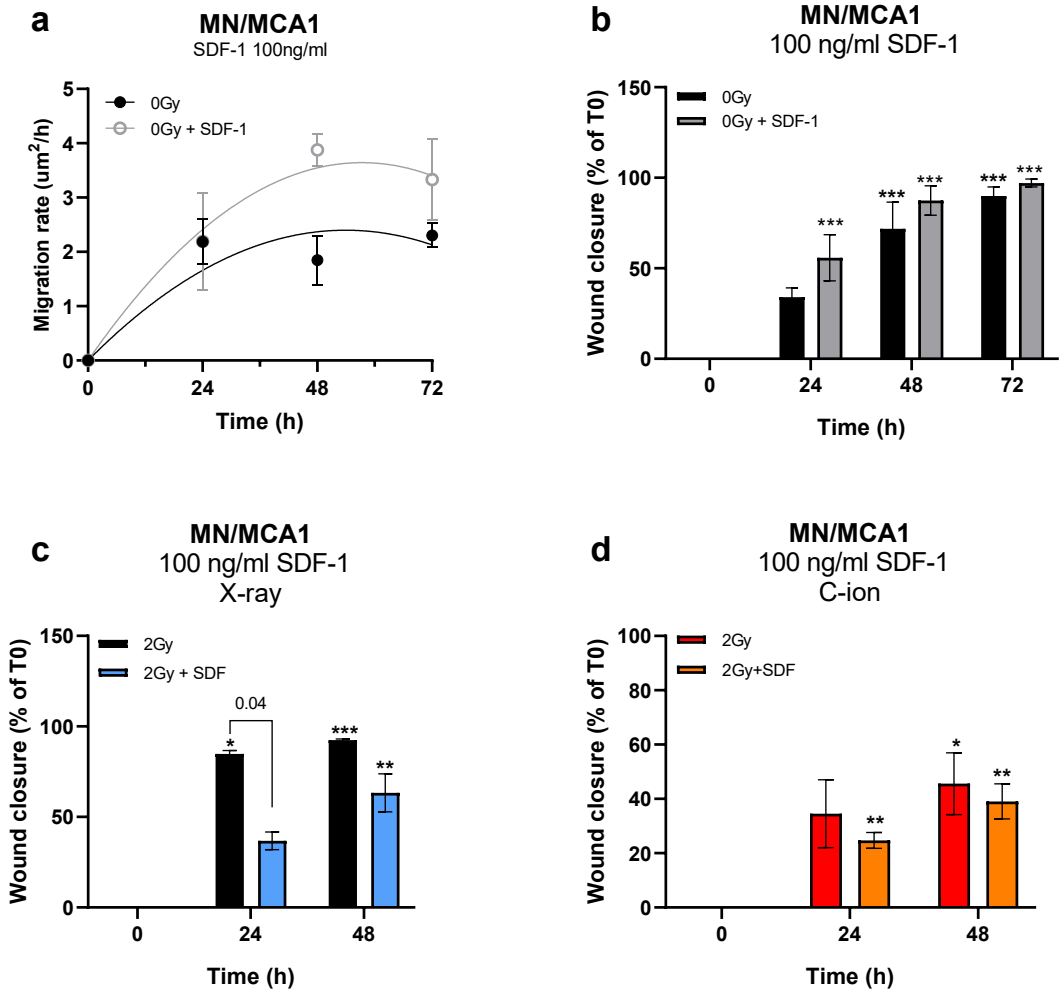

Figure 27: Migration evaluation by scratch assay of MN/MCA1 cell after X-ray or C-ion irradiation in the presence of SDF-1

Measurement of wound area (um2) at different time point (24h, 48h, 72h) following irradiation of MN/MCA1 cell and with SDF-1 incubation

(a) The data represent the migration rate (h^{-1}): $(A_{T0}-A_{Tn})/(A_{T0} *Tn)$ fit with quadratic polynomial formula using GraphPad Prism software. Statistical comparison using an F-test between incubation with and without SDF-1, revealing significant differences in the overall trends between treatment groups (p = 0.04). (b) Percentage of wound area closure over the time in MN/MCA1 with and without SDF-1 incubation. (c) Percentage of wound area closure over the time in MN/MCA1 irradiated with 2 Gy of X-ray with and without SDF-1 incubation. (d) Percentage of wound area closure over the time in MN/MCA1 irradiated with 2 Gy of C-ion with and without SDF-1 incubation. The wound area has been evaluated by Fiji software, and the data represents the mean ± SEM of 3 biological replicates normalised on wound area at time 0h. Statistical analysis was performed using two-way ANOVA followed by Sidak's multiple comparisons test. Statistical significance is indicated as follows: *p = 0.033, **p = 0.002, ***p < 0.001, representing differences relative to the corresponding time 0 h or control not irradiated. Differences between the two experimental conditions are reported as exact p-values directly on the graph.

Based on the results of migration rate 2 Gy of irradiation with X-ray and C-ion significantly reduce the migration velocity trigger by SDF-1 incubation in controls samples (*2 Gy X-ray p = 0.01, 2 Gy C-ion p =0.03*). In terms of migration rate the analyses revealed a significant increase with the incubation of SDF-1 also following C-ion irradiation **Figure 28a**. Consistent with the results in **Figure 24,** C-ion irradiation demonstrated a significantly higher efficacy in inhibiting migration compared to X-ray also with SDF-1 incubation **Figure 28a and b**.

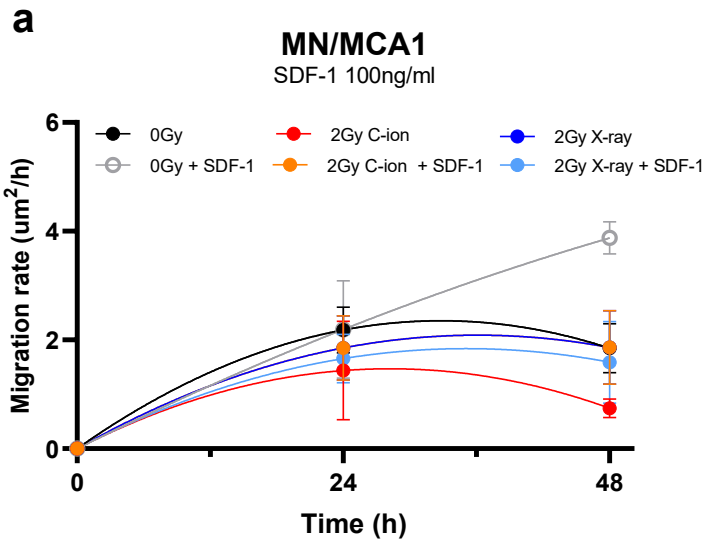

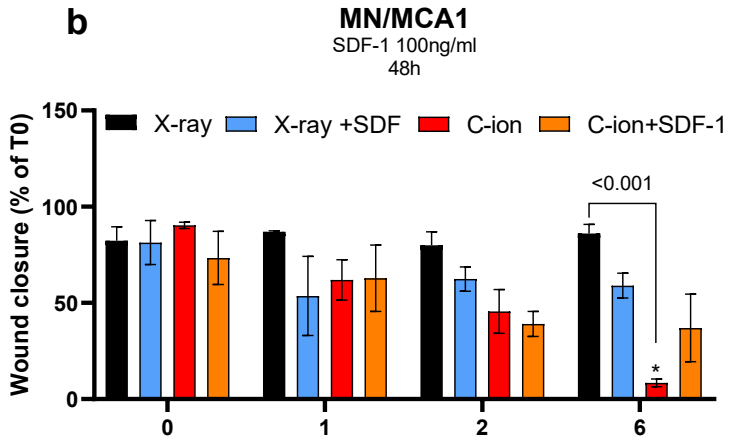

Figure 28:Comparison of X-ray and C-ion modulation of migration capacity by scratch assay of MN/with SDF-1 incubation

(a) The data represent the migration rate (h-1): (AT0-ATn)/(AT0 *Tn) fit with quadratic polynomial formula using GraphPad Prism software. With different colours (0 Gy grey, 2 Gy X-ray blue, 2 Gy C-ion red) are represented the migration rate of MN/MCA1 in comparison between 0 Gy and 2 Gy irradiation with X-ray and C-ion with and without SDF-1 incubation. Statistical comparison using an F-test. (b) The data represent the percentage of wound closure 48 after irradiation with X-ray and C-ion compering different doses (1,2,6, and 10 Gy) and incubation with SDF-1. The wound area has been evaluated by Fiji software, and the data represents the mean ± SEM of 3 biological replicates normalised on wound area at time 0. Data were analysed comparing each dose with respective 0 Gy in divided by time points using an ordinary two-way ANOVA with dose and time as independent factors, followed by Sidak's multiple comparisons test. Statistical significance is indicated as follows: *p = 0.033, **p = 0.002, ***p < 0.001, representing differences relative to the corresponding control not irradiated. Differences between the two experimental conditions are reported as exact p-values directly on the graph.

7.2.3.2. X-ray and C-ion reduce chemoattracted migration in MN/MCA1 cell line assessed by transwell assay

We tested the cell individual migration by chemotaxis with Transwell assay. At very low doses X-ray irradiation significantly boosted cell migration, especially following 1 Gy irradiation (*p-value = 0,0002*), while C-ion irradiation maintained the migration stable **(Figure 29a).** Starting from 2 Gy we can observe a dose-dependent decrease in migration, with C-ion resulting to be more efficient based on statistical analyses (*p-value 0 Gy-10 Gy= 0.0002*). The hypoxia reduced cell migration following X-ray irradiation compared to normoxic condition, with a significant difference only at very low doses, as shown in **Figure 29c** compare to C-ion where we do not see any significant changes between normoxic and hypoxic conditions **(Figure 29d)**.

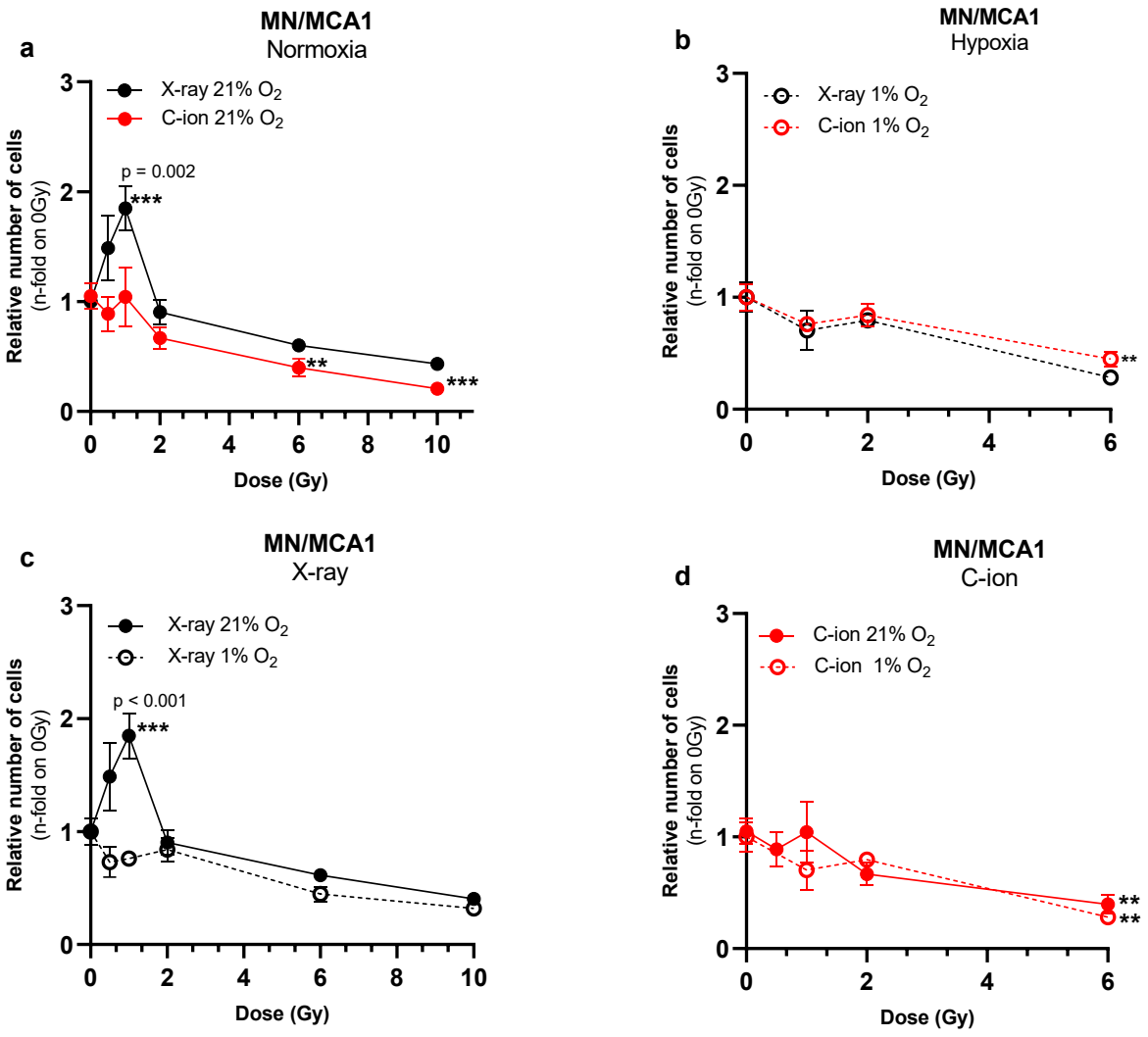

Figure 29: Evaluation of migration capacity of MN/MCA1 cell line

(a) Relative number of cells migrated 24h after X-ray and C-ion irradiation at increased doses, under normoxic condition and normalized on not irradiated samples. (b) Comparison between relative number of cells migrated 24h following X-ray and C-ion irradiation, cultured under hypoxic conditions (1%O_2) for two weeks. (c) Comparison between relative number of cells migrated 24h, following X-ray irradiation, cultured under normoxic and hypoxic condition for two weeks. (d) Comparison between relative number of cells migrated 24h, following C-ion irradiation, cultured under normoxic and hypoxic condition for two weeks. Data are presented as the mean and standard deviation (SEM) of three independent experiments. Statistical significance (p-value <0.05) was assessed using a Two-way ANOVA, followed by Sidak's post-hoc test for multiple comparison Statistical significance is indicated as follows: *p < 0.033, **p < 0.002, ***p < 0.001, representing differences relative to the corresponding control not irradiated. Differences between the two experimental conditions are reported as exact p-values directly on the graph.

7.3. Activation of immunogenic effect and immunostimulatory response by irradiation

7.3.1. X-ray irradiation induces chemokine release in dose dependent manner

To characterize the soluble inflammatory response to irradiation, we quantified the release of a type I interferon (IFN-β), an interferon-inducible chemokine (CXCL10/IP-10), a pro-inflammatory cytokine (IL-6, TNF- α), and a hematopoietic growth factor (GM-CSF), in the supernatant of MN/MCA1 cells. These cytokines were selected as representative components of the inflammatory profile produced by irradiated tumour cells. Their release was monitored at 48, 72, and 96 hours after X-ray exposure. Across most cytokines, a significant dose-dependent increase in release was observed, with IFN-β **(Figure 30a)**, IL-6 **(Figure 30e)**, TNF-α **(Figure 30d)** showing maximum concentrations 72 hours post-irradiation, while GM-CSF continued to rise and reached its highest levels at 96 hours **(Figure 30b)**. Among these, IL-6 **(Figure 30e)** and GM-CFS **(Figure 30b)** showed the most pronounced time-dependent increase after 8 Gy irradiation with significant difference, whereas IFN-β, TNF-α, and CXCL10 were induced too, but without significant differences emerged between the time point **(Figure 30).**

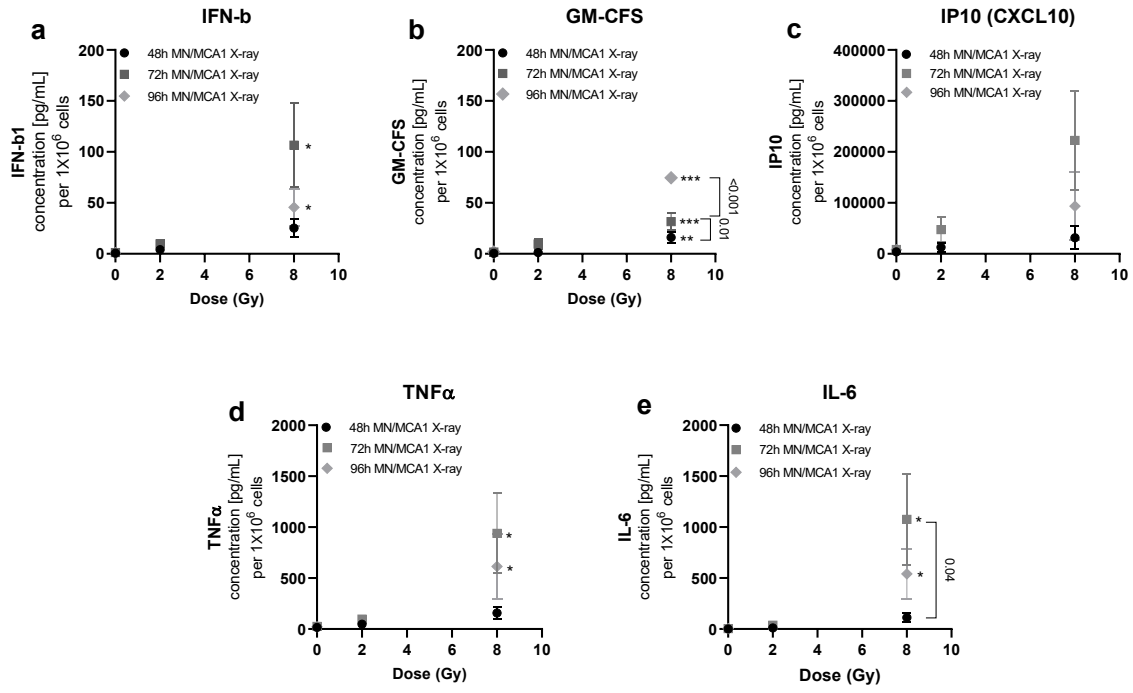

Figure 30: Induction of chemokine release by X-ray irradiation in MN/MCA1

Concentration of chemokine released by MN/MCA1 cells into the supernatant following X-ray irradiation.(a) IFN-β, (b) GM-CFS, (c) IP10 (CXCL10), (d) TNF-α, and (e) IL-6 levels were quantified in pg/mL and calculated per 1×10⁶ cells at different time points 48, 72, and 96h after

exposure to 2 Gy and 8 Gy X-ray. Data represent the mean of three biological replicates; error bars indicate standard error of the mean (SEM). Each biological replicate was measured in technical duplicates. Statistical significance (p-value <0.05) was assessed using a Two-way ANOVA, followed by Sidak's post-hoc test for multiple comparison. Statistical difference is indicated as follows: *p < 0.033, **p < 0.002, ***p < 0.001, representing differences relative to the corresponding control not irradiated. Differences between the experimental time points are reported as exact p-values directly on the graph.

7.3.2. Immunogenic cell death (ICD) signals induced by irradiation

High-LET ionizing radiations, such as carbon ions, are reported to be more immunogenic than conventional X-ray (Helm et al. 2021). This superior immunogenicity is characterized by the enhanced release of damage-associated molecular patterns (DAMPs), which serve as critical 'danger signals' that promote dendritic cell recruitment and trigger robust antitumour immune responses (Galluzzi et al. 2017). Among these, HMGB1 and calreticulin (CRT) represent central mediators of immunogenic cell death. In our experiments, we studied the concentration of HMGB1 release in MN/MCA1 supernatant following X-ray and C-ion irradiation at different time points and oxygen concentrations.

7.3.2.1. Irradiation and hypoxic condition modulate HMGB1 release in MN/MCA1 cells

The results, depicted in **Figure 31a,** show a dose-dependent increase after both X-ray and C-ion irradiation, with maximal levels detected 72 hours after treatment. Interestingly, photons induced slightly higher extracellular HMGB1 compared with carbon ions, at all measured time points (48-72–96 h).

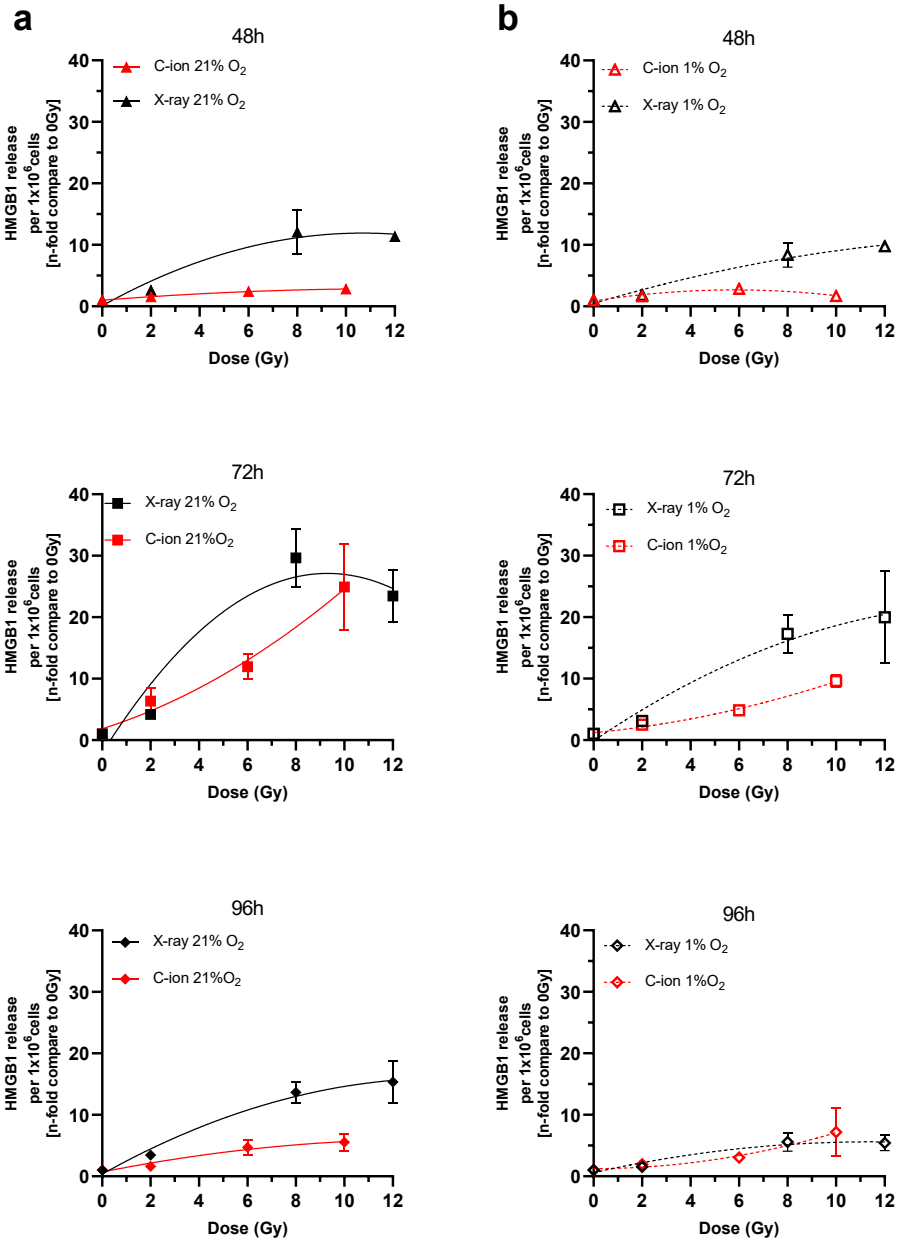

Figure 31: Irradiation induces HMGB1 release in MN/MCA1 cells

(a) Comparison of HMGB1 release after X-ray and C-ion by MN/MCA1 cell under normoxic conditions. The molecules were measured in cell supernatant and calculated based on $1x10^6$ cells at different time points (48h, 72h and 96h). The overall trend after X-ray irradiation is

significantly higher compared to C-ion, particularly at 72 h and 96 h $p < 0.001$. (b) The graphs show HMGB1 release, by MN/MCA1 cells, under hypoxic conditions (1%O_2), 48h, 72h and 96h following X-ray and C-ion irradiation. The HMGB1 release trend was fitted with polynomial quadratic model, and the statistical difference was calculated by extra sum of squares F text. Data represents the mean of three biological replicates; error bars indicate standard error of the mean (SEM). Each biological replicate was measured in technical duplicates.

As shown in **Figure 31b**, culturing the cells under low oxygen concentration (1% O_2) reduced the immune response in MN/MCA1 cells. In line with scratch migration assay and viability assay, our results suggest that maintaining the cells for two weeks at 1% O_2 concentration drastically reduces the immunogenic effect of irradiation after both irradiation qualities, in line with normoxic trend **Figure 32**.

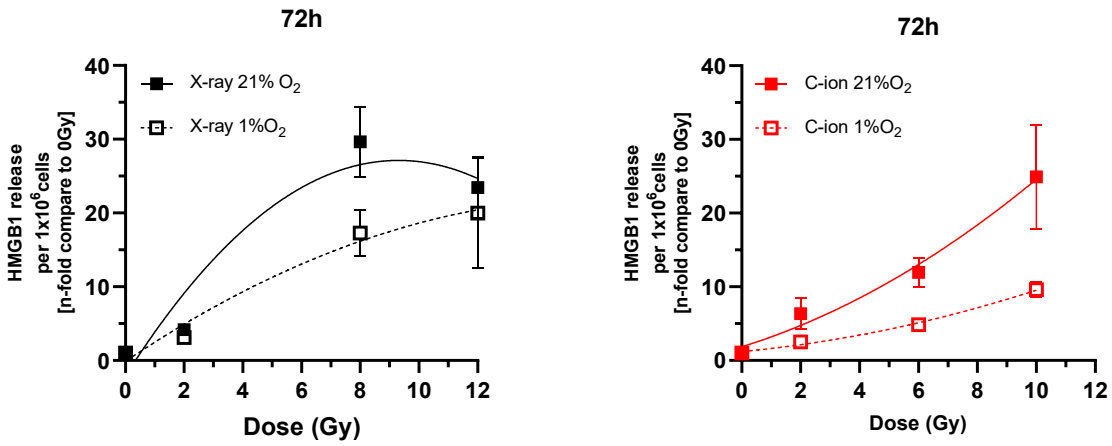

Figure 32: Effect of hypoxia in HMGB1 release after radiation of MN/MCA1 cells

Comparison in HMGB1 release X-ray (a) and C-ion (b) irradiations by MN/MCA1 cell under normoxic and hypoxic conditions. The exposition was evaluated at different time points (here show only 72h). The overall trend under normoxic conditions is significantly higher compared to hypoxia only following C-ion irradiation (C-ion $p = 0.0023$). The HMGB1 release trend was fitted with polynomial quadratic model, and the statistical difference was calculated by extra sum of squares F text. Data represents the mean of three biological replicates; error bars indicate standard error of the mean (SEM). Each biological replicate was measured in technical duplicates.

7.3.2.2. Irradiation triggers calreticulin exposure in MN/MCA1 cell line under normoxic and hypoxic conditions

Calreticulin, a key marker of immunogenic cell death, translocate from the endoplasmic reticulum to the cell surface upon ICD induction. We quantified CRT surface exposure by flow cytometry in

MN/MCA1 cells, following X-ray and C-ion irradiation. As shown in **Figure 33a**, both irradiation modalities triggered a dose-dependent increase in CRT exposure, with no significant differences observed between X-ray and C-ion across the time points analysed (48, 72, and 96 hours).

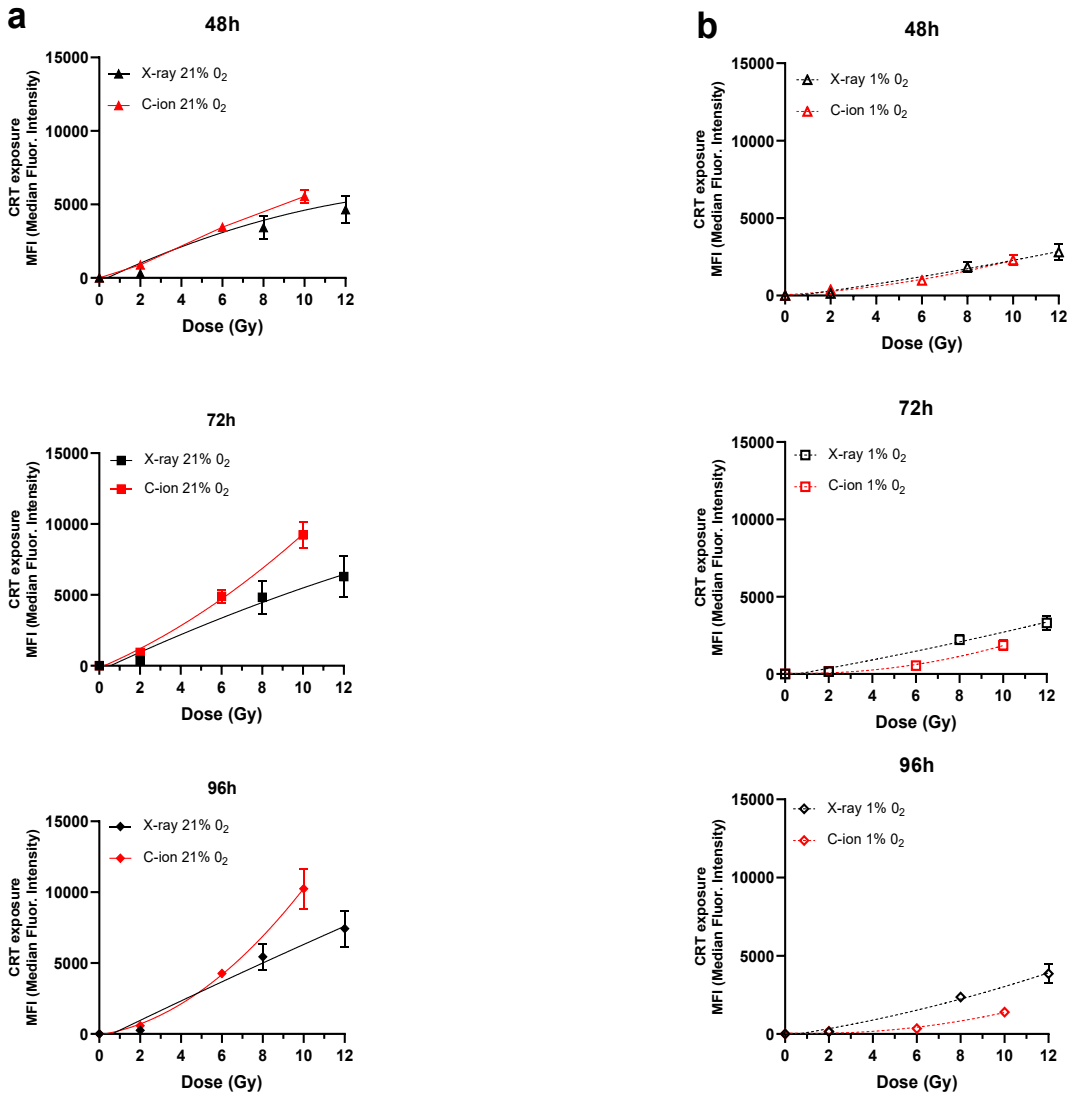

Figure 33: Irradiation induces calreticulin (CRT) exposure on MN/MCA1 cell surface. Comparison in CRT exposure after X-ray and C-ion irradiations by MN/MCA1 cell under normoxic conditions. The exposition was evaluated at different time points (48h, 72h and 96h). The overall trend after C-ion irradiation is significantly higher compared to X-ray at 72 h and 96 h after irradiation $p < 0.006$. (b) The graphs show CRT exposure, by MN/MCA1 cells, under hypoxic conditions ($1\%O_2$), 48h, 72h and 96h following X-ray and C-ion irradiation. Data represents the mean of the median of fluorescent intensity measured in 30000 events, for each biological replicate. Data represents the mean of three biological replicates; error bars indicate standard error of the mean (SEM). Each biological replicate was measured in technical duplicates. The trends were fitted with polynomial quadratic model, and the statistical difference was calculated by extra sum of squares F-text.

.

To assess the impact of hypoxia, CRT exposure was measured in cells maintained for two weeks at 1% O_2. **Figure 33b** describes CRT translocation following irradiation in hypoxic cells. In accordance with HMGB1 release, low oxygen presence reduces DAMPs following both radiation qualites **(Figure 34).** As for normoxic conditions, no significant differences were detected between irradiation types or among the different time points, in hypoxic cells. These results indicate that while CRT exposure is responsive to irradiation dose, it is largely independent of irradiation modality and time and is attenuated under hypoxic conditions.

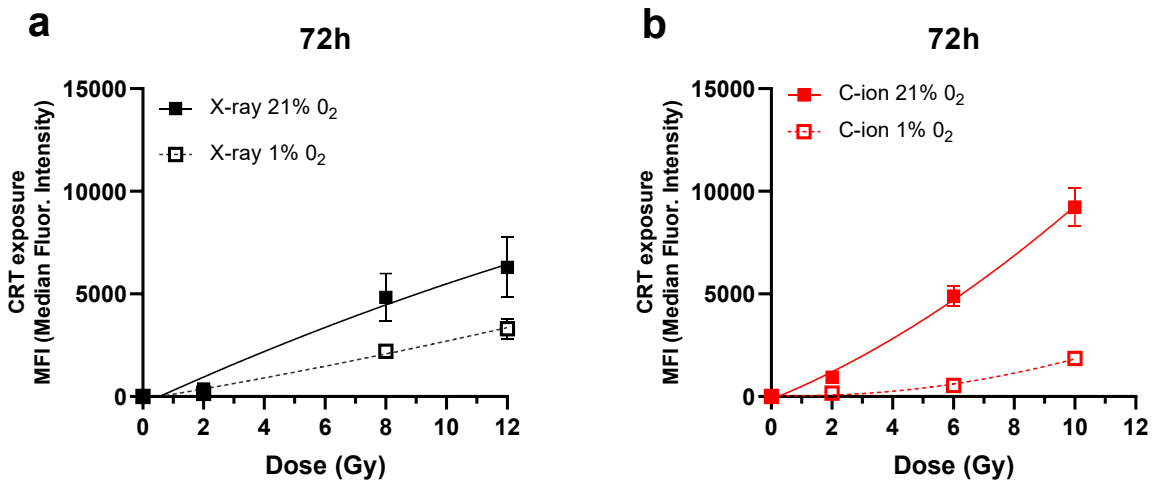

Figure 34: Effect of hypoxia in calreticulin exposure following irradiation

Comparison in CRT exposure after X-ray (a) and C-ion (b) irradiations by MN/MCA1 cell under normoxic and hypoxic conditions (1%O_2). The exposition was evaluated at different time points (here show only 72h). The overall trend that represents CRT increase through the doses under normoxic conditions is significantly higher compared to hypoxia (X-ray $p < 0.0068$, C-ion $p < 0.0001$). The HMGB1 release trend was fitted with polynomial quadratic model, and the statistical difference was calculated by extra sum of squares F text. Data represents the mean of three biological replicates; error bars indicate standard error of the mean (SEM). Each biological replicate was measured in technical duplicates.

7.4. Evaluation of complement system activation following X-ray and carbon ion irradiation, and influence of hypoxic condition

7.4.1. Irradiation induces general increase of C3 in MN/MCA1 cells

As previously described (**4.4.1.2***),* the complement system is a fundamental component of innate immunity, with emerging research underscoring its significant role in tumour progression. Within the tumour microenvironment (TME), complement factors are primarily exposed by infiltrating immune cells, while their expression by malignant cells is generally considered less frequent (Pio, Ajona, and Lambris 2013). MN/MCA1 shows a very low amount of C3 express on the cell surface that should be consider the active subunit **(**Figure 35**).**

To investigate whether MN/MCA1 cells actively influence complement activation following radiotherapy, we quantified both total C3 expression and membrane-bound C3 on MN/MCA1 cells at 24, 48, and 72 hours post-irradiation. Given its position in the complement cascade, C3 serves as the primary substrate for generating downstream anaphylatoxins.

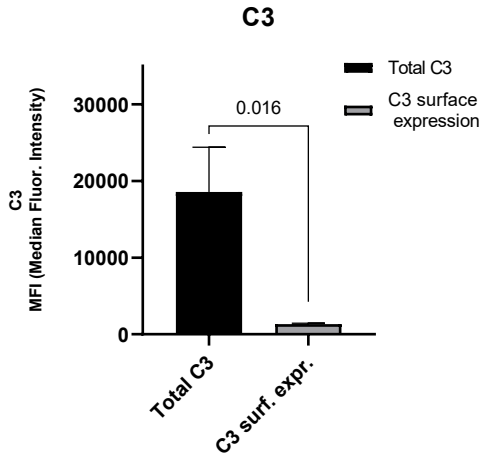

Figure 35: C3 base line expression in MN/MCA1 cell line

Comparison between total C3 quantification in MN/MCA1 cells following fixation and permeabilization and C3 surface expression. Significant difference calculated by Mann-Whitney test. Data are obtained from cells cultured in normoxic conditions, with heat inactivated FBS. Quantification by the median of fluorescent intensity in 30000 events for each biological replicate. Data show the mean ± SEM of 3 biological replicates.

Our results demonstrate no variation in total C3 expression in MN/MCA1 cells trough the time and an increased in a dose-dependent manner following irradiation. This total upregulation was observed across both radiation qualities, reaching the only significant increase 72 hours after 10 Gy C-ion irradiation (**Figure 36a**). A similar trend was observed for C3 surface expression, which showed a

marked increase compared to non-irradiated samples, particularly at higher doses and later time points after C-ion irradiation (6 and 10 Gy, 48h and 72h after irradiation) (**Figure 36b**). The difference between the two radiation qualities is visible only for the C3 surface expression, with a significant efficacy of C-ion 48h after irradiation compare to X-ray (**Figure 36b**) **(Figure S 4b)**.

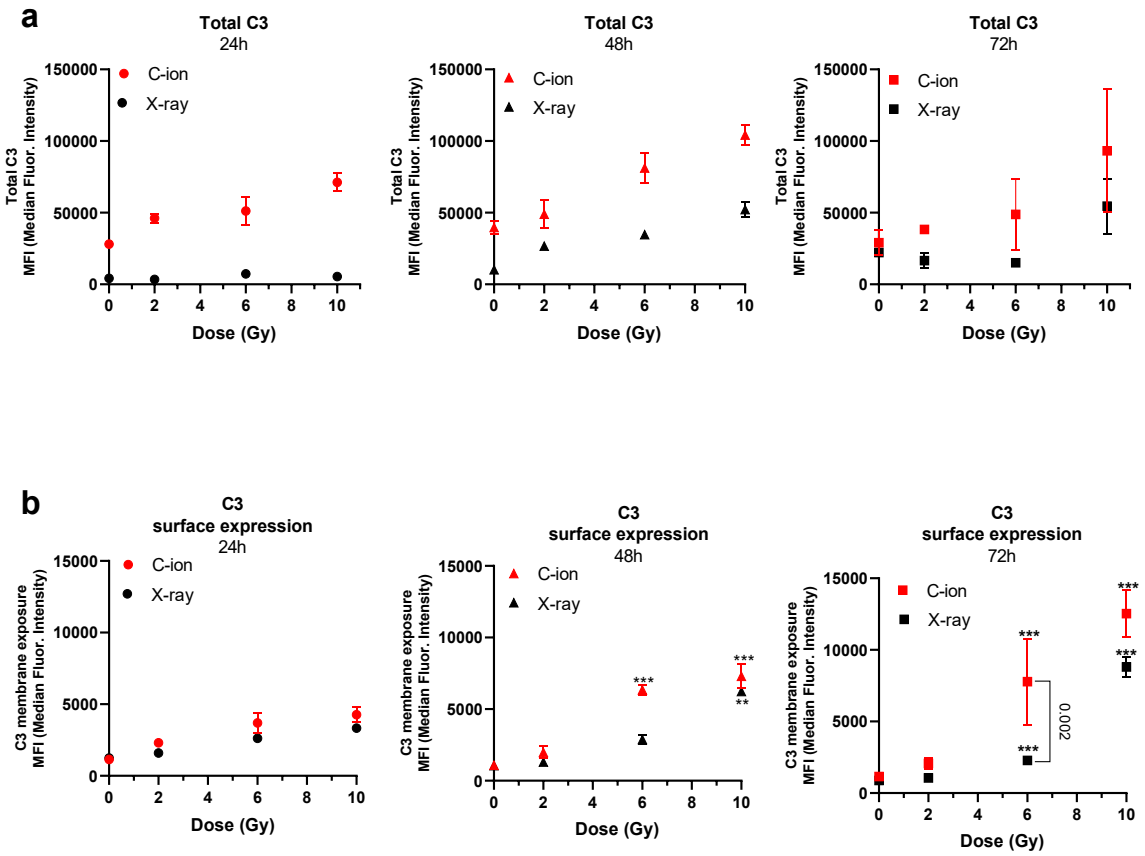

Figure 36: C3 complement factor expression in MN/MCA1 after X-ray and C-ion irradiation

(a) Total C3 quantification in MN/MCA1 cells after irradiation with fixation and permeabilization, to detect the amount of the protein also inside of the tumour cells at different time point (24h-48h-72h). (b) Detection of C3 expression on the cell surface 24-48-72h after X-ray and C-ion irradiation. Data are obtained from cells cultured in normoxic conditions, with heat inactivated FBS. Statistical significance determined using the ANOVA test and Holm-Sidak method correction, noted in the graphs with p-value for X-ray and C-ion comparison and with * p-value < 0.05 comparing 0 Gy with the other doses. Quantification by the median of fluorescent intensity in 30000 events for each biological replicate. Data show the mean ± SEM of 3 biological replicates. Statistical significance (p-value <0.05) was assessed using a Two-way ANOVA, followed by Sidak's post-hoc test for multiple comparison. Statistical difference is indicated as follows: *p < 0.033, **p < 0.002, ***p < 0.001, representing differences relative to the corresponding control not irradiated. Differences between the radiation qualities are reported as exact p-values directly on the graph.

7.4.2. Influence of irradiation on C3b deposition in MN/MCA1 cells

After confirming the ability of irradiation to increase total C3 levels, we investigated the production of C3 key activation products: C3b and C3a. To this end, C3b deposition was quantified 24 hours after exposing tumour cells to increasing doses of X-ray and carbon ions. In these conditions, the detected C3b reflects the cleavage of C3 produced by the tumour cells themselves, as they represent the only source of complement proteins in cell culture under serum free conditions.

Since the prevailing hypothesis in the field is that most of complement factors in the tumour microenvironment originate from systemic sources rather than from tumour cells (Pio et al. 2019), we intended to mimic this situation by incubating the irradiated cells with mouse serum, used here as a surrogate for circulating complement *in vivo*.

In MN/MCA1 cells, irradiation induced a clear dose-dependent increase in C3b deposition **(Figure 37)**. When cells were irradiated in the absence of serum, thereby limiting complement availability to that produced by tumour cells themselves, Carbon ion irradiation showed a tendency towards increased C3b deposition compared with X-rays, although this difference did not reach statistical significance. However, upon serum supplementation, which provides an exogenous source of complement similar to the *in vivo* situation, both irradiation qualities promoted a dose-dependent increase comparing the respective values for the same dose. Especially C-ion treatment shows a dose-dependent increase *($p = 0.004$ for 6 Gy and $p = 0.001$ for 10 Gy compared to control)* (**Figure 37a)**. Importantly, the presence of serum markedly amplified this effect, suggesting that complement activation is strongly potentiated when systemic components are available. This observation is consistent with previous reports describing a limited basal complement production by MN/MCA1 cells (Magrini et al. 2021).

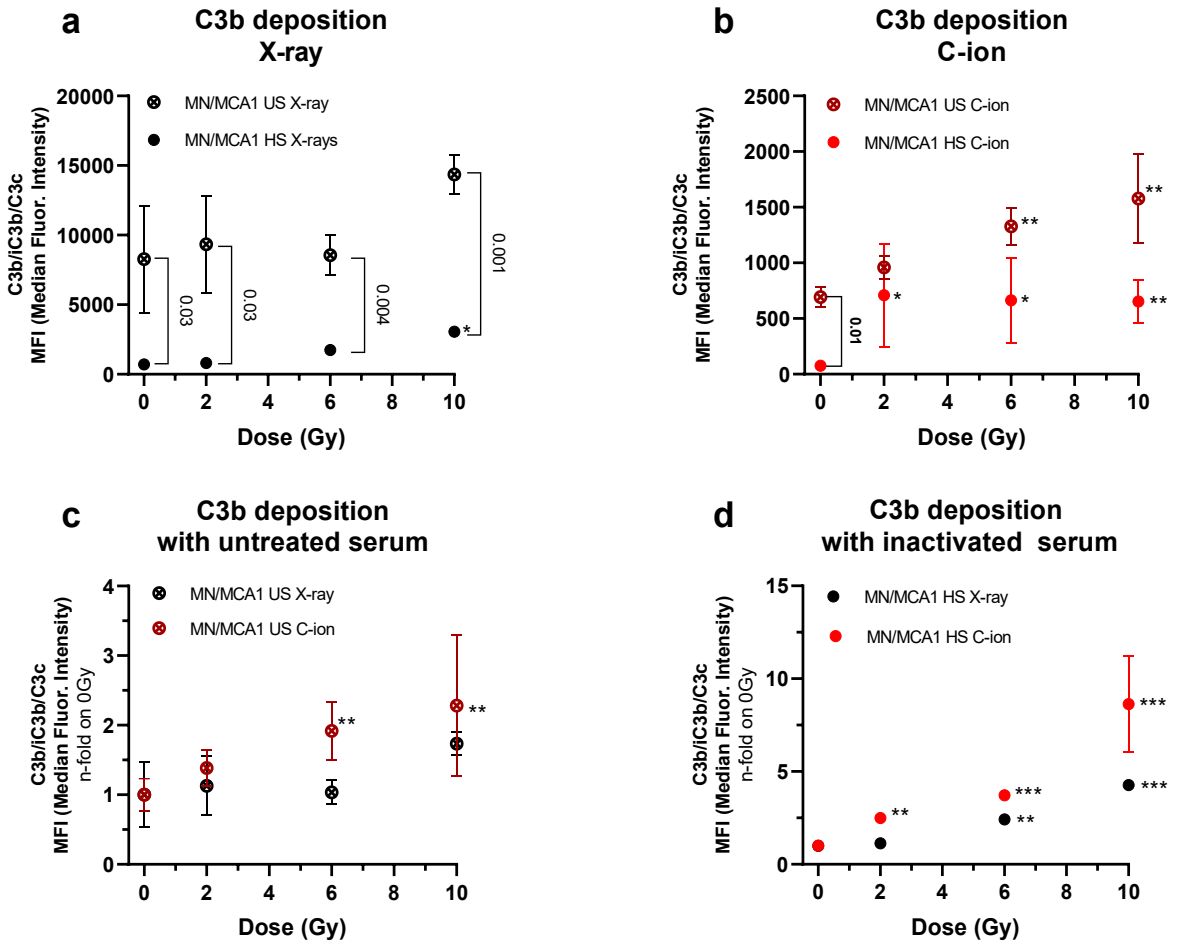

Figure 37: C3b deposition on MN/MCA1 cells following irradiation

(a) C3b deposition quantification 24h after X-ray irradiation and incubation with mouse serum, untreated (US) or heat inactivated (HS). (b) C3b deposition quantification 24h after C-ion irradiation and incubation with mouse serum untreated (US) and heat inactivated (HS). (c) Comparison of C3b deposition quantification 24h after X-ray and C-ion irradiation and incubation with mouse serum activated (US). (d) Comparison of C3b deposition quantification 24h after X-ray and C-ion irradiation with incubation with mouse serum heat inactivated (HS). C3b deposition quantified by the median of fluorescent intensity in 30000 events for each biological replicate. Data show the mean ± SEM of 3 biological replicates. Statistical significance (p-value <0.05) was assessed using a Two-way ANOVA, followed by Sidak's post-hoc test for multiple comparison. Statistical difference is indicated as follows: *p < 0.033, **p < 0.002, ***p < 0.001, representing differences relative to the corresponding control not irradiated. Differences between the experimental conditions (a, b) and radiation qualities (c, d) are reported as exact p-values directly on the graph.

We previously demonstrated that hypoxia (1% O_2) attenuates the immune response, specifically by reducing the release of damage-associated molecular patterns (DAMPs) **(Figure 31-Figure 33).**

Building upon these findings, we investigated whether chronic exposure to hypoxia (1% O_2 for two weeks) modulates complement activation in MN/MCA1 following irradiation.

As shown in **Figure 38b and c**, irradiation alone does not induce significant C3b deposition under hypoxic conditions. Notably, substantial C3b accumulation was only achieved following incubation with untreated mouse serum, suggesting that exogenous complement factors are required for robust activation in this environment. Furthermore, we observed a general downward trend of C3b deposition in cells cultured under hypoxia compared to normoxia, suggesting that low-oxygen conditions may drive an inhibitory effect on complement deposition.

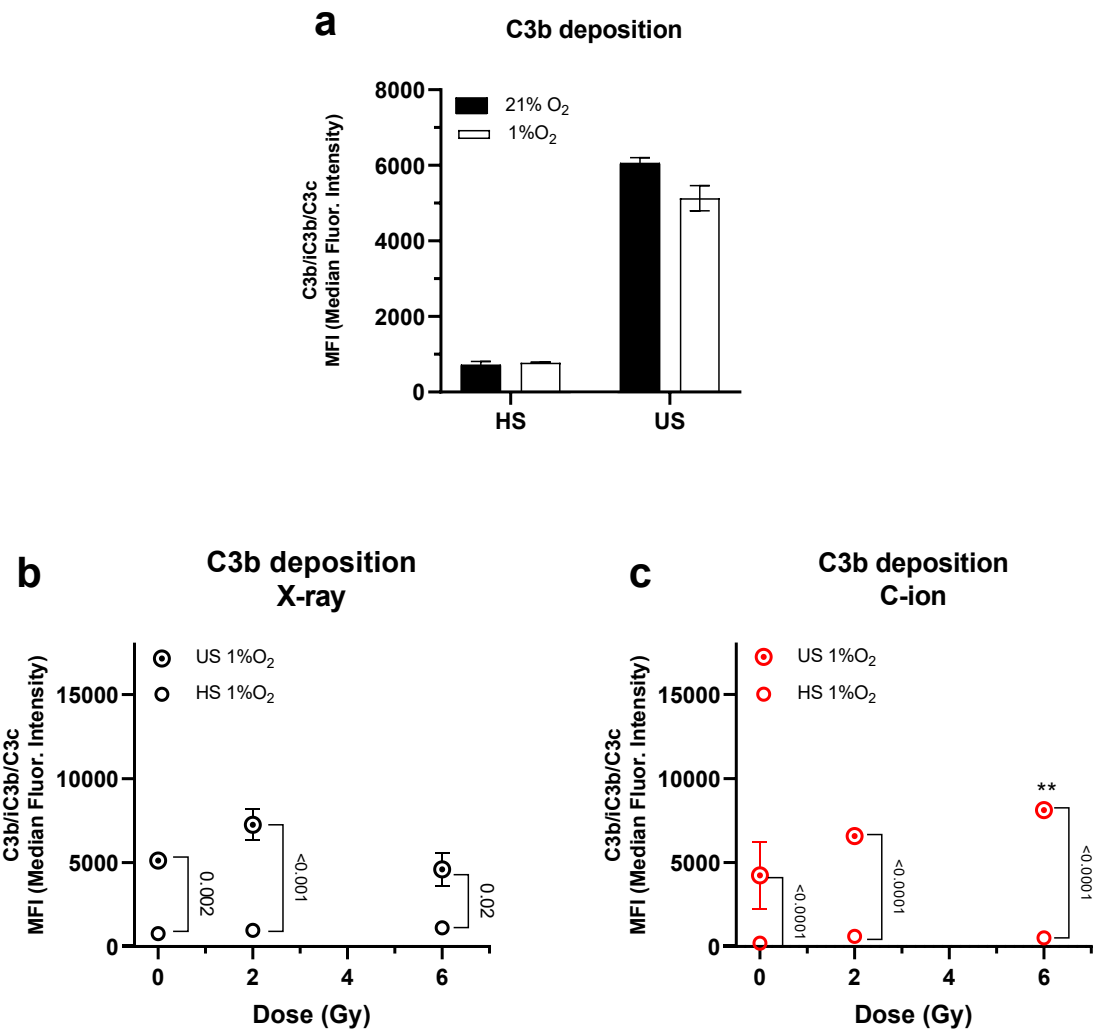

Figure 38: C3b deposition on MN/MCA1 cells following irradiation under hypoxic conditions

C3b deposition on MN/MCA1 culturing for two weeks under hypoxic conditions (1%O_2). (a) Comparison C3b deposition baseline in M/MCA1 under hypoxia and normoxic conditions with untreated mouse serum (US) and heat inactivated (HS) incubation. (b) Comparison in C3b deposition 24h after X-ray irradiation and incubation with untreated mouse serum (US) and heat

inactivated (HS). (b) Comparison in C3b deposition 24h after C-ion irradiation and incubation with mouse serum activated (US) and heat inactivated (HS)

Quantification by the median of fluorescent intensity in 30000 events for each biological replicate. Quantification by the median of fluorescent intensity in 30000 events for each biological replicate. Data show the mean ± SEM of 3 biological replicates. Statistical significance (p-value <0.05) was assessed using a Two-way ANOVA, followed by Sidak's post-hoc test for multiple comparison. Statistical difference is indicated as follows: *p < 0.033, **p < 0.002, ***p < 0.001, representing differences relative to the corresponding control not irradiated. Differences between experimental conditions are reported as exact p-values directly on the graph.

7.4.3. Cell line radiosensitivity and different complement base line expression influence complement system activation induced by irradiation

To further dissect the influence of intrinsic complement production and radiosensitivity on complement activation, we extended our analysis to additional tumour cell lines (4T1 and B16) with different baseline complement expression levels.

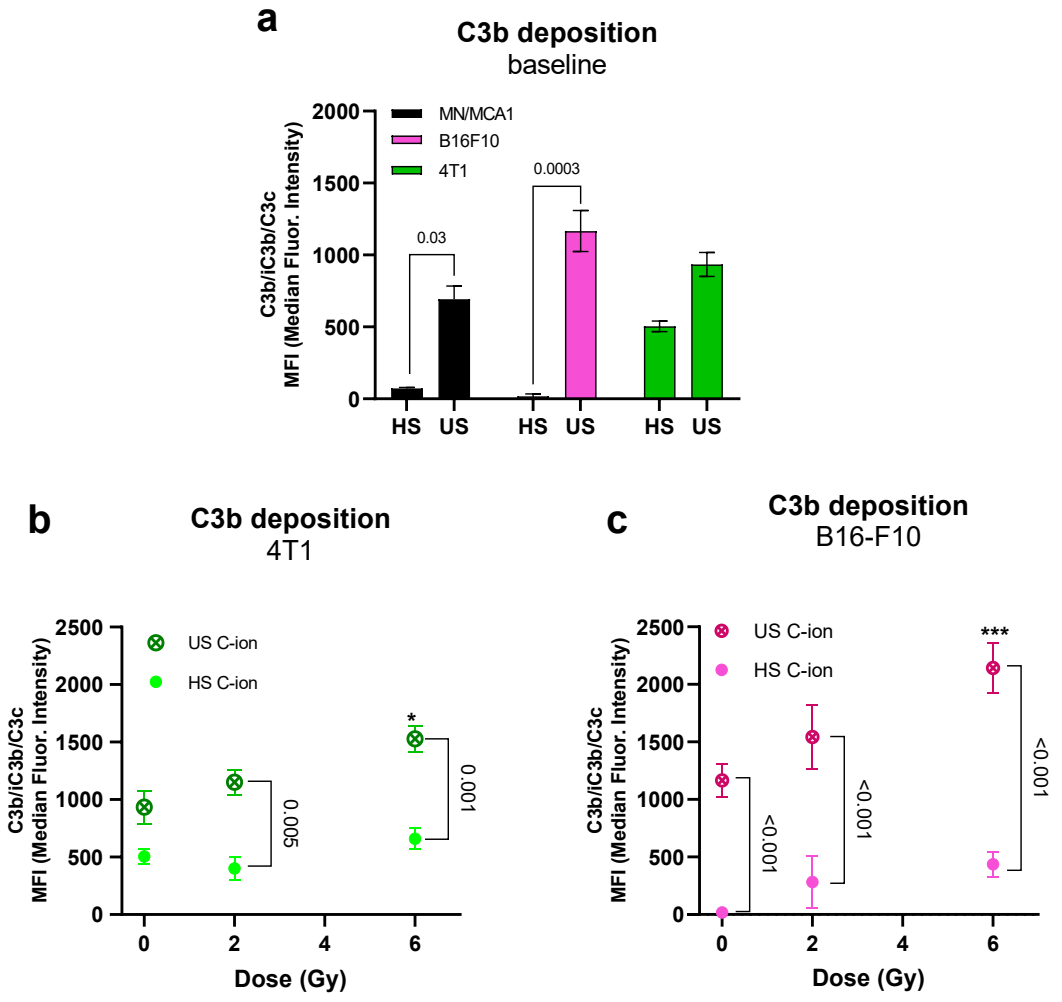

Figure 39: C3b deposition on 4T1 and B16-F10 cells following C-ion irradiation

(a) C3b deposition baseline quantification in MN/MCA1, 4T1 and B16F10 with mouse serum untreated (US) and heat inactivated (HS) incubation. (b) C3b deposition quantification in 4T1 cells 24h after C-ion irradiation with incubation with mouse serum untreated (US) and heat inactivated (HS). (c) C3b deposition quantification in B16-F10 cells 24h after C-ion irradiation with incubation with mouse serum untreated (US) and heat inactivated (HS). Quantification by the median of fluorescent intensity in 30000 events for each biological replicate. Data show the mean ± SEM of 3 biological replicates. Statistical significance (p-value <0.05) was assessed using a Two-way ANOVA, followed by Sidak's post-hoc test for multiple comparison. Statistical difference is indicated as follows: *p < 0.033, **p < 0.002, ***p < 0.001, representing differences relative to the corresponding control not irradiated. Differences between experimental conditions are reported as exact p-values directly on the graph.

As shown in **Figure 39a,** 4T1 breast carcinoma cells displayed markedly higher baseline levels of C3b deposition compared to MN/MCA1 and B16 melanoma cells. However, C-ion induced only a modest increase of these complement fragments in 4T1 cells, whereas B16 cells, which exhibited very low baseline levels of C3b, showed a more pronounced irradiation-induced enhancement and different radiosensitivity. Consistent with the findings in MN/MCA1 cells, the addition of mouse serum after Carbon ion irradiation further boosted complement activation in both B16 and 4T1 cells. The effect was particularly evident in B16-F10 cells **(Figure 39c)**, suggesting that the extent of complement activation following irradiation depends not only on the cell specific radiosensitivity but also on the intrinsic complement production capacity of the tumour cells and the availability of systemic complement sources.

7.4.4. Irradiation induced anaphylatoxins release: C3a release in MN/MCA1 cell line and C3aR receptor

To complete the analysis of complement activation induced by irradiation, we also investigated the release of anaphylatoxins, focusing on C3a. As shown in **Figure 40,** irradiation triggers C3a release into the cell culture supernatant in a dose-dependent manner. A modest increase was already detectable 24 hours after treatment, although no significant differences were observed between X-ray and carbon ions at this time point, under normoxic and hypoxic conditions **(Figure 40).** However, 72 hours post-irradiation under normoxic conditions C3a release was significantly increased, and a clear difference emerged between the two irradiation qualities, with carbon ions inducing a stronger response (supplementary Errore. L'origine riferimento non è stata trovata.**S 5**). These findings are in line with previous reports describing complement activation and anaphylatoxin release as part of the cellular stress and danger signalling triggered by irradiation (Surace et al. 2015).

C3a has been implicated not only in the amplification of inflammation but also in the modulation of anti-tumour immunity, where its effects can be context-dependent, either supporting immune activation or promoting immunosuppression within the tumour microenvironment. Therefore, our results suggest that carbon ion irradiation, by inducing a more pronounced release of C3a compared to photons, may differentially shape complement-mediated signalling in the tumour setting.

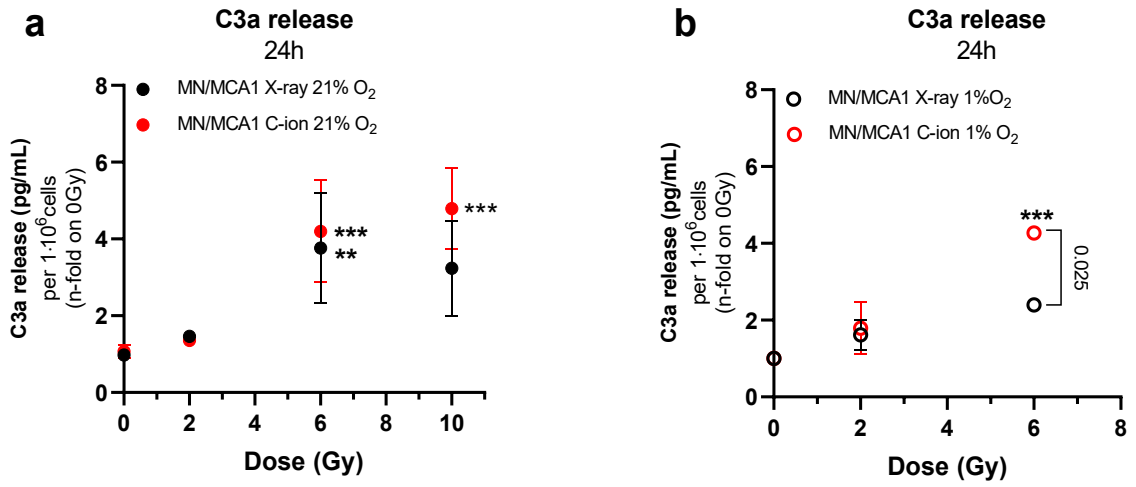

Figure 40: C3a release in MN/MCA1 supernatant following irradiation and at different oxygen concentrations

(a) C3a release in supernatant of MN/MCA1 cells 24h after irradiation with X-ray and C-ion, in normoxic condition (b) C3a release in MN/MCA1 cells' supernatant under chronic hypoxia, 24h following irradiation with X-ray and C-ion in normoxic condition. Data are obtained from supernatant of cells cultured with heat inactivated FBS. Data show the mean ± SEM of C3a concentration in pg/ml of 3 biological replicates. Statistical significance (p-value <0.05) was assessed using a Two-way ANOVA, followed by Sidak's post-hoc test for multiple comparison. Statistical difference is indicated as follows: *p < 0.033, **p < 0.002, ***p < 0.001, representing differences relative to the corresponding control not irradiated. Differences between radiation qualities are reported as exact p-values directly on the graph.

As discussed in the introduction **(4.4.1.2),** the anaphylatoxin C3a is a potent soluble mediator that exerts its biological effects by binding to the C3a receptor (C3aR). While C3aR is conventionally associated with immune cell populations, it is also expressed by various malignant cells, where it can modulate intracellular signalling.

We investigated whether ionising radiation influences C3aR expression and the subsequent activation of its downstream pathways in MN/MCA1. As shown in **Figure 41a**, both radiation qualities induced an upregulation of C3aR, with Carbon-ion (C-ion) irradiation eliciting a

significantly more pronounced effect at higher doses (6 and 10 Gy) compared to X-ray. C-ion treatment did not exhibit a strong temporal dependence, with elevated C3aR levels remaining relatively stable between 24 and 48 hours post-exposure **Figure 41b.** The concurrent increase in both C3a secretion and C3aR expression suggests an irradiation-induced activation of the complement axis.

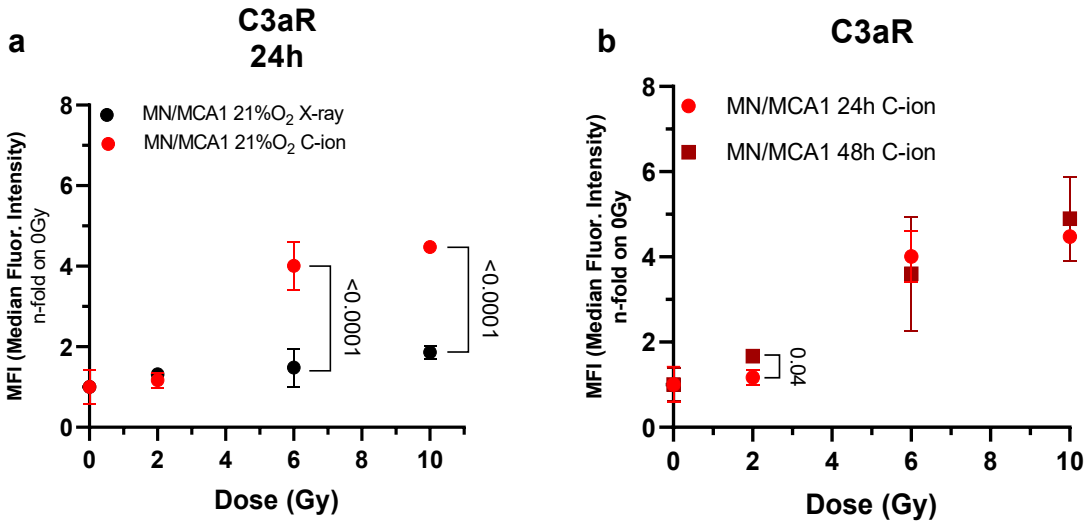

Figure 41: C3aR expression on MN/MCA1 cells following irradiation

(a) C3aR quantification in MN/MCA1 cells 24h after irradiation with X-ray and C-ion. (b) Detection of C3aR expression on the cell surface of MN/MCA1 cells 24 and 48h after C-ion irradiation. Data are obtained from cells cultured in normoxic conditions, with heat inactivated FBS. Quantification by the median of fluorescent intensity in 30000 events for each biological replicate. Each timepoint includes 3 biological replicates. Statistical significance was determined by two-way ANOVA followed by Sidak's post hoc test for multiple comparisons.

7.4.5. Irradiation influences complement inhibitors on the cellular surface

The complement system is a fundamental and complex cascade of protein activation, tightly controlled by various regulatory molecules such as CD55. CD55, also known as decay-accelerating factor, inhibits complement activation by preventing the formation of the C3 convertase through its interaction with membrane-bound C4b and C3b, thereby disrupting the polymerization required for convertase assembly (section 4.4.1.1). With this study we aim to investigate how irradiation influences these regulators. As shown in **Figure 42a**, radiation exposure yielded a dose-dependent increase in CD55 surface expression 24 hours post-irradiation, with higher efficacy following C-ion irradiation, particularly at higher doses (6 Gy and 10 Gy) **(Figure 42a)**. Furthermore, the expression

of this regulator did not appear to be significantly changed over time, with C-ion exposure **(Figure 42 b).**

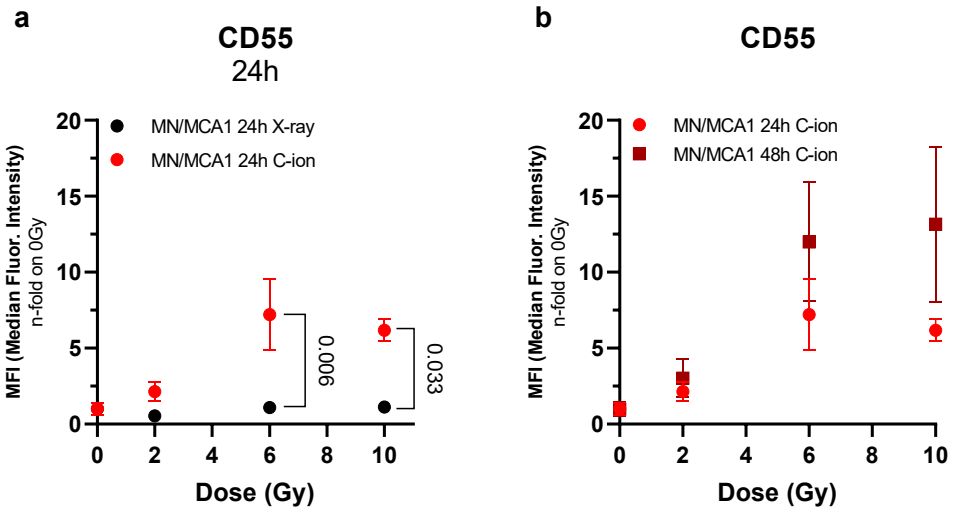

Figure 42: CD55 expression in MN/MCA1 following irradiation

(a) CD55 quantification in MN/MCA1 cells 24h after irradiation following X-ray and C-ion. (b) Detection of CD55 expression on the surface of MN/MCA1 cells 24h and 48h after C-ion irradiation. Data are obtained from cells cultured in normoxic conditions, with heat inactivated FBS. Quantification by the median of fluorescent intensity in 30000 events for each biological replicate. Each time points include 3 biological replicates. Statistical significance was determined by two-way ANOVA followed by Sidak's post hoc test for multiple comparisons.

7.5. *In vivo* experiments

After the subcutaneous inoculation of MN/MCA1 cells on the right limb of female C57BL mice, as explained in materials and methods section, (6.1.2), we measured the tumour growth regularly before and after the treatment with 6 Gy of X-ray. Irradiation with X-ray gradually reduced the tumour growth. In **Figure 43** we cans appreciate the significant difference in tumor volume following 6 Gy X-ray irradiation.

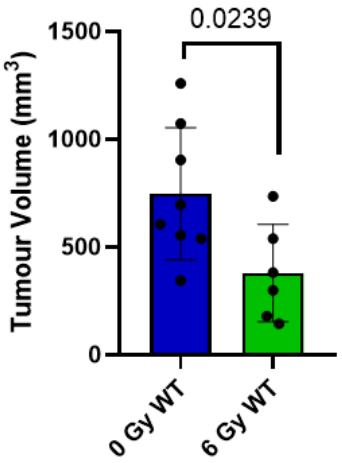

Figure 43: Tumour volume after MN/MCA1 inoculation and following X-ray irradiation
Measurement of tumour volume until 22 days after MN/MCA1 cells injection in the leg of wt C57BL female mice (mean ± SEM). The statistical analyses are performed using two tail t- test.

X-ray irradiation has been shown to modulate complement activation, as demonstrated by our *in vitro* results (section: results 7.4). To validate these findings in a physiological context, we performed *ex vivo* analyses on tumour tissues **(Figure 44a)** and mouse serum **(Figure 44b).** Our data revealed no significant increase in C3a expression within the tumour, following X-ray irradiation. Interestingly, the results confirmed that C3a was predominantly abundant in the serum, supporting the hypothesis that complement components in the tumour microenvironment were primarily of systemic origin.

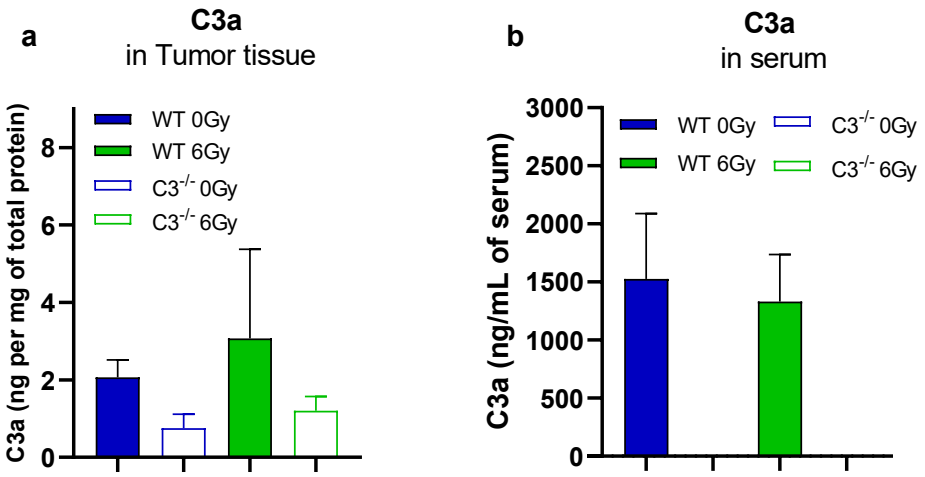

Figure 44: C3a expression in tumour tissue and mouse serum

(a) Local C3a concentration at the day of sacrifice (22 days post injection and 9 days post irradiation) measured in homogenised tumour tissue (WT 0 Gy n=4, WT 6 Gy n=2) (b) C3a concentration in mouse serum 9 days post X-ray irradiation (WT 0 Gy n=4, WT 6 Gy n=9).

To further validate the role of complement activation in our model, $C3^{-/-}$ knockout mice were utilized as a negative control. As expected, C3a anaphylatoxin levels within the tumor tissue exhibited a significant divergence between groups; while WT mice showed robust complement activation, levels in the $C3^{-/-}$ cohort remained negligible. Interestingly, while serum levels in WT mice were high, they were entirely undetectable in the knockout group. These findings were further endorsed by immunofluorescence staining of frozen sections **(Figure 45),** which revealed a stark contrast between the regional deposition of C3b in WT tissues and its total absence in the $C3^{-/-}$ samples. The preliminary results necessaries of co-staining to confirm the abundance of C3b deposition close to blood vessels or immune cells in line with the systemic origin of complement in TME.

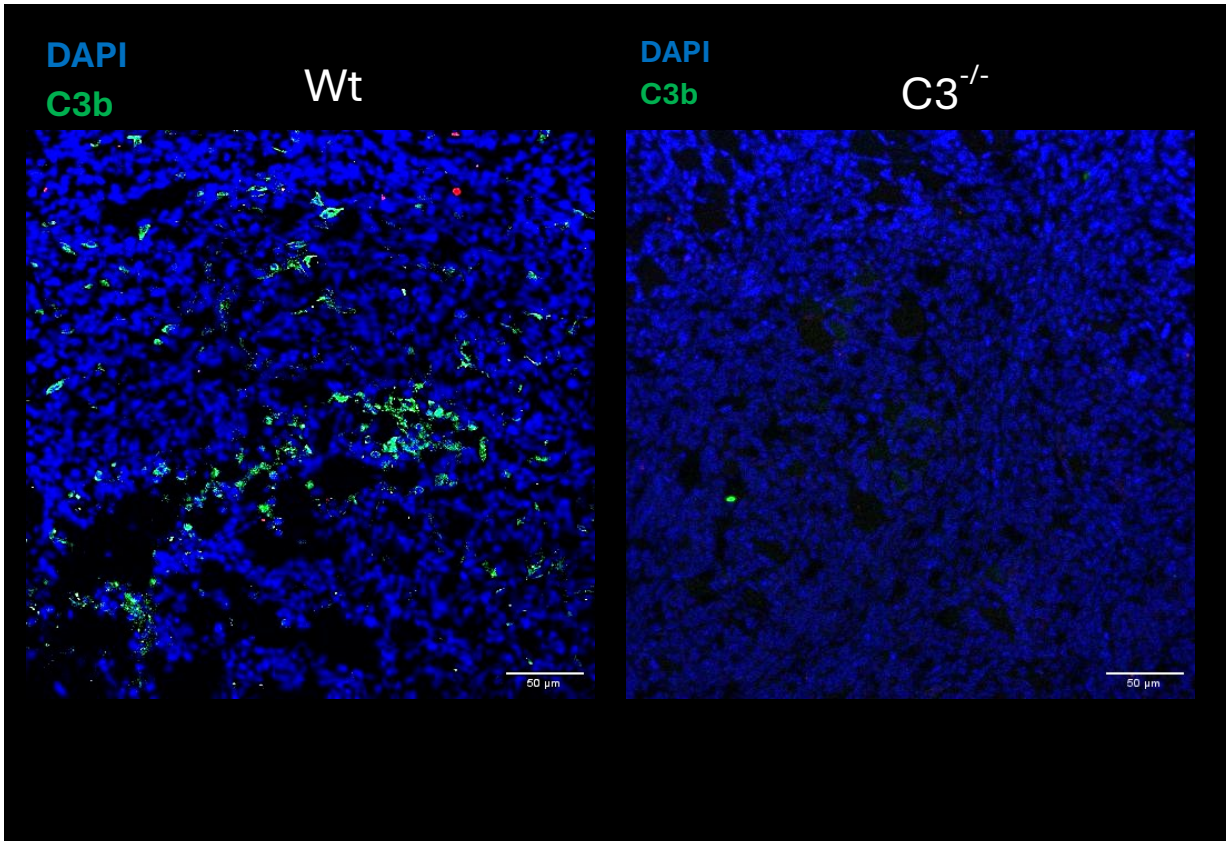

Figure 45: C3b deposition in mice tumor section

Representative tumor tissue sections stained with C3b antibody (green). On the right tissue section from wildtype mouse and the right tissue section from $C3^{-/-}$ knockout mouse. Picture collected from Leica DMI 4000B confocal microscope with N PLAN L 20x / NA 0.40, dry objective.

8. Discussion

8.1. Radiobiological characterization of MN/MCA1 fibrosarcoma: a comparative study on intrinsic radiosensitivity and hypoxia-induced resistance

For the first time, the MN/MCA1 fibrosarcoma cell line was radiobiologically characterized, allowing a direct comparison with the well-established 4T1 breast cancer cell line (Totis et al. 2025). The radiobiological characterization of a novel tumor model is a fundamental step in predicting its response to ionizing radiation and optimizing therapeutic strategies. The divergence between the observed RBE and the α/β ratio indicates that radiosensitivity is not solely defined by the cell's inherent resistance, but rather by the differential capacity to repair sublethal damage. In this model, the relatively high α/β ratio (6 Gy) suggests a limited 'shoulder' in the photon survival curve; consequently, the transition to high-LET carbon ions yields a lower RBE compared to more resistant lines, as the biological gain is mathematically constrained by the high baseline effectiveness of conventional X-rays (**Figure 19 and Table** 3**S 1)**. This indicates that, for the same physical dose of radiation, 4T1 cells are more radioresistant and it is indeed necessary to use a higher dose to achieve an equivalent level of cell killing especially for X-ray irradiation. The higher α value derived from the clonogenic survival curves of MN/MCA1 cells reflects a greater intrinsic radiosensitivity per unit dose, indicating that these cells accumulate lethal damage more efficiently upon X-ray exposure **(Table 2)(Figure 19).** The α/β ratios further highlight differences in fractionation sensitivity between the two cell lines **(Table S 1)**. Moreover, conventional X-ray radiotherapy is expected to be more effective against MN/MCA1 tumors, while for 4T1 and B16-F10 cells the administration of either higher X-ray doses or high-LET radiation, such as carbon ions, is required to achieve a comparable cell killing effect. These differences in radiosensitivity were further supported by viability assays, in which the IC_{50} values for 4T1 cells are nearly two fold higher compared to those measured in MN/MCA1 cells for both X-ray and carbon-ion irradiation, confirming the consistent pattern of relative radioresistance **(Figure 21 and Figure 22)**.

As mentioned in the introduction, fibrosarcoma tumors are frequently hypoxic, and hypoxia is a major contributor to radiation resistance (Helm and Fournier 2023) (section 4.2). Consistent with this, we demonstrated that in MN/MCA1 cells the duration of exposure to 1% O_2 is a critical factor for the effectiveness of the carbon-ion treatment **(Figure 20)**. It is well established that both the severity and the duration of hypoxia strongly influence radiotherapy outcomes(Hsieh et al. 2010; Sokol and Durante 2023; Wouters and Brown 1997). The results for clonogenic survival and viability showed a persistent radioresistant phenotype in MN/MCA1 cells after two weeks of culture

at 1% O_2 **(Figure 21a)**reduced for acute hypoxia **(Figure 21b).** The oxygen enhancement ratio (OER) of 1.4 observed following X-ray irradiation is consistent with the strong oxygen dependence in radiation response, representative of low-LET radiation.

Particle therapy is reported to be effective against hypoxic tumors (Tinganelli et al. 2015); however, in our model, radioresistance persists even after prolonged hypoxic exposure (two weeks). This phenomenon may arise from both biological and physico–chemical mechanisms. From a biological perspective, chronic hypoxia is not merely a transient stress condition but represents a powerful selective force that drives long-term cellular adaptation (Beckers, Pruschy, and Vetrugno 2024). As discussed by Lee and colleagues, prolonged exposure to low oxygen tension induces profound metabolic reprogramming, including a shift towards glycolytic metabolism, suppression of mitochondrial oxidative phosphorylation, and stabilization of hypoxia-inducible signalling pathways that promote cell survival under oxygen deprivation (Lee et al. 2023). Over time, these adaptations might result in clonal selection, favouring the expansion of subpopulations that are intrinsically more resistant to environmental stressors, including ionizing radiation. Such hypoxia-selected cells often exhibit altered redox balance, enhanced DNA damage tolerance, and reduced dependence on oxygen-mediated fixation of radiation-induced damage, all of which contribute to a more radioresistant phenotype. Other options for this outcome are discussed in detail in the subsequent section 8.5.4.

8.2. Radiation induced modulation of MN/MCA1 cell migration

As previously observed for survival and viability, also migration capacity of MN/MCA1 is reduced by X-ray and C-ion in a dose-dependent manner, with 2 Gy C-ion exposure inducing a significantly greater decrease in migration rate compared to an equivalent X-ray dose **(Figure 26b and Figure 29a)**. Notably, 2Gy of C ion irradiation induced a significant greater decrease in migration rate compared to an equivalent X ray dose **(Figure 26a)**. Most of the published studies demonstrate an increase in cell migration following X-ray irradiation, due to the activation of EMT and TGF-β-mediated pathways. Our results showed a significant increase in migration of MN/MCA1 cells only at very low doses after X-ray and a dose-dependent decrease after C-ion irradiation.

To better interpret these findings, mechanistic insights suggest that carbon ion therapy prevents HIF-1α stabilisation and inhibits MMP-2 expression even under hypoxic conditions, whereas photon may activate these factors (A.-S. Wozny et al. 2019). X-ray irradiation seams to not significantly influence MN/MCA1 migration **(Figure 28b, Figure 29a)** and this response can be explain by

predominance of cell killing and stress at higher doses and to the capacity of photon in triggering modulation in proteins adhesions or cell cycle arrest, as mentioned in the introduction **(Figure 6).**

Low-LET radiation has been shown to increase ROS production, leading to cytoskeletal alterations and abnormal cell migration and proliferation; however, these effects are highly dependent on cell type, highlighting the importance of considering cell-specific responses (Nakao et al. 2023). The influence of hypoxia on migration and stemness and stimulation of migration capacity is well established (Tinganelli and Durante 2020). Our results confirmed the capability of chronic hypoxia to increase migration rate compared to normoxic conditions (**Figure 24**: Evaluation of migration ability by scratch assay in MN/MCA1 cell line under hypoxic conditions**a)**, likely through activation of EMT transition pathways and stabilisation of HIF1α (Vito, El-Sayes, and Mossman 2020)**.** However, this effect is attenuated following X-ray **(Figure 29c)** and C-ion **(Figure 25 and Figure 29d)** irradiation and is demonstrated by two different assays, to evaluate two different migration effects: chemoattraction and group migration. Our results show comparable outcome between the two assays.

8.3. Possible role of CXCR4 SDF-1 axis

As explained in the introduction (section 4.3), one of the key mediators of tumour cell migration and viability is the CXCR4/SDF-1 axis, which can be modulated also by hypoxic conditions and irradiation (Eckert et al. 2018). Based on our results in MN/MCA1 cells, the radiation response, viability and migration was not significantly influenced by the CXCR4/SDF-1 **(**Errore. L'origine riferimento non è stata trovata.**, Figure 27 and Figure 29).** More precisely, the effect of SDF-1 incubation was detectable only at very low radiation doses and it stimulated migration exclusively in non-irradiated control samples **(Figure 27a and b).** These findings suggest that radiation may activate alternative signalling pathways that interfere with CXCR4/SDF-1 signalling or might induce functional alterations of the CXCR4 receptor. To clarify this aspect, further experiments are required to investigate CXCR4 expression levels after irradiation, its membrane localization, and the activation status of downstream signalling pathways such as PI3K/AKT and ERK, to determine whether radiation impairs receptor functionality rather than its expression (Busillo and Benovic 2007).

8.4. Radiation induces immune response in MN/MCA1 cells

Sarcomas are generally considered immunologically “cold” tumors, characterized by limited immune cell infiltration and poor responsiveness to immunotherapy (Petitprez et al. 2020; Tawbi et

al. 2017). In this context, radiotherapy has emerged as a potential strategy to enhance tumour immunogenicity. Ionizing radiation can promote immunogenic cell death (ICD) and stimulate the release of pro-inflammatory chemokines, thereby facilitating immune cell recruitment and activation (Demaria, Golden, and Formenti 2015; Galluzzi et al. 2017).

In our model, both X-rays and carbon ions induced immune-related responses, including chemokine release and ICD-associated signals, suggesting a shift towards a more immunostimulatory phenotype **(Figure 30, Figure 31, Figure 33)**. However, we also observed modulation of complement activation, which has been associated mainly with tolerogenic and immunosuppressive mechanisms within the tumor microenvironment **(Figure 37, Figure 40)**(Markiewski and Lambris 2009; Roumenina et al. 2019). These findings highlight the dual and potentially opposing immunological effects of radiation, which will be discussed in detail in the following sections.

8.4.1. X-ray and C-ion trigger immunogenic cell death in MN/MCA1 cells

Immunogenic cell death (ICD) is currently considered as a primary mechanism by which radiotherapy triggers systemic immune responses, effectively converting the irradiated tumor into an *in situ* vaccine. This process provides a mechanistic bridge between the direct cytotoxic power of radiation and the activation of durable, adaptive anticancer immunity. In our study, we demonstrated that both X-rays and C-ions possess the capacity to induce the release of high-mobility group box 1 (HMGB1), a hallmark Damage-Associated Molecular Pattern (DAMP). The kinetics of this release reached maximum levels 72 hours post-irradiation across both radiation modalities. Carbon ion irradiation resulted in a linear and dose-dependent increase 72h following irradiation, in contrast to X-ray irradiation that resulted in a peak of HMGB1 level at 8 Gy and a decrease after 12 Gy, suggesting that at higher doses C-ions may reach superior levels of HMGB1 release compared to X-rays **(Figure 31).**

The immunogenic quality of cell death is not characterized by a single marker, but by the net balance between immunostimulatory and immunosuppressive signals. This is further highlighted by our data on Calreticulin (CRT) exposure **(Figure 33).** CRT acts as a critical "eat-me" signal that translocate to the cell surface during the stress response, a "pre-mortem" phase of ICD that occurs before the cell dies (Galluzzi et al. 2023). We observed a robust, dose-dependent increase in CRT surface exposure that was significantly more pronounced following C-ion compared to X-ray irradiation at high doses (6 Gy and 10 Gy) between 72 and 96 hours **(Figure 33a).** This suggests that C-ions may more effectively engage the endoplasmic reticulum (ER) stress machinery, potentially leading to superior phagocytic uptake of tumour antigens by dendritic cells (DCs).

However, these *in vitro* findings should be interpreted with caution. While cell lines provide detailed molecular data, they cannot fully mimic the complex crosstalk between dying tumour cells, antigen-presenting cells, and effector lymphocytes. In a living organism, the TME acts as an immune modulator where the perception of cell death can be shifted from immunogenic to tolerogenic. For instance, high levels of extracellular ATP, a "find-me" signal for DCs, can be rapidly degraded into immunosuppressive adenosine by ecto-enzymes like CD39 and CD73 often overexpressed in the TME (Galluzzi et al. 2026).

Additionally, the specific Regulated Cell Death pathway triggered by radiation, i.e., apoptosis, necroptosis, or ferroptosis, significantly influence the immunological outcome. High-LET particles like C-ions are known to induce more complex, clustered DNA damage, which may favour more inflammatory pathways like necroptosis over the often immunologically silent apoptosis. Ultimately, the success of radiotherapy-induced ICD in patients undergoing radiotherapy depends on whether these radiation-induced signals can overcome the pre-existing immunosuppressive barriers of the TME, such as the presence of Tregs or M2 macrophages.

8.4.2. Irradiation modulates complement system in MN/MCA1 cells

The complement system is a phylogenetically ancient arm of innate immunity, traditionally considered as the first line of defence against pathogens. While historically it is viewed as a simple proteolytic cascade primarily operative in serum, research over the last decade has revealed a far more complex role for complement in oncology (Artero et al. 2025). Its function is nowadays considered to be highly context-dependent, capable of triggering both immunostimulatory and immunosuppressive responses, depending on the tumor type and stage (Garlanda, Dambra, and Magrini 2025). Notably, studies in the MN/MCA1 murine fibrosarcoma model, conducted by our collaborators at Humanitas University, have demonstrated that the complement system can act as a driver of tumor progression and immunosuppression. In this specific model, C3aR-dependent signalling facilitates the recruitment and M2-like polarization of tumor-associated macrophages (TAMs), which in turn suppress anti-tumour T cell responses (Magrini et al. 2021).

A final goal of the doctoral thesis presented here is to determine whether radiotherapy (RT) influences this immunosuppressive outcome by modulating complement activation in fibrosarcoma cells. Radiotherapy is known to induce tumour cell death, specifically necrosis and apoptosis, which releases DAMPs that can initiate the complement cascade (Pio et al. 2019). We focused our investigation on C3, the central convergence points for the classical, lectin, and alternative pathways. While the liver is the primary systemic source of complement proteins, emerging

evidence highlights the "complosome", an intracellular complement system where cells, particularly immune and tumour cells, produce and activate their own complement components (West and Kemper 2023). Our *in vitro* experiments investigated whether irradiation directly stimulates MN/MCA1 cells to produce and activate complement components. When cultured in heat-inactivated serum (to eliminate systemic complement interference), resting MN/MCA1 cells exhibited very low surface levels of C3 **(Figure 35)**. However, following irradiation, we observed a significant, dose-dependent increase in C3 membrane deposition **(Figure 36b)**. Specifically, a 6-fold increase was observed at 48 and 72 hours following at higher doses (6 Gy and 10 Gy), probably due to an accumulation of C3 fragments. Carbon-ion radiation demonstrated higher efficacy in C3 membrane deposition than X-rays, particularly at 6 Gy. To specify the nature of this deposition, we utilized a C3b/iC3b/C3c-specific antibody, and we focus on the earlier time point to see the immediate activation and avoid the possible accumulation of inactivated fragments (iC3b/C3dg)(Surace et al. 2015). To better approximate a physiologically relevant scenario, cells were cultured in heat-inactivated FBS and, following irradiation, incubated for 5 minutes with untreated mouse serum, while heat-inactivated serum was used as a negative control. With heat-inactivated mouse serum, X-ray irradiation induced a non-significant dose-dependent increase **(Figure 37a and d)**, whereas C-ion irradiation resulted in a significant rise in C3b deposition starting at 2 Gy, maintaining stable activation levels at higher doses **(Figure 37b and d)**. These initial findings confirm the ability of irradiation particularly C-ion to induce autocrine complement activation in MN/MCA1 cells. Considering the systemic origin of complement in the tumour microenvironment, cells were incubated with untreated mouse serum. The results confirmed that systemic complement is the main contributor to total surface deposition, as high levels of membrane-bound C3b were detected even in non-irradiated cells (Magrini et al. 2021). Although irradiation showed a trend toward increased C3b deposition in the presence of normal serum, the differences compared to unirradiated cells were not statistically significant **(Figure 37)**. A notable distinction, however, was observed between radiation qualities: X-ray-irradiated cells exhibited significant differences in C3b deposition between normal and heat-inactivated serum at all doses, whereas for C-ion-irradiated cells this difference was only significant at 0 Gy **(Figure 37)**. This may be related to the higher although not statistically significant increase in C3b deposition observed after C-ion irradiation in the presence of heat-inactivated serum.

The cleavage of C3 generates not only the membrane-bound opsonin C3b but also the soluble anaphylatoxin C3a, a potent inflammatory mediator. In MN/MCA1 cells, we detected a dose-dependent increase in C3a, reaching peak levels 24 hours after 6 Gy and 10 Gy irradiation (both X-ray and C-ion) **(Figure 40)**. The biological activity of C3a is mediated through its receptor, C3aR.

Our data indicate that surface expression of C3aR on MN/MCA1 cells also increases following 6 Gy and 10 Gy irradiation, with C-ion irradiation showing significantly higher efficacy than X-rays **(Figure 41)**. This finding is critical, as C3aR expression is generally observed in infiltrating myeloid cells rather than in tumour cells themselves. The induction of both the ligand (C3a) and its receptor (C3aR) on tumour cells suggests a potential autocrine signalling loop triggered by radiation. In other malignancies, such as lung and cutaneous squamous cell carcinomas, autocrine C3aR signalling has been shown to directly promote tumour cell proliferation, epithelial-mesenchymal transition (EMT), and resistance to therapy(Shi et al. 2024; Shu et al. 2020). These observations align with the results of a clinical study reported by Lawal et al., which correlated high expression of C3, C5, C3aR, and C5aR1 with tumour immune evasion and poor progression-free survival across various human cancers, including melanoma, brain tumor and carcinoma(Lawal et al. 2021). Our findings suggest that while radiotherapy is intended to kill tumour cells, it may simultaneously trigger a local complement response that could support an immunosuppressive microenvironment, if left unmodulated. Considering also the Surace et al, results testing the importance of complement for an anti-tumor effect of radiation in melanoma model. Understanding this radiation-induced complement activation will be vital for future *in vivo* studies, aimed at combining radiotherapy with complement inhibitors (such as C3aR antagonists) to prevent the recruitment of suppressive macrophages and unleash more effective anti-tumor T cell responses.

8.4.2.1. Complement activation following irradiation is cell line dependent

A central finding of this study is that complement activation in the tumour microenvironment (TME) is highly dependent on the specific cell line's molecular landscape. The 4T1 breast carcinoma and B16-F10 melanoma cell lines were selected as benchmarks for comparison with the MN/MCA1 fibrosarcoma model for several key reasons. First, both lines are well-established in radiobiological research and exhibit a more radioresistant phenotype compared to MN/MCA1 **(Table S1)**. Second, they provide a diverse baseline of complement C3 expression and regulatory components, allowing for a comprehensive analysis of how initial complement status influences radiation response. Notably, the 4T1 model has been previously characterized in the context of combined radiotherapy and complement activation, providing a robust reference framework for our findings. Our results demonstrated a clear stratification between MN/MCA1, B16-F10, and 4T1 cells regarding their susceptibility to C3b deposition. While MN/MCA1 and B16-F10 exhibited low baseline C3b levels, 4T1 cells displayed a high constitutive level of C3b deposition even prior to exogenous serum stimulation. Upon incubation with Untreated Mouse Serum (US), all lines showed increased C3b

levels; however, the highest fold-increase was observed in the B16-F10 line *(p=0.001)* with and without C-ion irradiation **(Figure 39a)(Table 4)**.

Table 4: n-fold value of C3b deposition with US and HS incubation

Doses (Gy)	MN/MCA1	4T1	B16
0	9.14537	1.85327	68.6078
2	1.350399	2.871155	5.447585
6	1.998996	2.31531	4.913609

This differential sensitivity likely stems from differences in membrane architecture and the density of membrane-bound complement regulatory proteins (mCRPs). Specifically, data reported by others suggest that B16-F10 cells express reduced levels of Crry, a regulator important for complement homeostasis, which impairs their ability to degrade C3b once the cascade is initiated (Kim et al. 1995; Elvington et al. 2014; Wu et al. 2008). The low level of inhibitory molecules on the cell surface makes B16-F10 cells highly susceptible to activation of the alternative complement pathway. Upon exposure to external mouse serum factors, this promotes the amplification loop, leading to enhanced C3 cleavage and increased C3b deposition on the cell surface (Geller and Yan 2019). We further investigated how irradiation triggers complement activation. For the 4T1 cell line, irradiation had a negligible effect on C3b deposition after irradiation compared to its baseline, but we have significant difference in radiation qualities effect: 6 Gy X-ray **(Figure S 6a)** demonstrate to be more effective in compare to C-ion **(Figure 39 and Figure S 6b)**, and a dose-dependent increase with serum incubation treated and untreated is significant only after X-ray irradiation **(Figure S 6b and c)**. In contrast to 4T1 cells, B16-F10 cells showed a dose-dependent increase, particularly at 6 Gy, where a significant boost in C3b was observed when combined with active serum **(Figure 39).**

This divergence may be explained by the inherent radiosensitivity profiles of these cell lines. Based on established α/β ratios, the 4T1 cell line is considered the most radioresistant line in this panel that were investigated in the frame of this thesis. As noted by Surace et al., radiotherapy-induced complement activation often relies on the exposure of "neo-epitopes" or damage-associated

molecular patterns (DAMPs) on the cell surface (Adamiak et al. 2017; Mannes et al. 2021; Ricklin and Lambris 2007). The radioresistance of 4T1 cells may involve mechanisms that stabilize the cell membrane or upregulate mCRPs even under stress **(Figure S5)**, thereby preventing the "burst" of C3b deposition, seen in the more susceptible B16-F10 line. The most remarkable result is the synergy between serum incubation and irradiation in B16-F10 cells **(Figure 39).** While heat-inactivated serum (HS) failed to trigger deposition in all cell lines, the combination of 6 Gy and untreated mouse serum led to a massive deposition event. As discussed by Elvington and colleagues, radiation-induced cell stress acts as a primer that "sensitizes" the tumor surface to complement-mediated attack. In B16 cells, irradiation likely compromises an already weak regulatory shield (low Crry), allowing for an unhindered deposition of C3b that could potentially enhance downstream opsonisation or the formation of the Membrane Attack Complex (MAC).

8.4.3. Complement system activation *in vivo* mouse model

As established by our *in vitro* results **(Figure 37)** and detailed in the introduction (section 4.4.1.2), the liver serves as the primary source of the complement system, meaning that its presence within the tumour microenvironment is largely a result of systemic uptake. Our preliminary *in vivo* experiments confirmed C3b deposition within localized regions of tumour sections **(Figure 45)** and completely absent in C3 knockout mice like in Magrini and colleague paper. This is also the confirmation that the major contribution in complement activation in MN/MCA1 mouse model does not come from the tumour cells. Our subsequent goal is to validate its colocalization with blood vessels and immune cells, consistent with the findings of Magrini et al. (2021). Following the establishment of our experimental protocol, we already planned for next experiments to investigate the potential modulation of the complement system in response to radiotherapy. In the meanwhile, we confirmed the efficacy of X-ray irradiation (a single 6 Gy fraction) in reducing tumor growth **(Figure 43)**. A non-ablative dose was selected to ensure a controlled therapeutic response while maintaining a viable tumor mass. This experimental design allowed for the collection of post-irradiation tissues, enabling a detailed study of the biological and immunological dynamics triggered by the treatment. Moreover, preliminary results indicated no significant differences in C3a concentrations within the tumour or mouse serum after irradiation at the time of sacrifice **(Figure 44)**. This experiment was conducted 9 days post-irradiation; however, given that the kinetics of the complement cascade is rapid and the half-life of its components is notably short, it is highly probable that the acute response was missed (Surace et al. 2015). Consequently, the current data likely reflects only baseline C3a levels rather than the immediate post-treatment flux. To address this, we planned subsequent experiments involving blood collection at multiple time points post-treatment, to

accurately characterize the temporal kinetics of complement activation and its influence on radiation response.

8.5. Importance of hypoxia in radiation response modulation

As established in the literature, hypoxia remains a primary driver of radiotherapy failure, profoundly modulating cellular proliferation, stemness, and migratory potential. Specially for fibrosarcoma models, which are known to develop extensive and heterogeneous hypoxic regions *in vivo*, it is important to investigate the role of hypoxia (Staab et al. 2007).

8.5.1. Temporal dynamics of post-irradiation hypoxic response

Our findings emphasize the time-dependent nature of these biological responses, which follow a longitudinal progression from immediate reactive shifts to persistent adaptive reprogramming **(Figure 6)**. The cellular response to hypoxia can be categorized by its duration, with distinct molecular consequences at each stage (Lee et al. 2023). The acute phase (seconds to hours) is characterized by reduced activity in oxygen-dependent enzymes, triggering the unfolded protein response (UPR) and a global inhibition of mRNA translation to preserve ATP. In contrast, the long-term phase (hours to weeks) involves a systemic reprogramming of the transcriptome and epigenome, favouring angiogenesis, glycolytic metabolic shifts, and pH homeostasis.

An additional critical aspect in the interpretation of chronic hypoxia experiments is the routine handling of cells outside the hypoxic workstation during passaging, which, in our case, requires at least one hour of exposure to normoxic conditions. According to established hypoxia timelines, repeated transitions between hypoxia and normoxia more closely resemble cyclic rather than strictly chronic hypoxia (Bader, Dewhirst, and Hammond 2021). Cyclic hypoxia is biologically distinct from sustained hypoxia and is characterized by dynamic oxygen fluctuations that activate additional signalling pathways not typically engaged under constant low oxygen conditions (Bader, Dewhirst, and Hammond 2021; Saxena and Jolly 2019). Prior to irradiation, cells were subjected to at least 48 hours of hypoxia to establish a chronic hypoxic phenotype. It should be considered that reoxygenation cycles may activate compensatory pathways that could influence experimental outcomes. Our experimental data regarding viability and survival following irradiation highlight the clinical significance of these temporal dynamics showing the higher radioresistence of cells maintained two weeks at 1% O_2 concentration **(Figure 20a and Figure 21c)**. The observed divergence in radiation response between chronic and acute hypoxia supports the conclusion that after approximately two weeks of exposure to 1% O_2, cells successfully initiate an adaptive program. This transition results in a state of hypoxia tolerance, where long-term adaptation, likely mediated by chromatin remodelling, provides the cells with the plasticity needed to survive in increasingly hostile environments and radiation **(Figure 20b and Figure 21)**.

8.5.2. Impact of hypoxia and radiotherapy on migration

Hypoxia is a potent catalyst for metastatic potential, promoting the epithelial-to-mesenchymal transition (EMT) and inducing a switch toward amoeboid migration **(Figure 24)** (Friedl and Wolf 2003). While conventional X-rays may inadvertently stimulate these processes by stabilizing HIF-1α, Carbon-ion (C-ion) irradiation offers a distinct therapeutic advantage.

In our model, both X-ray and C-ion irradiation reduced migratory capacity under hypoxic conditions, though C-ions demonstrated superior efficacy. This superiority is framed due to their high LET, C-ions produce dense, clustered DNA damage that is harder to repair than the sparse lesions produced by photons (A. S. Wozny and Rodriguez-Lafrasse 2023). The observed reduction in migration following X-ray exposure despite the cells' inherent radioresistance may be attributed to radiation-induced stress on the cytoskeleton, specifically the inhibition of Rho-GTPases or other pathways essential for cellular motility (Moncharmont et al. 2014)(Akino et al. 2009).

8.5.3. Immune response under hypoxic conditions following irradiation

For immune response evaluation we maintained the two weeks hypoxia protocol, to evaluate a possible long-term effect. As mentioned in the introduction, hypoxia influences also immune responses (section 4.2). Our results showed a significant reduction in immunogenic response under 1% O_2 concentration in terms of HMGB1 release and CRT exposure **(Figure 32 and Figure 34)**.These results may be attributed to several factors, including the challenges in reproducing and measuring immune responses *in vitro*, as explained by Huang and colleagues (Huang et al. 2020). Through selective pressure, hypoxia has been widely shown to favour the survival of more resistant and aggressive cells (Koshikawa et al. 2006)(Quartieri et al. 2023).

Moreover, we did not see any significant changes related to innate immunity, with C3b deposition showing no change in complement activation compared to normoxic condition **(Figure 39).** Several studies demonstrated that hypoxia modulates the expression of complement regulators on the cellular surface, thereby influencing the activation of the complement cascade (Moon, Petersson, and Olcina 2022; Okroj et al. 2009). Nevertheless, as previously mentioned, complement activation is reported to be rapidly induced under stress conditions (Surace et al. 2015), and after two weeks under hypoxic condition the complement activation is likely to be resolved, suggesting that cells may adapt to maintain a balance under extremely low oxygen levels. Therefore, investigating the kinetics of complement activation, including C3b deposition, under hypoxic condition and following irradiation is necessary to better clarify the mechanism.

8.5.4. Physical and biological constraints: the importance of LET and O_2 tension

The sustained radioresistant behaviour seen in MN/MCA1 cells following carbon ion irradiation is most plausibly attributed to a combination of biological selection processes and limitations inherent to the physical properties of the radiation beam. As highlighted by Sokol & Durante (2023) and Jansen et al. (2025), C-ion irradiation at a dose-averaged LET of approximately 75 keV/µm occupies a transitional regime (Jansen et al. 2026; Sokol and Durante 2023). At this LET, the "oxygen effect" is only partially suppressed. The 75 keV/µm threshold frequently falls below the levels required to fully overcome hypoxia-induced resistance, supporting the consensus that heavier ions (e.g., Oxygen or Neon) capable of sustaining LETd > 100 keV/µm may be necessary to maximize RBE across the spread-out Bragg peak. Furthermore, the 1% O_2 concentration represents an "intermediate" hypoxic state. According to the Oxygen Fixation Hypothesis, maximum radioresistance is typically only reached at much lower levels (0.1%). The mandatory hypoxia-reoxygenation cycles during cell passage likely triggered periodic bursts of ROS, activating stress-responsive pathways (such as NF-κB and MAPK) that further modulate the DNA damage response. Lastly, as noted by Ma and colleagues the influence of cell-cycle distribution under these specific conditions adds another layer of complexity (Ma et al. 2013). These findings underscore the necessity of further investigation into the synergistic mechanisms of time, oxygen concentration, and cell-cycle dynamics to fully characterize the radiobiological response of the tumour microenvironment.

9. Conclusions

This research provides the first radiobiological characterization of the MN/MCA1 fibrosarcoma line, identifying it as more intrinsically radiosensitive than the 4T1 breast cancer model. Based on the *in vitro* data C-ion irradiation appears more effective for cell killing (**Figure 46(1))** and it reduces migration (**Figure 46(3))**. A central finding is the dual nature of radiation-induced immunity. Both modalities trigger immunogenic cell death (ICD), with C-ions showing superior efficacy in engaging ER stress and CRT exposure at high doses **Figure 46(4)**. In MN/MCA1 cells, irradiation significantly increases complement activation in MN/MCA1 tumor cells, but this was only observed following higher doses C-ion and in the presence of mouse serum, containing complement factors **Figure 46(4).** The inhibition of complement system together with C-ion irradiation treatment can be a good strategy based on the immunosuppressive role of complement demonstrated by Magrini et al., in our fibrosarcoma model. Conversely, the B16-F10 line exhibited massive complement deposition, proving that these responses are highly cell-line dependent. Finally, chronic hypoxia remains a critical limit: two weeks of exposure to 1% O_2 induces a persistent radioresistant phenotype that high-LET radiation only partially overcomes **Figure 46 (2)**.

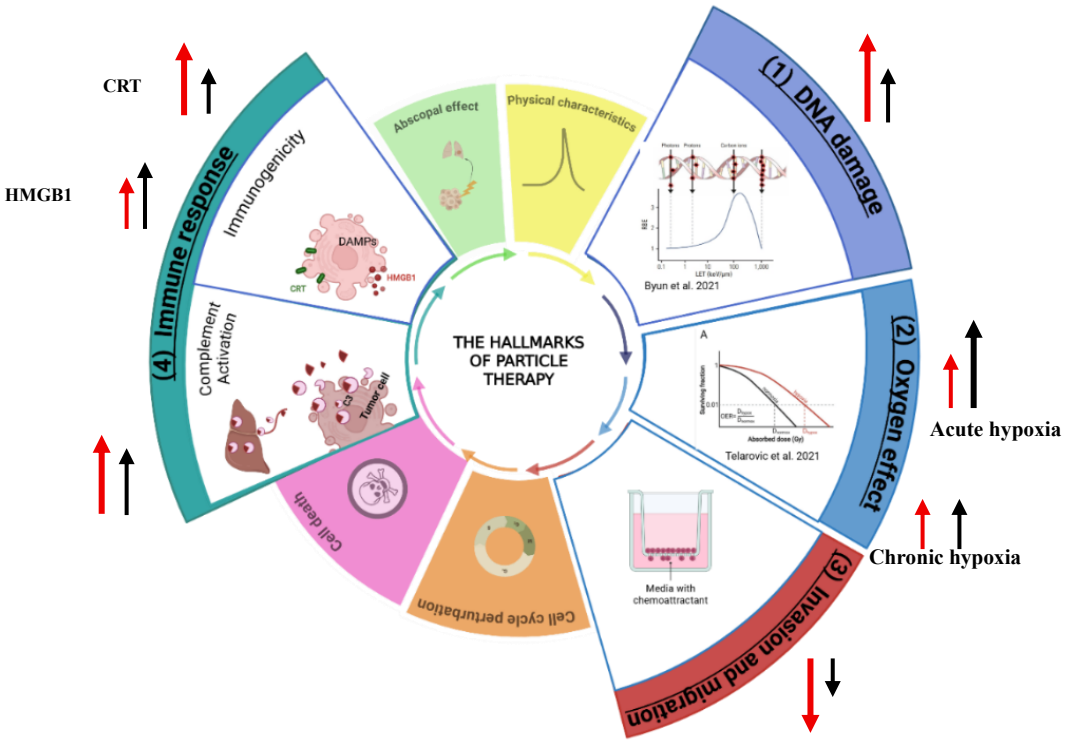

Figure 46: Conclusion of the thesis highlighted in the hallmarks of particle therapy influenced by irradiation

Thickness and length of the arrows proportional with the increase/decrease in response of irradiation with X-ray (black) and C-ion (red). Inspired by **(Hanahan 2022)** created in https://BioRender.com

Since these findings are primarily derived from *in vitro* studies, the possibility of differing responses *in vivo* remains, particularly due to interactions with the tumor microenvironment (TME) and the predominant role of immune cells in complement activation. Based on these preliminary results that future clinical strategies must look beyond physical beam parameters to incorporate hypoxia-targeting agents or complement inhibitors, tailored to the specific tumor type. As show in this work the combination of complement modulation and radiotherapy represent a promising strategy for personalised therapy. The transition of these strategies from preclinical models to the clinical applications is facilitated by a robust existing complement-targeting agents already established in non-oncological practice. For instance, the C3 inhibitor pegcetacoplan is already undergoing evaluation in early-phase trials alongside pembrolizumab to determine if upstream blockade can sensitize immunologically "cold" tumors (Werner et al. 2025). Similarly, C5a receptor antagonists, such novel agent IPH5401, are being investigated for their capacity to disrupt the recruitment of myeloid-derived suppressor cells (MDSCs) within the TME (Massard et al. 2019).

Ultimately, the clinical efficacy of these strategies depends on the precise temporal coordination between radiotherapy and pharmacological blockade. Identifying the optimal therapeutic window, corresponding to the peak of radiation-induced ICD, is essential to drive the immune response toward durable activation rather than compensatory immunosuppression. By integrating established complement inhibitors with the unique high-LET lethal DNA damage, this dual-modality approach aims to shift the tumor–immune crosstalk from a tolerogenic to an immunogenic state. This combination is designed to overcome the limitations of localized treatment, potentially inducing a systemic anti-tumor response to improve long-term outcomes in patients with metastatic or radioresistant disease.

10. Supplementary figure

10.1. Comparison of cell growth and survival curve performed at CNAO and GSI facilities

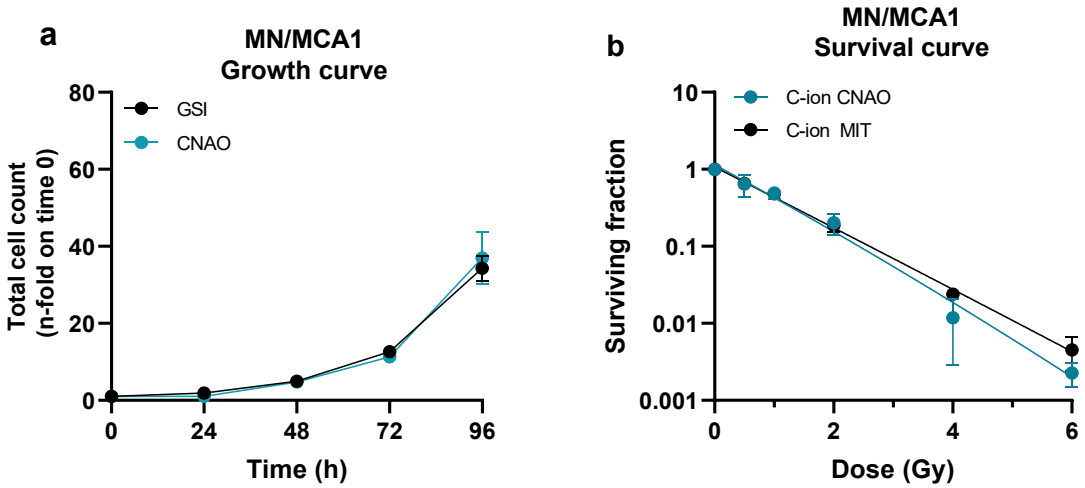

Figure S 1 : Cross-facility validation: experimental results obtained from different facilities

(a) MN/MCA1 cell growth curve experiment performed in GSI (in black) and in CNAO (in blue).

(b) Comparison of cell survival curve following C-ion irradiation in CNAO (blue) and at Marburg Ion Beam Therapy Center (MIT) (black).

Table S 1: α,β values, α/β ratio and RBE of different cell lines (MN/MCA1. 4T1 and B16-F10) following X-ray and C-ion irradiation

Cell line	X-ray	C-ion	RBE
MN/MCA1	6 (α: 0.44 β: 0.079)	≈0 (α: 0.971 β: 0.0143)	1.6
4T1	3.18 (α: 0.116 β: 0.036)	≈0 (α: 0.829 β: 0.0005)	2
B16	2.37 (α: 0.197 β: 0.083)	≈0 (α: 0.655 β ≈ 0)	1.1

10.2. Influence of irradiation and hypoxia on migration capacity in MN/MCA1 cell line

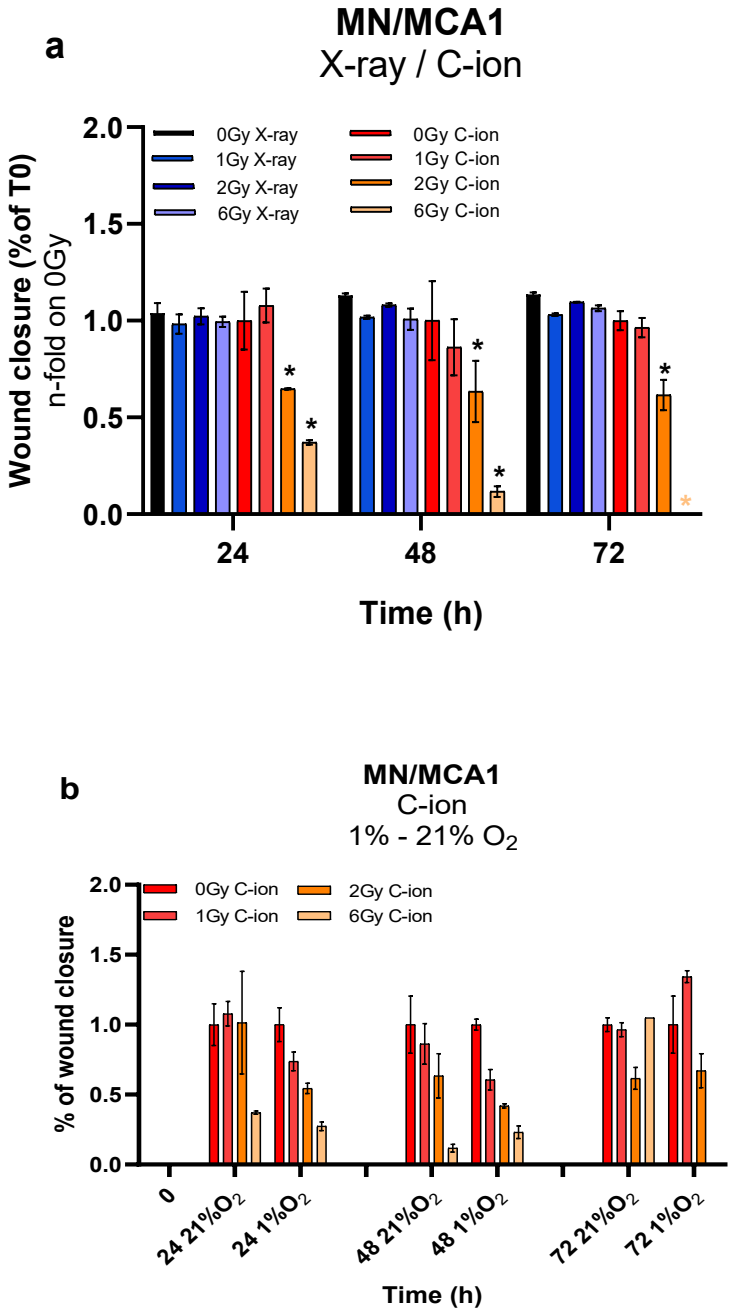

Figure S 2: Influence of hypoxia on MN/MCA1 migration capacity following C-ion and X-ray irradiation

(a) Wound area measured at different time points after scratch (24h, 48h and 72h) is shown with bar plot to compare the influence of X-ray (blue shades) and C-ion (red nuance). (b) Wound area measured at different time points after scratch (24h, 48h and 72h) is shown with bar plot to compare the influence of hypoxic condition (1%O_2) after C-ion irradiation.

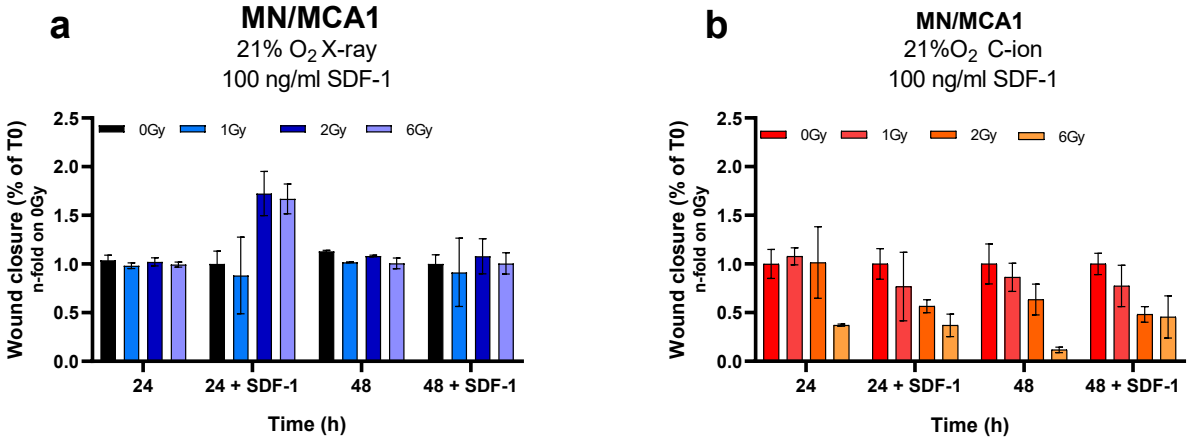

Figure S 3: Influence of SDF-1 on MN/MCA1 migration capacity following C-ion and X-ray irradiation

Wound area values measured at different time points after scratch (24h, 48h) are shown with bar plot to compare the influence of SDF-1 100ng/ml. Bar plot represents wound closure percentage following X-ray (a) and C-ion (b) irradiation.

10.3. Complement activation in MN/MCA1 following irradiation

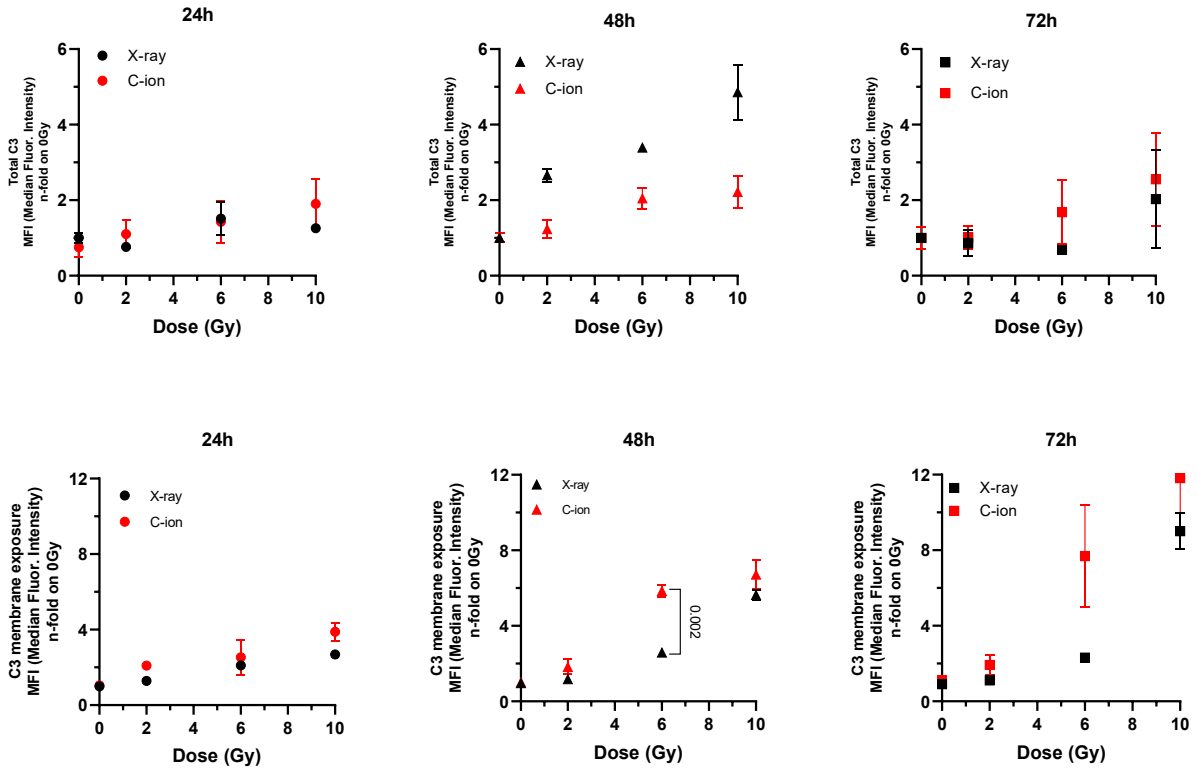

Figure S 4: X-ray and C-ion induce C3 expression on MN/MCA1 cell surface

(b) Detection of C3 expression on the cell surface 24-48-72h after X-ray and C-ion irradiation in cells cultured with heat inactivated FBS. Quantification by median fluorescent intensity across 30000 events for each biological replicate.

Significant differences relative to the 0 Gy baseline are indicated by * ($p < 0.05$). Data were analysed using a two-way ANOVA with Sidak's correction for multiple comparisons. Data show the mean ± SEM of 3 biological replicates

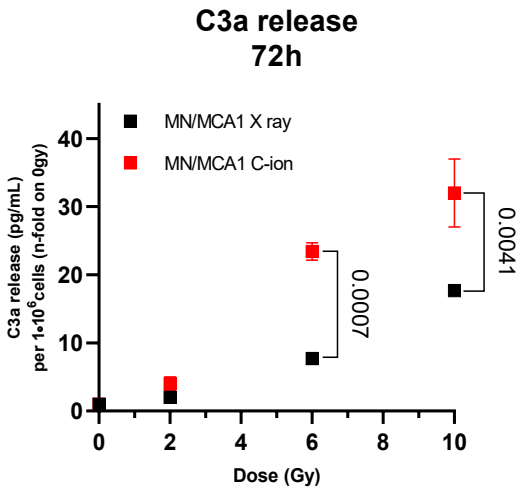

Figure S 5: C3a release in MN/MCA1 cell line following X-ray and C-ion irradiation

C3a release in MN/MCA1 supernatant 72h following irradiation with X-ray and C-ion in normoxic condition. Data are obtained from cells cultured in normoxic conditions, with heat inactivated FBS. Data show the mean ± SEM of C3a concentration in pg/ml of 3 biological replicates. Statistical significance was determined by two-way ANOVA followed by Sidak's post hoc test for multiple comparisons.

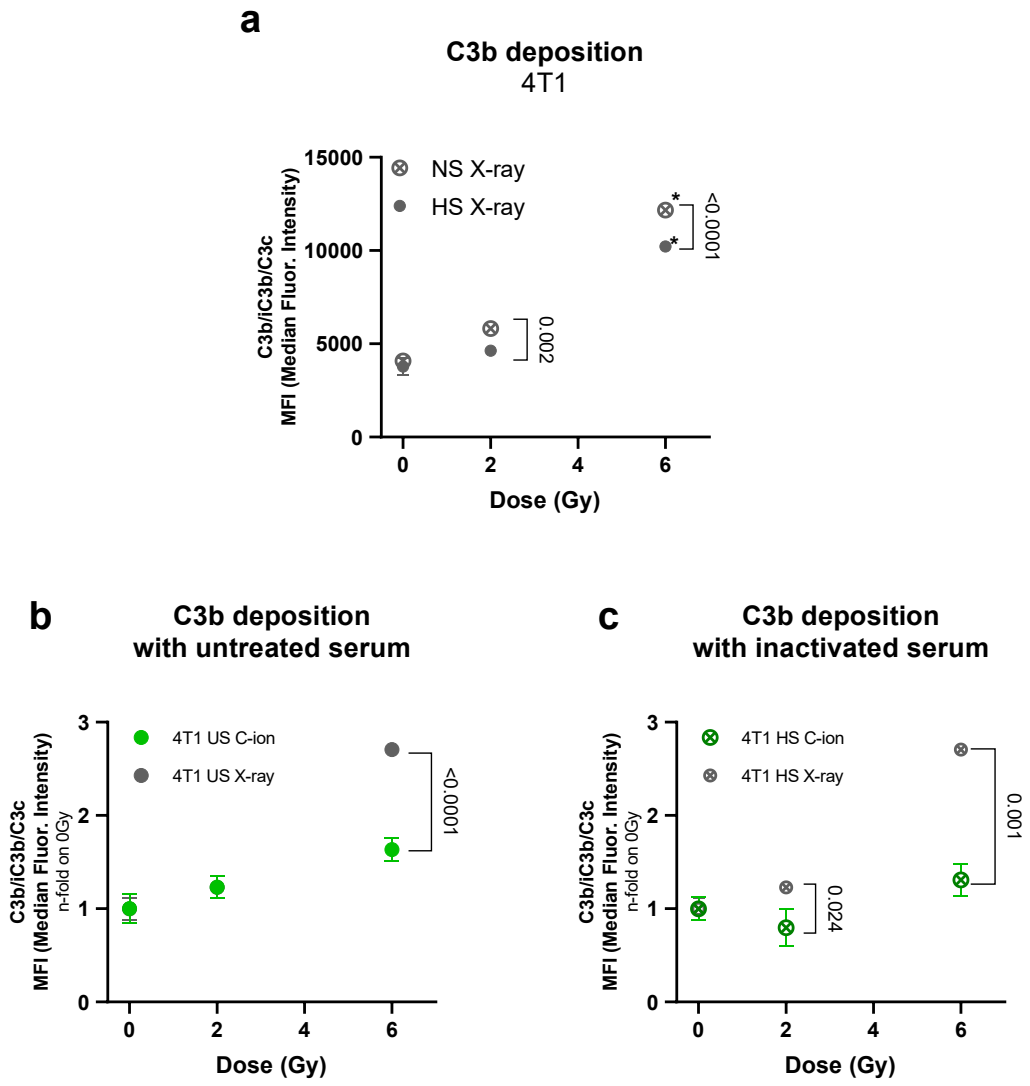

Figure S 6: C3b deposition on 4T1 cells following irradiation

(a) C3b deposition quantification 24h after X-ray irradiation and incubation with mouse serum, untreated (US) or heat inactivated (HS). (b) Comparison of C3b deposition quantification 24h after X-ray and C-ion irradiation and incubation with mouse serum activated (US). (d) Comparison of C3b deposition quantification 24h after X-ray and C-ion irradiation with incubation with mouse serum heat inactivated (HS). C3b deposition quantified by the median of fluorescent intensity in 30000 events for each biological replicate. Each time points include 3 biological replicates. Statistical significance determined using the ANOVA test and Holm-Sidak method correction, noted in the graphs with p-value for X-ray and C-ion comparison and with * p-value < 0.05 comparing 0 Gy with the other doses.

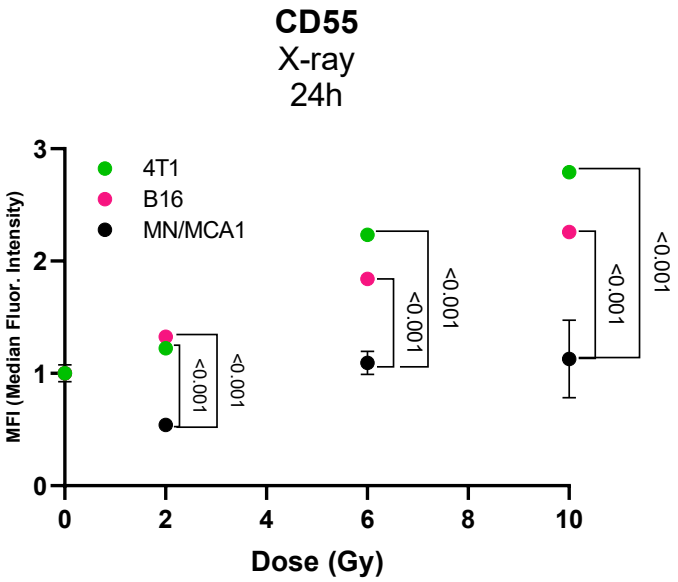

Figure S 7: Comparison in CD55 (DAF) expression on different cell lines

CD55 expression on cell surface in MN/MCA1, B16 and 4T1 cells surface 24h following X-ray irradiation. Data show the mean ± SEM of 3 biological replicates for MN/MCA1 and 4T1 and 2 biological replicates for B16. Quantification by the median of fluorescent intensity in 30000 events for each biological replicate. Statistical significance was determined by two-way ANOVA followed by Sidak's post hoc test for multiple comparisons.

11. Bibliography

Adamiak, M, A Abdelbaset-Ismail, M Suszynska, A Abdel-Latif, J Ratajczak, and M Z Ratajczak. 2017. “Novel Evidence That the Mannan-Binding Lectin Pathway of Complement Activation Plays a Pivotal Role in Triggering Mobilization of Hematopoietic Stem/Progenitor Cells by Activation of Both the Complement and Coagulation Cascades.” *Leukemia* 31(1): 262–65. doi:10.1038/leu.2016.278.

Ajona, Daniel, Sergio Ortiz-Espinosa, Haritz Moreno, Teresa Lozano, María J Pajares, Jackeline Agorreta, Cristina Bértolo, et al. 2017. “A Combined PD-1/C5a Blockade Synergistically Protects against Lung Cancer Growth and Metastasis.” *Cancer Discovery* 7(7): 694–703. doi:10.1158/2159-8290.CD-16-1184.

Akino, Yuichi, Teruki Teshima, Ayaka Kihara, Yuko Kodera-Suzumoto, Miho Inaoka, Shigeki Higashiyama, Yoshiya Furusawa, and Nariaki Matsuura. 2009. “Carbon-Ion Beam Irradiation Effectively Suppresses Migration and Invasion of Human Non–Small-Cell Lung Cancer Cells.” *International Journal of Radiation Oncology*Biology*Physics* 75(2): 475–81. doi:https://doi.org/10.1016/j.ijrobp.2008.12.090.

Artero, Mikel Rezola, Andrea Minery, Leon Nedelcev, Maria Radanova, and Lubka T. Roumenina. 2025. “Complement and the Hallmarks of Cancer.” *Seminars in Immunology* 78(April): 101950. doi:10.1016/j.smim.2025.101950.

Augsburger, Daniela, Peter J Nelson, Thomas Kalinski, Andrej Udelnow, Thomas Knösel, Monika Hofstetter, Ji Wei Qin, et al. 2017. “Current Diagnostics and Treatment of Fibrosarcoma - Perspectives for Future Therapeutic Targets and Strategies.” *Oncotarget* 8(61): 104638–53. doi:10.18632/oncotarget.20136.

B. Mustapha; B. Aydogan; J. Nolen; A. Nassiri; J. Noonan; M. Pankuch; J. Welsh; R. Schulte; J. Robb AIP. 2020. “Prospects for an Advanced Heavy Ion Therapy Center in the Chicago Area.” 050009.

Bader, Samuel B., Mark W. Dewhirst, and Ester M. Hammond. 2021. “Review Cyclic Hypoxia: An Update on Its Characteristics, Methods to Measure It and Biological Implications in Cancer.” *Cancers* 13(1): 1–20. doi:10.3390/cancers13010023.

Baldacchino, Gérard, Emilie Brun, Ibtihel Denden, Sarah Bouhadoun, Raphael Roux, and Hicham Khodja. 2019. “Importance of Radiolytic Reactions during High - LET Irradiation Modalities : LET Effect , Role of O 2 and Radiosensitization by Nanoparticles.” *Cancer Nanotechnology*: 1–21. doi:10.1186/s12645-019-0047-y.

Barcellini, Amelia, Alexandra Charalampopoulou, Gustavo Baldassarre, Sandro Pignata, Giorgia Mangili, Giuseppe Magro, Alessandra Dall’Acqua, et al. 2025. “Quality of Radiation Shapes Survival, Invasiveness, and Migration in Ovarian Cancer Cell Lines with Different Molecular Profiles and Varying Alpha/Beta Ratios: An in Vitro Study on Behalf of the Multicenter Italian Trials in Ovarian Cancer (MITO) Group.” *International journal of radiation biology* 101(9): 973–81. doi:10.1080/09553002.2025.2531909.

Barker, Holly E, James T E Paget, Aadil A Khan, and Kevin J Harrington. 2015. “The Tumour Microenvironment after Radiotherapy: Mechanisms of Resistance and Recurrence.” *Nature reviews. Cancer* 15(7): 409–25. doi:10.1038/nrc3958.

Beckers, Claire, Martin Pruschy, and Irene Vetrugno. 2024. “Tumor Hypoxia and Radiotherapy: A Major Driver of Resistance Even for Novel Radiotherapy Modalities.” *Seminars in Cancer Biology* 98(September 2023): 19–30. doi:10.1016/j.semcancer.2023.11.006.

Bennion, Alexandra, Joanne Lysaght, and Niamh Lynam-Lennon. 2026. “The Insider’s Perspective: The Intracellular Complosome and Immune Cell Dynamics in Cancer.” *Clinical and translational medicine* 16(2): e70628. doi:10.1002/ctm2.70628.

Berridge, Michael V, Patries M Herst, and An S Tan. 2005. “Tetrazolium Dyes as Tools in Cell Biology: New Insights into Their Cellular Reduction.” *Biotechnology annual review* 11: 127–52. doi:10.1016/S1387-2656(05)11004-7.

Bray, Freddie, Mathieu Laversanne, Hyuna Sung, Jacques Ferlay, Rebecca L. Siegel, Isabelle Soerjomataram, and Ahmedin Jemal. 2024. “Global Cancer Statistics 2022: GLOBOCAN Estimates of Incidence and Mortality Worldwide for 36 Cancers in 185 Countries.” *CA: A Cancer Journal for Clinicians* 74(3): 229–63. doi:10.3322/caac.21834.

Brown, J. Martin, and William R. Wilson. 2004. “Exploiting Tumour Hypoxia in Cancer Treatment.” *Nature Reviews Cancer* 4(6): 437–47. doi:10.1038/nrc1367.

Busillo, John M, and Jeffrey L Benovic. 2007. “Regulation of CXCR4 Signaling.” *Biochimica et biophysica acta* 1768(4): 952–63. doi:10.1016/j.bbamem.2006.11.002.

Camazzola, Gianmarco, Daria Boscolo, Emanuele Scifoni, Alexander Dorn, Marco Durante, Michael Krämer, Valentino Abram, and Martina C Fuss. 2023. “TRAX-CHEMxt : Towards the Homogeneous Chemical Stage of Radiation Damage.”

Chen, Daniel S., and Ira Mellman. 2013. “Oncology Meets Immunology: The Cancer-Immunity Cycle.” *Immunity* 39(1): 1–10. doi:10.1016/j.immuni.2013.07.012.

Damerell, Victoria, Michael S. Pepper, and Sharon Prince. 2021. “Molecular Mechanisms Underpinning Sarcomas and Implications for Current and Future Therapy.” *Signal Transduction and Targeted Therapy* 6(1). doi:10.1038/s41392-021-00647-8.

Demaria, Sandra, C Norman Coleman, and Silvia C Formenti. 2016. “Radiotherapy: Changing the Game in Immunotherapy.” *Trends in cancer* 2(6): 286–94. doi:10.1016/j.trecan.2016.05.002.

Demaria, Sandra, Encouse B. Golden, and Silvia C. Formenti. 2015. “Role of Local Radiation Therapy in Cancer Immunotherapy.” *JAMA Oncology* 1(9): 1325–32. doi:10.1001/jamaoncol.2015.2756.

Ding, Peipei, Yanqing Xu, Luying Li, Xinyue Lv, Ling Li, Jianfeng Chen, Danlei Zhou, et al. 2022. “Intracellular Complement C5a/C5aR1 Stabilizes β-Catenin to Promote Colorectal Tumorigenesis.” *Cell Reports* 39(9): 110851. doi:10.1016/j.celrep.2022.110851.

Downs-Canner, Stephanie, Deepa Magge, Roshni Ravindranathan, Mark E O'Malley, Lily Francis, Zuqiang Liu, Z Sheng Guo, Natasa Obermajer, and David L Bartlett. 2016. "Complement Inhibition: A Novel Form of Immunotherapy for Colon Cancer." *Annals of surgical oncology* 23(2): 655–62. doi:10.1245/s10434-015-4778-7.

Duda, Dan G., Sergey V. Kozin, Nathaniel D. Kirkpatrick, Lei Xu, Dai Fukumura, and Rakesh K. Jain. 2011. "CXCL12 (SDF1α)-CXCR4/CXCR7 Pathway Inhibition: An Emerging Sensitizer for Anticancer Therapies?" *Clinical Cancer Research* 17(8): 2074–80. doi:10.1158/1078-0432.CCR-10-2636.

Durante, Marco, Jürgen Debus, and Jay S. Loeffler. 2021. "Physics and Biomedical Challenges of Cancer Therapy with Accelerated Heavy Ions." *Nature Reviews Physics* 3(12): 777–90. doi:10.1038/s42254-021-00368-5.

Durante, Marco, and Jay S. Loeffler. 2010. "Charged Particles in Radiation Oncology." *Nature Reviews Clinical Oncology* 7(1): 37–43. doi:10.1038/nrclinonc.2009.183.

Durante, Marco, Roberto Orecchia, and Jay S. Loeffler. 2017. "Charged-Particle Therapy in Cancer: Clinical Uses and Future Perspectives." *Nature Reviews Clinical Oncology* 14(8): 483–95. doi:10.1038/nrclinonc.2017.30.

Eckert, Franziska, Karin Schilbach, Lukas Klumpp, Lilia Bardoscia, Efe Cumhur Sezgin, Matthias Schwab, Daniel Zips, and Stephan M. Huber. 2018. "Potential Role of CXCR4 Targeting in the Context of Radiotherapy and Immunotherapy of Cancer." *Frontiers in Immunology* 9(December): 1–17. doi:10.3389/fimmu.2018.03018.

Elvington, Michelle, Melissa Scheiber, Xiaofeng Yang, Katherine Lyons, Dustin Jacqmin, Casey Wadsworth, David Marshall, Kenneth Vanek, and Stephen Tomlinson. 2014. "Complement-Dependent Modulation of Antitumor Immunity Following Radiation Therapy." *Cell Reports* 8(3): 818–30. doi:10.1016/j.celrep.2014.06.051.

Enterline, H T, and D R Coman. 1950. "The Ameboid Motility of Human and Animal Neoplastic Cells." *Cancer* 3(6): 1033–38. doi:10.1002/1097-0142(1950)3:6<1033::aid-cncr2820030612>3.0.co;2-r.

Formenti, Silvia C., and Sandra Demaria. 2013. "Combining Radiotherapy and Cancer Immunotherapy: A Paradigm Shift." *Journal of the National Cancer Institute* 105(4): 256–65. doi:10.1093/jnci/djs629.

Fournier, Claudia, Marcus Winter, Sebastian Zahnreich, Elena Nasonova, Larissa Melnikova, and Sylvia Ritter. 2007. "Interrelation amongst Differentiation, Senescence and Genetic Instability in Long-Term Cultures of Fibroblasts Exposed to Different Radiation Qualities." *Radiotherapy and Oncology* 83(3): 277–82. doi:https://doi.org/10.1016/j.radonc.2007.04.022.

Friedl, Peter, and Katarina Wolf. 2003. "TUMOUR-CELL INVASION AND MIGRATION : DIVERSITY AND ESCAPE MECHANISMS." 3(May): 362–74. doi:10.1038/nrc1075.

Fucikova, Jitka, Radek Spisek, Guido Kroemer, and Lorenzo Galluzzi. 2021. “Calreticulin and Cancer.” *Cell Research* 31(1): 5–16. doi:10.1038/s41422-020-0383-9.

Galluzzi, Lorenzo, Molykutty J Aryankalayil, C Norman Coleman, and Silvia C Formenti. 2023. “Emerging Evidence for Adapting Radiotherapy to Immunotherapy.” *Nature reviews. Clinical oncology* 20(8): 543–57. doi:10.1038/s41571-023-00782-x.

Galluzzi, Lorenzo, Aitziber Buqué, Oliver Kepp, Laurence Zitvogel, and Guido Kroemer. 2017. “Immunogenic Cell Death in Cancer and Infectious Disease.” *Nature Reviews Immunology* 17(2): 97–111. doi:10.1038/nri.2016.107.

Galluzzi, Lorenzo, Oliver Kepp, Laurence Zitvogel, Daolin Tang, and Guido Kroemer. 2026. “Cancer Cell Death: Cell-Autonomous and Immunogenic Dimensions.” *Cancer Cell* (2025). doi:10.1016/j.ccell.2025.12.005.

Garlanda, Cecilia, Monica Dambra, and Elena Magrini. 2025. “Interplay between the Complement System and Other Immune Pathways in the Tumor Microenvironment.” *Seminars in Immunology* 78(January). doi:10.1016/j.smim.2025.101951.

Geller, Anne, and Jun Yan. 2019. “The Role of Membrane Bound Complement Regulatory Proteins in Tumor Development and Cancer Immunotherapy.” *Frontiers in Immunology* 10(MAY): 1–13. doi:10.3389/fimmu.2019.01074.

Giavazzi, R., G. Alessandri, F. Spreafico, S. Garattini, and A. Mantovani. 1980. “Metastasizing Capacity of Tumour Cells from Spontaneous Metastases of Transplanted Murine Tumours.” *British Journal of Cancer* 42(3): 462–72. doi:10.1038/bjc.1980.259.

Glaviano, Antonino, Hannah Si-Hui Lau, Lukas M Carter, E Hui Clarissa Lee, Hiu Yan Lam, Elena Okina, Donavan Jia Jie Tan, et al. 2025. “Harnessing the Tumor Microenvironment: Targeted Cancer Therapies through Modulation of Epithelial-Mesenchymal Transition.” *Journal of hematology & oncology* 18(1): 6. doi:10.1186/s13045-024-01634-6.

Goetze, Kristina, Marius Scholz, G Taucher-Scholz, and Wolfgang Mueller-Klieser. 2009. “The Impact of Conventional and Heavy Ion Irradiation on Tumor Cell Migration in Vitro.” *International journal of radiation biology* 83: 889–96. doi:10.1080/09553000701753826.

Graeff, Christian, Lennart Volz, and Marco Durante. 2023. “Emerging Technologies for Cancer Therapy Using Accelerated Particles.” *Progress in Particle and Nuclear Physics* 131: 104046. doi:10.1016/J.PPNP.2023.104046.

Hall, Eric J. & Giaccia, Amato J. 2018. “Eric J. Hall and Amato J. Giaccia: Radiobiology for the Radiologist: Wolters Kluwer, Philadelphia, PA, 2019, Eighth Edition, 624 Pp, ISBN: 978-1496335418.” *Australasian Physical & Engineering Sciences in Medicine* 41. doi:10.1007/s13246-018-0684-1.

Hanahan, Douglas. 2022. “Hallmarks of Cancer: New Dimensions.” *Cancer Discovery* 12(1): 31–46. doi:10.1158/2159-8290.CD-21-1059.

Hanley, Rachel, Francesca Pagliari, Daniel Garcia Calderón, Joana Fernandes Guerreiro, Géraldine Genard, Jeannette Jansen, Clelia Nisticò, et al. 2023. "Radio - Resistance of Hypoxic Tumors : Exploring the Effects of Oxygen and X - Ray Radiation on Non - Small Lung Cancer Cell Lines." *Radiation Oncology*: 1–14. doi:10.1186/s13014-023-02275-8.

Helm, Alexander, and Claudia Fournier. 2023. "High-LET Charged Particles: Radiobiology and Application for New Approaches in Radiotherapy." *Strahlentherapie und Onkologie* 199(12): 1225–41. doi:10.1007/s00066-023-02158-7.

Helm, Alexander, Walter Tinganelli, Palma Simoniello, Fuki Kurosawa, Claudia Fournier, Takashi Shimokawa, and Marco Durante. 2021. "Reduction of Lung Metastases in a Mouse Osteosarcoma Model Treated With Carbon Ions and Immune Checkpoint Inhibitors." *International Journal of Radiation Oncology Biology Physics* 109(2): 594–602. doi:10.1016/j.ijrobp.2020.09.041.

Hsieh, Chia-Hung, Cheng-Hung Lee, Ji-An Liang, Chun-Yen Yu, and Woei-Cherng Shyu. 2010. "Cycling Hypoxia Increases U87 Glioma Cell Radioresistance via ROS Induced Higher and Long-Term HIF-1 Signal Transduction Activity." *Oncology reports* 24(6): 1629–36. doi:10.3892/or_00001027.

Huang, Yangle, Qingting Huang, Jingfang Zhao, Yuanli Dong, Lijia Zhang, Xumeng Fang, Pian Sun, Lin Kong, and Jiade Jay Lu. 2020. "The Impacts of Different Types of Radiation on the CRT and PDL1 Expression in Tumor Cells Under Normoxia and Hypoxia." *Frontiers in oncology* 10: 1610. doi:10.3389/fonc.2020.01610.

Jain, Rakesh K. 2005. "Normalization of Tumor Vasculature: An Emerging Concept in Antiangiogenic Therapy." *Science (New York, N.Y.)* 307(5706): 58–62. doi:10.1126/science.1104819.

Jansen, Jeannette, Olga Sokol, Yolanda Prezado, and Marco Durante. 2026. "Back with Weight: Revisiting Very Heavy Ions for Precision Radiotherapy." *Radiation Research*. doi:10.1667/rade-25-00177.1.

Jeon, Hyungtaek, Seung Ro Han, Suhyuk Lee, Sang June Park, Joo Heon Kim, Seung Min Yoo, and Myung Shin Lee. 2018. "Activation of the Complement System in an Osteosarcoma Cell Line Promotes Angiogenesis through Enhanced Production of Growth Factors." *Scientific Reports* 8(1): 1–11. doi:10.1038/s41598-018-23851-z.

Justus, Calvin R, Mona A Marie, Edward J Sanderlin, and Li V Yang. 2023. "Transwell In Vitro Cell Migration and Invasion Assays." *Methods in molecular biology (Clifton, N.J.)* 2644: 349–59. doi:10.1007/978-1-0716-3052-5_22.

Kepp, Oliver, and Guido Kroemer. 2023. "Immunogenic Cell Stress and Death Sensitize Tumors to Immunotherapy." *Cells* 12(24). doi:10.3390/cells12242843.

Kim, Y U, T Kinoshita, H Molina, D Hourcade, T Seya, L M Wagner, and V M Holers. 1995. "Mouse Complement Regulatory Protein Crry/P65 Uses the Specific Mechanisms of Both Human

Decay-Accelerating Factor and Membrane Cofactor Protein." *Journal of Experimental Medicine* 181(1): 151–59. doi:10.1084/jem.181.1.151.

King, Ben C., and Anna M. Blom. 2023. "Intracellular Complement: Evidence, Definitions, Controversies, and Solutions." *Immunological Reviews* 313(1): 104–19. doi:10.1111/imr.13135.

Kolev, Martin, Madhumita Das, Monica Gerber, Scott Baver, Pascal Deschatelets, and Maciej M. Markiewski. 2022. "Inside-Out of Complement in Cancer." *Frontiers in Immunology* 13(July): 1–14. doi:10.3389/fimmu.2022.931273.

Koshikawa, N, C Maejima, K Miyazaki, A Nakagawara, and K Takenaga. 2006. "Hypoxia Selects for High-Metastatic Lewis Lung Carcinoma Cells Overexpressing Mcl-1 and Exhibiting Reduced Apoptotic Potential in Solid Tumors." *Oncogene* 25(6): 917–28. doi:10.1038/sj.onc.1209128.

Krysko, Dmitri V., Abhishek D. Garg, Agnieszka Kaczmarek, Olga Krysko, Patrizia Agostinis, and Peter Vandenabeele. 2012. "Immunogenic Cell Death and DAMPs in Cancer Therapy." *Nature Reviews Cancer* 12(12): 860–75. doi:10.1038/nrc3380.

Kunachowicz, Dominika, Paulina Tomecka, Mikołaj Sędzik, Jarosław Kalinin, Jacek Kuźnicki, and Nina Rembiałkowska. 2025. "Influence of Hypoxia on Tumor Heterogeneity, DNA Repair, and Cancer Therapy: From Molecular Insights to Therapeutic Strategies." *Cells* 14(14). doi:10.3390/cells14141057.

Lawal, Bashir, Sung-Hui Tseng, Janet Olayemi Olugbodi, Sitthichai Iamsaard, Omotayo B Ilesanmi, Mohamed H Mahmoud, Sahar H Ahmed, Gaber El-Saber Batiha, and Alexander T H Wu. 2021. "Pan-Cancer Analysis of Immune Complement Signature C3/C5/C3AR1/C5AR1 in Association with Tumor Immune Evasion and Therapy Resistance." *Cancers* 13(16). doi:10.3390/cancers13164124.

Lee, Sandy Che-eun S, Andrea Hye, An Pyo, and Marianne Koritzinsky. 2023. "Longitudinal Dynamics of the Tumor Hypoxia Response : From Enzyme Activity to Biological Phenotype." 6409: 1–16. doi:10.1126/sciadv.adj6409.

Li, Qian, Xu Lei, Jing Zhu, Yanping Zhong, Junjie Yang, Jincheng Wang, and Huabing Tan. 2023. "Radiotherapy/Chemotherapy-Immunotherapy for Cancer Management: From Mechanisms to Clinical Implications." *Oxidative medicine and cellular longevity* 2023: 7530794. doi:10.1155/2023/7530794.

Liu, Beilei, Hongyu Zhou, Licheng Tan, Kin To, Hugo Siu, and Xin-Yuan Guan. 2024. "Exploring Treatment Options in Cancer: Tumor Treatment Strategies." doi:10.1038/s41392-024-01856-7.

Loeffler, Jay S., and Marco Durante. 2013. "Charged Particle Therapy-Optimization, Challenges and Future Directions." *Nature Reviews Clinical Oncology* 10(7): 411–24. doi:10.1038/nrclinonc.2013.79.

Loh, Chin-Yap, Jian Yi Chai, Ting Fang Tang, Won Fen Wong, Gautam Sethi, Muthu Kumaraswamy Shanmugam, Pei Pei Chong, and Chung Yeng Looi. 2019. "The E-Cadherin and N-Cadherin Switch in Epithelial-to-Mesenchymal Transition: Signaling, Therapeutic Implications, and Challenges." *Cells* 8(10). doi:10.3390/cells8101118.

Ma, Ning-Yi, Walter Tinganelli, Andreas Maier, Marco Durante, and Wilma Kraft-Weyrather. 2013. "Influence of Chronic Hypoxia and Radiation Quality on Cell Survival." *Journal of radiation research* 54 Suppl 1(Suppl 1): i13-22. doi:10.1093/jrr/rrs135.

Magrini, Elena, Sabrina Di Marco, Sarah N. Mapelli, Chiara Perucchini, Fabio Pasqualini, Alessia Donato, Maria de la Luz Guevara Lopez, et al. 2021. "Complement Activation Promoted by the Lectin Pathway Mediates C3aR-Dependent Sarcoma Progression and Immunosuppression." *Nature Cancer* 2(2): 218–32. doi:10.1038/s43018-021-00173-0.

Mannes, Marco, Christoph Q. Schmidt, Bo Nilsson, Kristina N. Ekdahl, and Markus Huber-Lang. 2021. "Complement as Driver of Systemic Inflammation and Organ Failure in Trauma, Burn, and Sepsis." *Seminars in Immunopathology* 43(6): 773–88. doi:10.1007/s00281-021-00872-x.

Markiewski, Maciej M., and John D. Lambris. 2009. "Unwelcome Complement." *Cancer Research* 69(16): 6367–70. doi:10.1158/0008-5472.CAN-09-1918.

De Martino, Mara, Camille Daviaud, and Claire Vanpouille-Box. 2021. "Radiotherapy: An Immune Response Modifier for Immuno-Oncology." *Seminars in Immunology* 52(March): 101474. doi:10.1016/j.smim.2021.101474.

Massard, C, P Cassier, J C Bendell, D B Marie, M Blery, C Morehouse, M Ascierto, et al. 2019. "Preliminary Results of STELLAR-001, a Dose Escalation Phase I Study of the Anti-C5aR, IPH5401, in Combination with Durvalumab in Advanced Solid Tumours." *Annals of Oncology* 30: v492. doi:10.1093/annonc/mdz253.029.

Mellman, Ira, Daniel S. Chen, Thomas Powles, and Shannon J. Turley. 2023. "The Cancer-Immunity Cycle: Indication, Genotype, and Immunotype." *Immunity* 56(10): 2188–2205. doi:10.1016/j.immuni.2023.09.011.

Meri, Seppo, Elena Magrini, Alberto Mantovani, and Cecilia Garlanda. 2023. "The Yin Yang of Complement and Cancer." *Cancer Immunology Research* 11(12): 1578–88. doi:10.1158/2326-6066.CIR-23-0399.

Mittal, Deepak, Matthew M Gubin, Robert D Schreiber, and Mark J Smyth. 2014. "New Insights into Cancer Immunoediting and Its Three Component Phases--Elimination, Equilibrium and Escape." *Current opinion in immunology* 27: 16–25. doi:10.1016/j.coi.2014.01.004.

Mohamad, Osama, Brock J. Sishc, Janapriya Saha, Arnold Pompos, Asal Rahimi, Michael D. Story, Anthony J. Davis, and D. W.Nathan Kim. 2017. "Carbon Ion Radiotherapy: A Review of Clinical Experiences and Preclinical Research, with an Emphasis on DNA Damage/Repair." *Cancers* 9(6): 1–30. doi:10.3390/cancers9060066.

Moncharmont, Coralie, Antonin Levy, Jean Baptiste Guy, Alexander T. Falk, Matthieu Guilbert, Jane Chloé Trone, Gersende Alphonse, et al. 2014. "Radiation-Enhanced Cell Migration/Invasion Process: A Review." *Critical Reviews in Oncology/Hematology* 92(2): 133–42. doi:10.1016/j.critrevonc.2014.05.006.

Monica M Olcina. 2019. "The Tumour Microenvironment Links Complement System Dysregulation and Hypoxic Signalling." *British Journal of Radiology* 92(1093): 1–11. doi:10.1259/bjr.20189005.

Moon, Eui Jung, Kristoffer Petersson, and Monica M. Olcina. 2022. "The Importance of Hypoxia in Radiotherapy for the Immune Response, Metastatic Potential and FLASH-RT." *International Journal of Radiation Biology* 98(3): 439–51. doi:10.1080/09553002.2021.1988178.

Morgan, B Paul. 2016. "The Membrane Attack Complex as an Inflammatory Trigger." *Immunobiology* 221(6): 747–51. doi:10.1016/j.imbio.2015.04.006.

Nakao, Lia S, Michael F Olson, José Pablo Vázquez-Medina, and Alejandra Valdivia. 2023. "Editorial: Reactive Oxygen Species (ROS) Signaling during Cytoskeleton Dynamics." *Frontiers in cell and developmental biology* 11: 1295263. doi:10.3389/fcell.2023.1295263.

O'Brien, Rebecca M, Aoife Cannon, John V Reynolds, Joanne Lysaght, and Niamh Lynam-Lennon. 2021. "Complement in Tumourigenesis and the Response to Cancer Therapy." *Cancers* 13(6). doi:10.3390/cancers13061209.

O'Brien, Rebecca M., Niamh Lynam-Lennon, and Monica M. Olcina. 2023. "Thinking inside the Box: Intracellular Roles for Complement System Proteins Come into Focus." *British Journal of Cancer* 128(2): 165–67. doi:10.1038/s41416-022-02116-7.

Okroj, Marcin, Leticia Corrales, Anna Stokowska, Ruben Pio, and Anna M. Blom. 2009. "Hypoxia Increases Susceptibility of Non-Small Cell Lung Cancer Cells to Complement Attack." *Cancer Immunology, Immunotherapy* 58(11): 1771–80. doi:10.1007/s00262-009-0685-8.

Orth, Michael, Kirsten Lauber, Maximilian Niyazi, Anna A. Friedl, Minglun Li, Cornelius Maihöfer, Lars Schüttrumpf, et al. 2013. "Current Concepts in Clinical Radiation Oncology." *Radiation and Environmental Biophysics 2013 53:1* 53(1): 1–29. doi:10.1007/S00411-013-0497-2.

Petitprez, Florent, Aurélien de Reyniès, Emily Z Keung, Tom Wei-Wu Chen, Cheng-Ming Sun, Julien Calderaro, Yung-Ming Jeng, et al. 2020. "B Cells Are Associated with Survival and Immunotherapy Response in Sarcoma." *Nature* 577(7791): 556–60. doi:10.1038/s41586-019-1906-8.

Pio, Ruben, Daniel Ajona, and John D. Lambris. 2013. "Complement Inhibition: A Promising Concept for Cancer Treatment." *Seminars in immunology* 25(1): 54–64. doi:10.1016/j.smim.2013.04.001.Complement.

Pio, Ruben, Daniel Ajona, Sergio Ortiz-Espinosa, Alberto Mantovani, and John D. Lambris. 2019. "Complementing the Cancer-Immunity Cycle." *Frontiers in Immunology* 10(APR): 1–12. doi:10.3389/fimmu.2019.00774.

Pourjafar, Mona, and Vijay K Tiwari. 2024. "Plasticity in Cell Migration Modes across Development, Physiology, and Disease." *Frontiers in cell and developmental biology* 12: 1363361. doi:10.3389/fcell.2024.1363361.

Quartieri, Martina, Anggraeini Puspitasari, Tamara Vitacchio, Marco Durante, and Walter Tinganelli. 2023. "The Role of Hypoxia and Radiation in Developing a CTCs-like Phenotype in Murine Osteosarcoma Cells." *Frontiers in cell and developmental biology* 11: 1222809. doi:10.3389/fcell.2023.1222809.

Reda, Moataz, Alexander F. Bagley, Husam Y. Zaidan, and Wassana Yantasee. 2020. "Augmenting the Therapeutic Window of Radiotherapy: A Perspective on Molecularly Targeted Therapies and Nanomaterials." *Radiotherapy and Oncology* 150: 225–35. doi:10.1016/j.radonc.2020.06.041.

Revel, Margot, Marie V Daugan, Catherine Sautés-Fridman, Wolf H Fridman, and Lubka T Roumenina. 2020. "Complement System: Promoter or Suppressor of Cancer Progression?" *Antibodies* 9(4). doi:10.3390/antib9040057.

Ricklin, Daniel, and John D Lambris. 2007. "Complement-Targeted Therapeutics." *Nature biotechnology* 25(11): 1265–75. doi:10.1038/nbt1342.

Rodriguez, Luis G, Xiaoyang Wu, and Jun-Lin Guan. 2005. "Wound-Healing Assay." *Methods in molecular biology (Clifton, N.J.)* 294: 23–29. doi:10.1385/1-59259-860-9:023.

Rossi, Sandro. 2015. "The National Centre for Oncological Hadrontherapy (CNAO): Status and Perspectives." *Physica Medica: European Journal of Medical Physics* 31(4): 333–51. doi:10.1016/j.ejmp.2015.03.001.

Roumenina, Lubka T., Marie V. Daugan, Florent Petitprez, Catherine Sautès-Fridman, and Wolf Herman Fridman. 2019. "Context-Dependent Roles of Complement in Cancer." *Nature Reviews Cancer* 19(12): 698–715. doi:10.1038/s41568-019-0210-0.

Saxena, Kritika, and Mohit Kumar Jolly. 2019. "Acute vs. Chronic vs. Cyclic Hypoxia: Their Differential Dynamics, Molecular Mechanisms, and Effects on Tumor Progression." *Biomolecules* 9(8). doi:10.3390/biom9080339.

Sbaraglia, Marta, Elena Bellan, and Angelo P Dei Tos. 2021. "The 2020 WHO Classification of Soft Tissue Tumours: News and Perspectives." *Pathologica* 113(2): 70–84. doi:10.32074/1591-951X-213.

Schardt, Dieter, Thilo Elsässer, and Daniela Schulz-Ertner. 2010. "Heavy-Ion Tumor Therapy: Physical and Radiobiological Benefits." *Reviews of Modern Physics* 82(1): 383. doi:10.1103/RevModPhys.82.383.

Sengedorj, Azzaya, Michael Hader, Benjamin Frey, Rainer Fietkau, Oliver J. Ott, Udo S. Gaipl, and Michael Rückert. 2022. "Interaction of Radiotherapy and Hyperthermia with the Immune System: A Brief Current Overview." *Current Stem Cell Reports* 8(3): 129–38. doi:10.1007/S40778-022-00215-Y/FIGURES/2.

Shi, Saimeng, Longyun Ye, Kaizhou Jin, Xianjun Yu, Duancheng Guo, and Weiding Wu. 2024. "The Complement C3a/C3aR Pathway Is Associated with Treatment Resistance to Gemcitabine-Based Neoadjuvant Therapy in Pancreatic Cancer." *Computational and structural biotechnology journal* 23: 3634–50. doi:10.1016/j.csbj.2024.09.032.

Shu, Chi, Haoran Zha, Haixia Long, Xinxin Wang, Fei Yang, Jianbao Gao, Chunyan Hu, et al. 2020. "C3a-C3aR Signaling Promotes Breast Cancer Lung Metastasis via Modulating Carcinoma Associated Fibroblasts." *Journal of experimental & clinical cancer research : CR* 39(1): 11. doi:10.1186/s13046-019-1515-2.

Sokol, Olga, and Marco Durante. 2023. "Carbon Ions for Hypoxic Tumors: Are We Making the Most of Them?" *Cancers* 15(18): 1–18. doi:10.3390/cancers15184494.

Sonderegger, Stefan E., Silvia Manzanero, Trent M. Woodruff, Jad Farouqa, Jamileh Nabizadeh, Nadya Panagides, and Barbara E. Rolfe. 2023. Clinical Immuno-Oncology *The Role of the Complement System in Cancer Etiology and Management*. 1st ed. Elsevier Inc. doi:10.1016/B978-0-323-87763-3.00012-5.

Sørensen, Brita Singers, and Michael R. Horsman. 2020. "Tumor Hypoxia: Impact on Radiation Therapy and Molecular Pathways." *Frontiers in Oncology* 10(April): 1–11. doi:10.3389/fonc.2020.00562.

Staab, Adrian, Jürgen Loeffler, Harun M Said, Désirée Diehlmann, Astrid Katzer, Melanie Beyer, Markus Fleischer, et al. 2007. "Effects of HIF-1 Inhibition by Chetomin on Hypoxia-Related Transcription and Radiosensitivity in HT 1080 Human Fibrosarcoma Cells." *BMC cancer* 7: 213. doi:10.1186/1471-2407-7-213.

Surace, Laura, Veronika Lysenko, Andrea Orlando Fontana, Virginia Cecconi, Hans Janssen, Antonela Bicvic, Michal Okoniewski, et al. 2015. "Complement Is a Central Mediator of Radiotherapy-Induced Tumor-Specific Immunity and Clinical Response." *Immunity* 42(4): 767–77. doi:10.1016/j.immuni.2015.03.009.

Tawbi, Hussein A, Melissa Burgess, Vanessa Bolejack, Brian A Van Tine, Scott M Schuetze, James Hu, Sandra D'Angelo, et al. 2017. "Pembrolizumab in Advanced Soft-Tissue Sarcoma and Bone Sarcoma (SARC028): A Multicentre, Two-Cohort, Single-Arm, Open-Label, Phase 2 Trial." *The Lancet Oncology* 18(11): 1493–1501. doi:10.1016/S1470-2045(17)30624-1.

Telarovic, Irma, Roland H Wenger, and Martin Pruschy. 2021. "Interfering with Tumor Hypoxia for Radiotherapy Optimization." *Journal of Experimental & Clinical Cancer Research* 40(1): 197. doi:10.1186/s13046-021-02000-x.

Tenforde, T S, S B Curtis, K E Crabtree, S D Tenforde, W A Schilling, J Howard, and J T Lyman. 1980. "In Vivo Cell Survival and Volume Response Characteristics of Rat Rhabdomyosarcoma

Tumors Irradiated in the Extended Peak Region of Carbon- and Neon-Ion Beams." *Radiation Research* 83(1): 42–56.

Thiery, Jean Paul. 2002. "Epithelial–Mesenchymal Transitions in Tumour Progression." *Nature Reviews Cancer* 2(6): 442–54. doi:10.1038/nrc822.

Thomlinson, R H, and L H Gray. 1955. "The Histological Structure of Some Human Lung Cancers and the Possible Implications for Radiotherapy." *British journal of cancer* 9(4): 539–49. doi:10.1038/bjc.1955.55.

Tinganelli, Walter, and Marco Durante. 2020. 12 Cancers *Carbon Ion Radiobiology*. doi:10.3390/cancers12103022.

Tinganelli, Walter, Marco Durante, Ryoichi Hirayama, Michael Krämer, Andreas Maier, Wilma Kraft-Weyrather, Yoshiya Furusawa, Thomas Friedrich, and Emanuele Scifoni. 2015. "Kill-Painting of Hypoxic Tumours in Charged Particle Therapy." *Scientific Reports* 5: 1–13. doi:10.1038/srep17016.

Totis, Cristina, Nicole B Averbeck, Burkhard Jakob, Maik Schork, Gaia Volpi, Dennis F Hintze, Marco Durante, Claudia Fournier, and Alexander Helm. 2025. "Induction of Cytoplasmic DsDNA and CGAS-STING Immune Signaling After Exposure of Breast Cancer Cells to X-Ray or High-Energetic Carbon Ions." *Advances in radiation oncology* 10(6): 101783. doi:10.1016/j.adro.2025.101783.

Tufail, Muhammad, Can-Hua Jiang, and Ning Li. 2025. "Immune Evasion in Cancer: Mechanisms and Cutting-Edge Therapeutic Approaches." *Signal Transduction and Targeted Therapy* 10(1): 227. doi:10.1038/s41392-025-02280-1.

Vadrevu, Surya Kumari, Navin K Chintala, Sharad K Sharma, Priya Sharma, Clayton Cleveland, Linley Riediger, Sasikanth Manne, et al. 2014. "Complement C5a Receptor Facilitates Cancer Metastasis by Altering T-Cell Responses in the Metastatic Niche." *Cancer Research* 74(13): 3454–65. doi:10.1158/0008-5472.CAN-14-0157.

Vaupel, Peter, Arnulf Mayer, and Michael Höckel. 2004. "Tumor Hypoxia and Malignant Progression." *Methods in enzymology* 381: 335–54. doi:10.1016/S0076-6879(04)81023-1.

Vischioni, Barbara, Amelia Barcellini, Giuseppe Magro, Marco Rotondi, Marco Durante, Angelica Facoetti, Juliette Thariat, and Ester Orlandi. 2025. "For Patients Selections." *International Journal of Particle Therapy* 15(December 2024): 100737. doi:10.1016/j.ijpt.2024.100737.

Vito, Alyssa, Nader El-Sayes, and Karen Mossman. 2020. "Hypoxia-Driven Immune Escape in the Tumor Microenvironment." *Cells* 9(4): 1–20. doi:10.3390/cells9040992.

Wang, Hui, Heng Jiang, Melissa Van De Gucht, and Mark De Ridder. 2019. "Hypoxic Radioresistance : Can ROS Be the Key To." doi:10.3390/cancers11010112.

Wang, Yu, Sheng-Nan Sun, Qing Liu, Yang-Yang Yu, Jian Guo, Kun Wang, Bao-Cai Xing, et al. 2016. "Autocrine Complement Inhibits IL10-Dependent T-Cell–Mediated Antitumor

Immunity to Promote Tumor Progression." *Cancer Discovery* 6(9): 1022–35. doi:10.1158/2159-8290.CD-15-1412.

Wennerberg, Erik, Claire Vanpouille-Box, Sophia Bornstein, Takahiro Yamazaki, Sandra Demaria, and Lorenzo Galluzzi. 2017. "Immune Recognition of Irradiated Cancer Cells." *Immunological reviews* 280(1): 220–30. doi:10.1111/imr.12568.

Werner, Sarah, Thejaswini Giridharan, A N M Nazmul Khan, Luxue Deng, Ashley Duhon, Sora Suzuki, Celia DeJohn, et al. 2025. "Complement C3 Inhibition with Pegcetacoplan Controls Malignant Effusions in Recurrent Ovarian Cancer: Interim Results from a Phase II Trial." *Gynecologic Oncology* 200: 125–26. doi:10.1016/j.ygyno.2025.04.144.

West, Erin E, and Claudia Kemper. 2023. "Complosome — the Intracellular Complement System." *Nature Reviews Nephrology* 19(7): 426–39. doi:10.1038/s41581-023-00704-1.

Williams, Jacqueline. 2019. "Basic Clinical Radiobiology." *International Journal of Radiation Biology* 95(6): 797–797. doi:10.1080/09553002.2019.1569781.

Wouters, B G, and J M Brown. 1997. "Cells at Intermediate Oxygen Levels Can Be More Important than the 'Hypoxic Fraction' in Determining Tumor Response to Fractionated Radiotherapy." *Radiation research* 147(5): 541–50.

Wozny, Anne Sophie, and Claire Rodriguez-Lafrasse. 2023. "The 'Stealth-Bomber' Paradigm for Deciphering the Tumour Response to Carbon-Ion Irradiation." *British Journal of Cancer* 128(8): 1429–38. doi:10.1038/s41416-022-02117-6.

Wozny, Anne-sophie, Guillaume Vares, Gersende Alphonse, Alexandra Lauret, Caterina Monini, Nicolas Magn, Charlotte Cuerq, et al. 2019. "ROS Production and Distribution : A New Paradigm to Explain the Di Ff Erential E Ff Ects of X-Ray and Carbon Ion Irradiation on Cancer Stem Cell Migration and Invasion."

Wozny, Anne-Sophie, Guillaume Vares, Gersende Alphonse, Alexandra Lauret, Caterina Monini, Nicolas Magné, Charlotte Cuerq, et al. 2019. "ROS Production and Distribution: A New Paradigm to Explain the Differential Effects of X-Ray and Carbon Ion Irradiation on Cancer Stem Cell Migration and Invasion." *Cancers* 11(4). doi:10.3390/cancers11040468.

Yang, Ronghui, Di Fu, and Aijun Liao. 2025. "The Role of Complement in Tumor Immune Tolerance and Drug Resistance: A Double-Edged Sword." *Frontiers in Immunology* 16(January): 1–12. doi:10.3389/fimmu.2025.1529184.

Zha, Haoran, Xinxin Wang, Ying Zhu, Diangang Chen, Xiao Han, Fei Yang, Jianbao Gao, et al. 2019. "Intracellular Activation of Complement C3 Leads to PD-L1 Antibody Treatment Resistance by Modulating Tumor-Associated Macrophages." *Cancer Immunology Research* 7(2): 193–207. doi:10.1158/2326-6066.CIR-18-0272.

Zink, Klemens, Kilian Simon Baumann, Ulrike Theiss, Florentine Subtil, Sonja Lahrmann, Fabian Eberle, and Sebastian Adeberg. 2024. "Organization and Operation of Multi Particle Therapy

Facilities: The Marburg Ion-Beam Therapy Center, Germany (MIT).” *Health and Technology* 14(5): 929–38. doi:10.1007/s12553-024-00881-4.

Web References:

International Agency for Research on Cancer (IARC), "Global Cancer Observatory – Cancer today (data visualization)", [Online]. Available: https://gco.iarc.who.int/today/en/dataviz/pie?mode=population&group_populations=0. [Accessed: February 12, 2026].

International Agency for Research on Cancer (IARC), "Global Cancer Observatory – Cancer Tomorrow (data visualization)", [Online]. Available: https://gco.iarc.who.int/tomorrow/en/dataviz/bars. [Accessed: February 12, 2026].

Particle Therapy Co-Operative Group (PTCOG), "User Registration", [Online]. Available: https://www.ptcog.site/index.php/registration. [Accessed: January 20, 2026].

Fondazione CNAO (National Centre for Oncological Hadrontherapy), "Pathologies that can be treated", [Online]. Available: https://fondazionecnao.it/en/pathologies-than-can-be-treated. [Accessed: February 10, 2026].

Acknowledgement

The research path leading to this thesis has been an international journey, developed between the National Center for Oncological Hadrontherapy (CNAO) in Pavia and the GSI Helmholtzzentrum für Schwerionenforschung in Darmstadt. This "split doctorate" between Italy and Germany presented several organizational challenges and initial uncertainties, but it became an extraordinary opportunity thanks to the constant support of the people who accompanied me.

I would like to express my gratitude to my supervisor, Professor Angelica Facoetti, Head of the *Radiobiology Group* at CNAO. I thank her not only for making this project possible but, above all, for the trust she placed in me, granting me the freedom to explore new research horizons and guiding me towards full scientific independence.

I would also like to thank Professor Andrea Spanu for the interest shown in my work and for his insightful and productive suggestions during our discussions.

A special recognition goes to Professor Marco Durante, Director of the Biophysics Department at GSI, for welcoming me to his center. Engaging with such a stimulating environment has been an honor and a great source of inspiration.

In Germany, my thanks go to Professor Claudia Fournier, PI of the *Immune System and Tissue Radiobiology* research group, who supported me with dedication in all my ideas. Her listening skills and her invaluable help in coordinating this complex thesis work were fundamental to the organisation of the project.

Alongside her, I would like to thank Dr. Alexander Helm. A sincere thank you for his constant support and for being a point of reference; his presence made it much easier to face the daily challenges of research.

Finally, I would like to thank my two research groups: the CNAO Radiobiology group and the Immune System and Tissue Radiobiology group, including both current and past members who helped me throughout these three years of work.